GEOSCIENCE CANADA
JOURNAL OF THE GEOLOGICAL ASSOCIATION OF CANADA
JOURNAL DE L'ASSOCIATION GÉOLOGIQUE DU CANADA

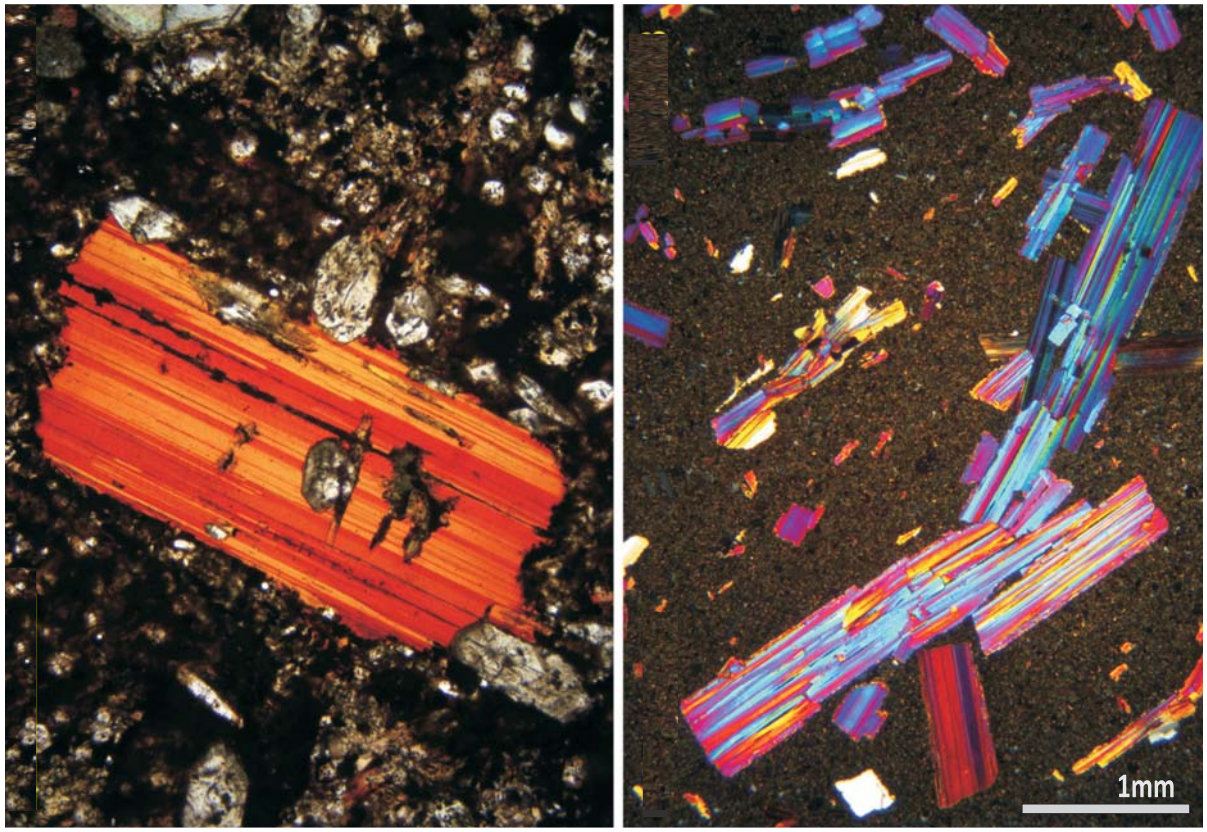

Tectonics in Action: Deconstructing Constructive Collisions

Lamproites - Deeply diverse and sometimes sparkling

Brunswick: An Influential and Truly Giant Canadian VMS

2020 VOLUME 47

Publisher/Éditeur
Geological Association of Canada
Alexander Murray Bld., Rm ER4063
Memorial University of Newfoundland
St. John's, NL, Canada, A1B 3X5
Tel: (709) 864-7660
Fax: (709) 864-2532
gac@mun.ca
www.gac.ca

Print Edition: ISSN 0315-0941
Online Edition: ISSN 1911-4850

Volume 47

A journal published quarterly by the Geological Association of Canada, incorporating the Proceedings.
Une revue trimestrielle publiée par l'Association géologique du Canada et qui en diffuse les actes.

Subscriptions: Receiving four issues of Geoscience Canada per year for $50 is one of the benefits of being a GAC member. To obtain institutional subscriptions, please contact Érudit: www.erudit.org

Abonnement: Recevoir quatre numéros par année pour 50,00 $ du magazine Geoscience est l'un des avantages réservés aux membres de l'AGC. Pour les abonnements institutionnels, s'il vous plaît contacter Érudit: www.erudit.org

Those wishing to submit material for publication in Geoscience Canada should refer to the Instructions to Authors on the journal's website, www.geosciencecanada.ca

AUTHORS PLEASE NOTE:
Please use the web address http://journals.hil.unb.ca/index.php/GC/index for submissions; please do not submit articles directly to the editor.

The Mission of the Geological Association of Canada is to facilitate the scientific well-being and professional development of its members, the learned discussion of geoscience in Canada, and the advancement, dissemination and wise use of geosciences in public, professional and academic life. Articles in Geoscience Canada are freely available one year after their publication date, unless authors have arranged for immediate open access. Opinions expressed and interpretations presented are those of the authors and do not necessarily reflect those of the editors, publishers and other contributors. Your comments are welcome.

Cover Image: Spectacular polysynthetic twinning in titanian phlogopites in lamproites from the diamond-bearing Ellendale Province, western Australia. Photos in cross-polarized light. For more information, see the paper by Mitchell (this issue). Photo credit: R.H. Mitchell.

ANDREW HYNES SERIES: TECTONIC PROCESSES

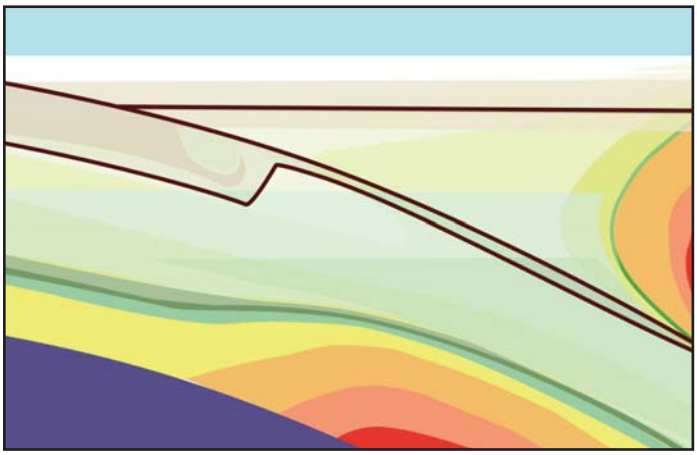

Accretion, Soft and Hard Collision: Similarities, Differences and an Application from the Newfoundland Appalachian Orogen

Cees van Staal[1,2] and Alexandre Zagorevski[3]

[1]Geological Survey of Canada
1500-605 Robson Street, Vancouver, British Columbia, V6B 5J3 Canada

[2]Department of Earth and Environmental Sciences
University of Waterloo, Waterloo, Ontario, N2L 3G1, Canada
E-mail: cees.vanstaal@canada.ca

[3]Geological survey of Canada
601 Booth Street, Ottawa, Ontario, K1A 0E8, Canada

Cees van Staal received the 2019 GAC Logan Medal; this paper is contribution number 6 of the Journal's Logan Medallist series.

SUMMARY

We argue there is no distinction between accretion and collision as a process, except when accretion is used in the sense of incorporating small bodies of sedimentary and/or volcanic rocks into an accretionary wedge by off-scraping or underplating. There is also a distinction when these terms are used in classifying mountain belts into accretionary and collisional orogens, although such classifications are commonly based on a qualitative assessment of the scale and nature of the accreted terranes and continents involved in formation of mountain belts.

Soft collisions occur when contractional deformation and associated metamorphism are principally concentrated in rocks of the leading edge of the partially pulled-down buoyant plate and the upper plate forearc terrane. Several young arc-continent collisions show evidence for partial or wholesale subduction of the forearc such that the arc is structurally juxtaposed directly against lower plate rocks. This process may explain the poor preservation of forearcs in the geological record. Soft collisions generally change into hard collisions over time, except if the collision is rapidly followed by formation of a new subduction zone due to step-back or polarity reversal. Thickening and metamorphism of the arc's suprastructure and retro-arc part of upper plate due to contractional deformation and burial are the characteristics of a hard collision or an advancing Andean-type margin. Strong rheological coupling of the converging plates and lower and upper crust in the downgoing continental margin promotes a hard collision.

Application of the soft–hard terminology supports a structural juxtaposition of the Taconic soft collision recorded in the Humber margin of western Newfoundland with a hard collision recorded in the adjacent Dashwoods block. It is postulated that Dashwoods was translated dextrally along the Cabot-Baie Verte fault system from a position to the north of Newfoundland where the Notre Dame arc collided ca. 10 m.y. earlier with a wide promontory in a hyperextended segment of the Laurentian margin.

RÉSUMÉ

Nous soutenons qu'il n'y a pas de distinction entre l'accrétion et la collision en tant que processus, sauf lorsque l'accrétion est utilisée dans le sens d'incorporer de petits corps de roches sédimentaires et/ou volcaniques dans un prisme d'accrétion par raclage ou sous-placage. Il y a également une distinction lorsque ces termes sont utilisés pour classer les chaînes de montagne en orogènes d'accrétion et de collision, bien que ces classifications soient généralement basées sur une évaluation qualitative de l'échelle et de la nature des terranes accrétés et des continents impliqués dans la formation des chaînes de montagnes.

Des collisions molles se produisent lorsque la déformation par contraction et le métamorphisme associé sont principalement concentrés dans les roches du front de la plaque

chevauchante partiellement abaissée et du terrane d'avant-arc de la plaque supérieure. Plusieurs jeunes collisions arc-continent montrent des preuves d'une subduction partielle ou totale de l'avant-arc de telle sorte que l'arc est directement structurellement juxtaposé contre les roches de la plaque inférieure. Ce processus peut expliquer la mauvaise préservation des avant-arcs dans les archives géologiques. Les collisions molles se transforment généralement en collisions dures au fil du temps, sauf si la collision est rapidement suivie de la formation d'une nouvelle zone de subduction en raison d'un recul ou d'une inversion de polarité. L'épaississement et le métamorphisme de la suprastructure de l'arc et de la partie rétro-arc de la plaque supérieure dus à la déformation par contraction et à l'enfouissement sont les caractéristiques d'une collision dure ou d'une marge de type andin en progression. Un fort couplage rhéologique des plaques convergentes et de la croûte inférieure et supérieure dans la marge continentale descendante favorise une collision dure.

L'application de la terminologie molle-dure corrobore une juxtaposition structurelle de la collision molle taconique enregistrée dans la marge de Humber de l'ouest de Terre-Neuve avec une collision dure enregistrée dans le bloc de Dashwoods adjacent. Il est postulé que le bloc de Dashwoods a été déplacé de manière dextre le long du système de failles Cabot-Baie Verte à partir d'une position au nord de Terre-Neuve où l'arc Notre Dame est entré en collision environ 10 m.a. plus tôt avec un large promontoire dans un segment en hyper-extension de la marge laurentienne.

Traduit par la Traductrice

INTRODUCTION

Subduction of oceanic lithosphere ultimately leads to the amalgamation of allochthonous (exotic) terranes with buoyant, unsubductable lithosphere and formation of orogenic belts. The actual process of amalgamation is described in the literature using a variety of terms, including docking, suturing, accretion, and collision. Whereas docking and suturing are commonly used as non-genetic descriptors of amalgamation of terranes, collision and accretion commonly carry different connotations to different authors. Accretion and collision have been used to classify mountain belts into accretionary and collisional orogens (e.g. Windley 1992; Cawood et al. 2009), suggesting to some (e.g. Wang et al. 2006) that accretion and collision of terranes represent fundamentally different processes. In Windley's (1992) view, accretion results in mountain belts characterized by significant addition of new juvenile crust, whereas collision generally does not. Collisions have been further subdivided into 'soft' and 'hard' by some workers (see below). The terminology used in analyzing orogenic belts is compounded by numerous other classifying schemes, based on tectonic (e.g. Şengör and Natal'in 1996; Şengör et al. 2018) or metamorphic characteristics (e.g. Brown 2009). Such classifications can be useful for purposes of comparative orogenesis and whether there were any secular changes in tectonic processes (e.g. Stern 2005; Brown 2007), but it is important to keep in mind that they are arbitrary and commonly depend on the scale of studies (see following).

In this contribution, we review and examine some of the common terminology and classifications that are used in orogenic analysis. We discuss the differences in terminology and assess their implications for tectonic analyses of some orogenic belts. In addition, we present an application from the Newfoundland Appalachians where a distinction between soft and hard collision helps in the tectonic analysis of the Ordovician Taconic–Grampian orogen.

Accretion Versus Collision

Accretionary orogens mainly form by tectonic addition of exotic allochthonous terranes such as island arcs, continental ribbons, oceanic plateaus and oceanic crust to continental margins or relatively stable, isolated terranes, prior to terminal closure of oceans. The growing accretionary orogen is more or less viewed as a large-scale accretionary orogenic wedge. Within this orogenic wedge, allochthonous terranes sequentially accrete to cratonized lithosphere, analogous to scraped-off sedimentary and volcanic rocks in accretionary prisms. In contrast, collisional orogens are commonly thought to form where an ocean fully closes between two converging continent-size terranes. The large size of the collided continental terranes generally prevents tectonic reworking of the intervening accreted terranes by any new subduction set-up outboard of the collisional orogen after termination of convergence between the continental colliders. Reworking is more common in an accretionary orogen, because the accreted terranes are generally relatively small and hence, more prone to be overprinted by subsequent tectonism following the rapid renewal of subduction by stepping outboard behind the accreted terrane. Hence, scale can play a significant role in discriminating between accretionary and collisional 'endmembers' of this classification system. Transfer of smaller sedimentary and volcano-plutonic packages from the downgoing plate to the overlying accretionary wedge by scraping-off, clipping-off or underplating is generally considered to be accretion (e.g. Kimura and Ludden 1995). This commonly occurs below sea level and does not typically form emergent mountains. The individual accretionary events are commonly too short and localized to identify them as distinct events in the ancient geological record. Nonetheless, 'steady-state' accretion or episodic accretion of larger underplated rocks or terranes can result in significant uplift and deformation in modern settings (Fig. 1A, B; e.g. Platt et al. 1985; Brandon et al. 1998; Soh et al. 1998) and can leave their footprint in the form of structures and metamorphism in the geological record (e.g. van Staal et al. 2008; Wells et al. 2014; Zagorevski et al. 2015).

The perspective of the authors can play a significant and rather arbitrary role in the distinction between accretion and collision. For example, docking of the Ontong Java plateau with the Solomon arc along the Vitiaz trench (Fig. 1C) led to imbrication of the Ontong Java plateau, local emergence of islands (Malaita and Santa Isabel), and a subduction reversal along the Solomon trench (Taira et al. 2004). This event is generally viewed as a collision (Mann and Taira 2004). Similarly, docking of the Crescent-Siletzia terrane to North America along the Cascadia subduction zone (Fig. 1B) led to imbrica-

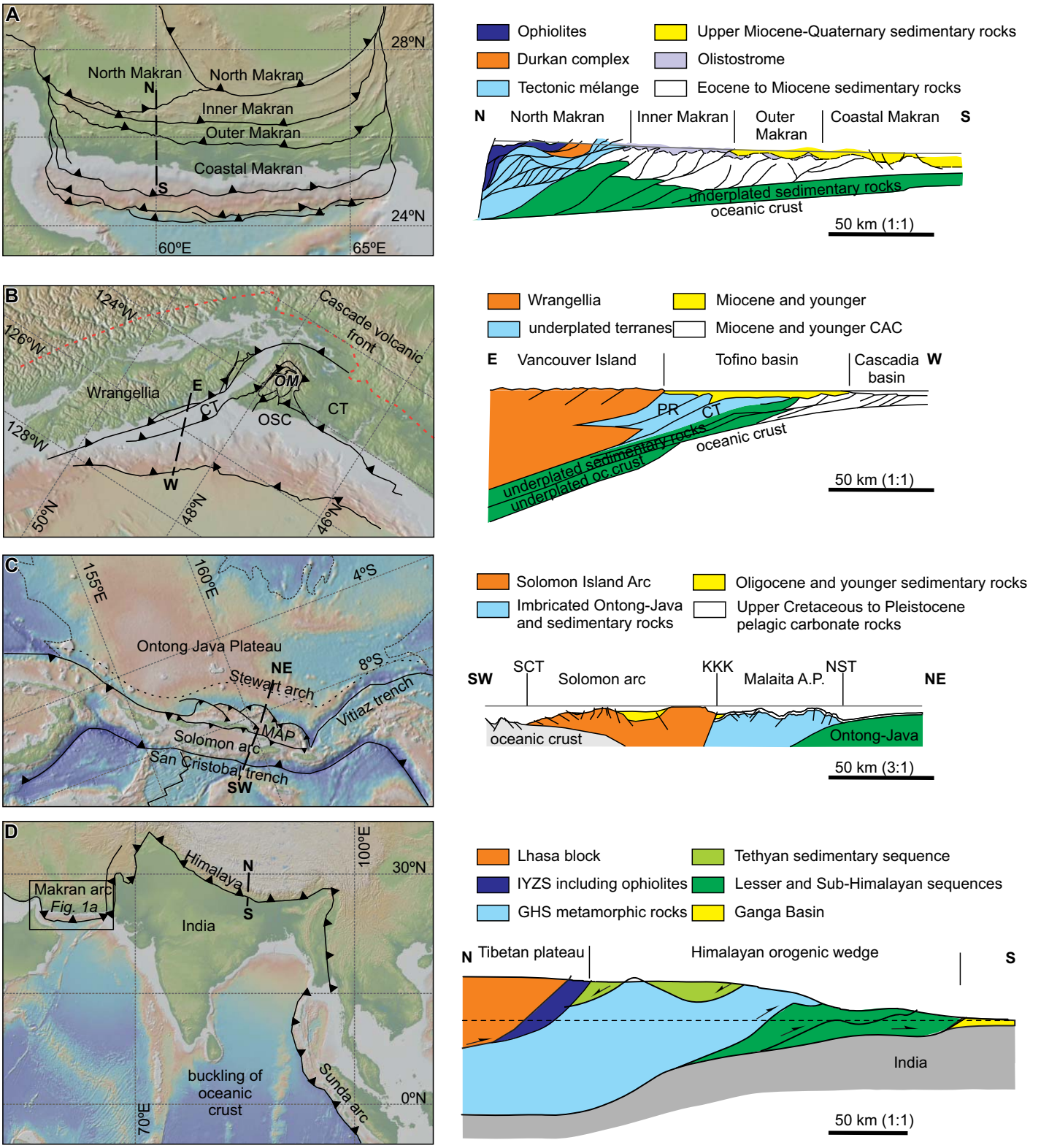

Figure 1. Figures showing the simplified geometries of: (A) the Makran subduction zone immediately west of the India–Eurasia collision zone (modified after Burg 2018). Location of the Makran with respect to India and the Himalayan mountain belt is shown in Fig. 1D, (B) the Cascadia subduction complex along the west coast of British Columbia and Washington (modified after Calvert 1996 and Brandon et al. 1998; CAC – Cascadia accretionary complex; CT – Crescent terrane and equivalents; OM – Olympic Mountains; OSC – Olympic Subduction Complex), (C) the Ontong Java–Solomon arc collision zone (modified after Mann and Taira 2004 and Taira et al. 2004; KKK Kia-Kaipito-Korigole fault zone MAP – Malaita Accretionary Prism, NST North Solomon trench; SCT – San Cristobal trench), and (D) the Himalayan India–Eurasia collision zone (modified after Godin et al. 2018; GHS – Greater Himalayan sequence; IYZS – Indus-Yalung Zangbo Suture zone; location of Figure 1A outlined). Background images and some plate boundaries were generated from www.geomapapp.org.

https://doi.org/10.12789/geocanj.2020.47.161

tion of the partly subducted and underplated Crescent-Siletzia terrane and rocks in the overlying and emerging forearc terrane (e.g. Wells et al. 2014). Yet this is considered an accretionary event by most workers (e.g. Calvert 1996; Groome et al. 2003) rather than a collisional event, although some use these terms interchangeably (e.g. Wells et al. 2014), because it occurred along a continental margin, resulted in growth of an accretionary wedge and continued subduction by stepping back behind the accreted terrane.

Temporal evolution and lateral differences can also play significant roles in the distinction between accretion and collision, which is illustrated in the following thought experiment. The Himalayan mountain belt is generally considered as the type example of a collisional orogen that formed following the closure of the Neotethys Ocean and ongoing India–Eurasia collision (Fig. 1D). However, there is still ongoing subduction of the Indian Ocean beneath the Makran arc to the west and the Sunda arc to the southeast (Fig. 1D). Hence, continental collision occurred only along a relatively short segment of the Neotethys Ocean between India and Eurasia, whereas accretion is ongoing in the adjacent Makran and Sunda accretionary prisms. The India–Eurasia collision generated large intraplate compressive stresses within the subducting Indian plate, which are transferred southwards into the oceanic lithosphere south of India where they are causing large scale buckling and crustal-scale thrust faulting (Fig. 1D; e.g. Beekman et al. 1996). Continued convergence may result in either lateral propagation of the Makran subduction zone along the continental margin of western India or initiation of new subduction south of India along one of the crust-penetrating thrust faults in the deformed oceanic lithosphere along this nascent plate boundary (Coudurier-Curveur et al. 2020). If this occurs, the Himalayan orogenic belt could be viewed as part of an accretionary rather than a collisional orogenic system, albeit one that accreted continental scale, cratonized terranes.

In terms of the process itself, there is no concrete distinction between processes of subduction-induced accretion and collision and hence, these two terms can be used interchangeably. Both of these processes refer to amalgamation of terranes and/or continents following the subduction of the intervening oceanic lithosphere.

Constraining Collision/Accretion Events

The onset of collision or accretion of a continent, an arc or an oceanic plateau to another tectonic element is commonly difficult to constrain and may vary among collision zones. The initiation of collision or accretion occurs when the two converging terranes and/or continents make first contact and the leading edge of the terrane or continent on the downgoing plate enters the foredeep (trench; Fig. 2A). This foredeep, situated between the upper and lower plates, evolves into a foreland basin as tectonic loading leads to flexural subsidence of the leading edge of the underthrust terrane (Fig. 2B). In some collision zones, strong coupling between the forearc and the subducting plate leads to forearc subduction (see following). In these cases, the forearc will experience a similar syn-collisional history to the underthrust terrane.

The onset of collision can result in a number of changes in the upper and lower plates including continental contamination and cessation of arc magmatism (e.g. Huang et al. 2006; Harris 2011), uplift of the upper plate and/or accretionary prism (e.g. Dorsey 1992; Soh et al. 1998; Liu et al. 2001; Lin et al. 2003; Huang et al. 2008), development of fold and thrust belt (Byrne et al. 2011) and flexural subsidence of the lower plate (e.g. Saqab et al. 2017). Continental contamination and/or cessation of arc magmatism (e.g. Huang et al. 2006) are not always a reliable indicator for the onset of collision because arc magmatism may continue for some time and there may be only a short time gap between arc and post-collisional magmatism (Mann and Taira 2004; Harris 2011). Similarly, the record of uplift is typically incomplete and preferentially records the final stages (Soh et al. 1998; Byrne et al. 2011). The deformation record also may be incomplete, lithology-dependent and is commonly difficult to date.

In contrast, the stratigraphy, provenance, and deformation of the syn-collisional foreland and forearc basins can provide some of the best constraints on the initiation of the collision and the evolution of the growing orogen. Foreland basins have an excellent preservation potential and initiate by rapid subsidence of the downgoing plate (Soh et al. 1998; Byrne et al. 2011; Saqab et al. 2017). As the collision progresses, the syn-collisional basins receive detritus from the emerging orogen, starting with uplift and exhumation of the accretionary prism (sedimentary provenance), progressing to the arc upper crust (volcanic and/or ophiolitic provenance), arc middle crust (plutonic provenance), and deeply exhumed orogen (metamorphic provenance). This sedimentary provenance progression provides a detailed record of exhumation of the mountain belt (e.g. Stevens 1970; Nelson and Casey 1979; Dewey and Mange 1999; Huang et al. 2006; Waldron et al. 2012). Careful analysis of the syn-collisional basins therefore is an important tool in orogenic research.

Collisional Styles

The modifiers 'soft and hard' are commonly used qualitatively with respect to collisions in orogenic research by tectonicists outside of the Americas (e.g. Pubellier et al. 1991; Mann and Taira 2004; Matte 2006; Brown 2009; Burg and Bouilhol 2019) with a few exceptions in the Americas (e.g. Zagorevski and van Staal 2011; Iturralde-Vinent et al. 2016). These modifiers have not been defined or described in detail by anybody as far as we know, although attempts have been made (Zagorevski and van Staal 2011). John Dewey introduced these terms in 1996 to the first author who was a visiting scientist in Oxford at the time. Although Dewey never explicitly explained what he meant with these modifiers, it was obvious that he referred to the scale of the structural 'damage' done to the colliding elements, not the rheology of the rocks. 'Soft' referred to collisions where the deformation was relatively light and localized mainly in rocks of the lower plate, and at least in part occurred below sea level. In contrast, hard collisions implied intense penetrative deformation in wide cross-sections of both the lower and upper plates caught up in the damage zone, while the progressively emerging mountains supplied ample sediment to the

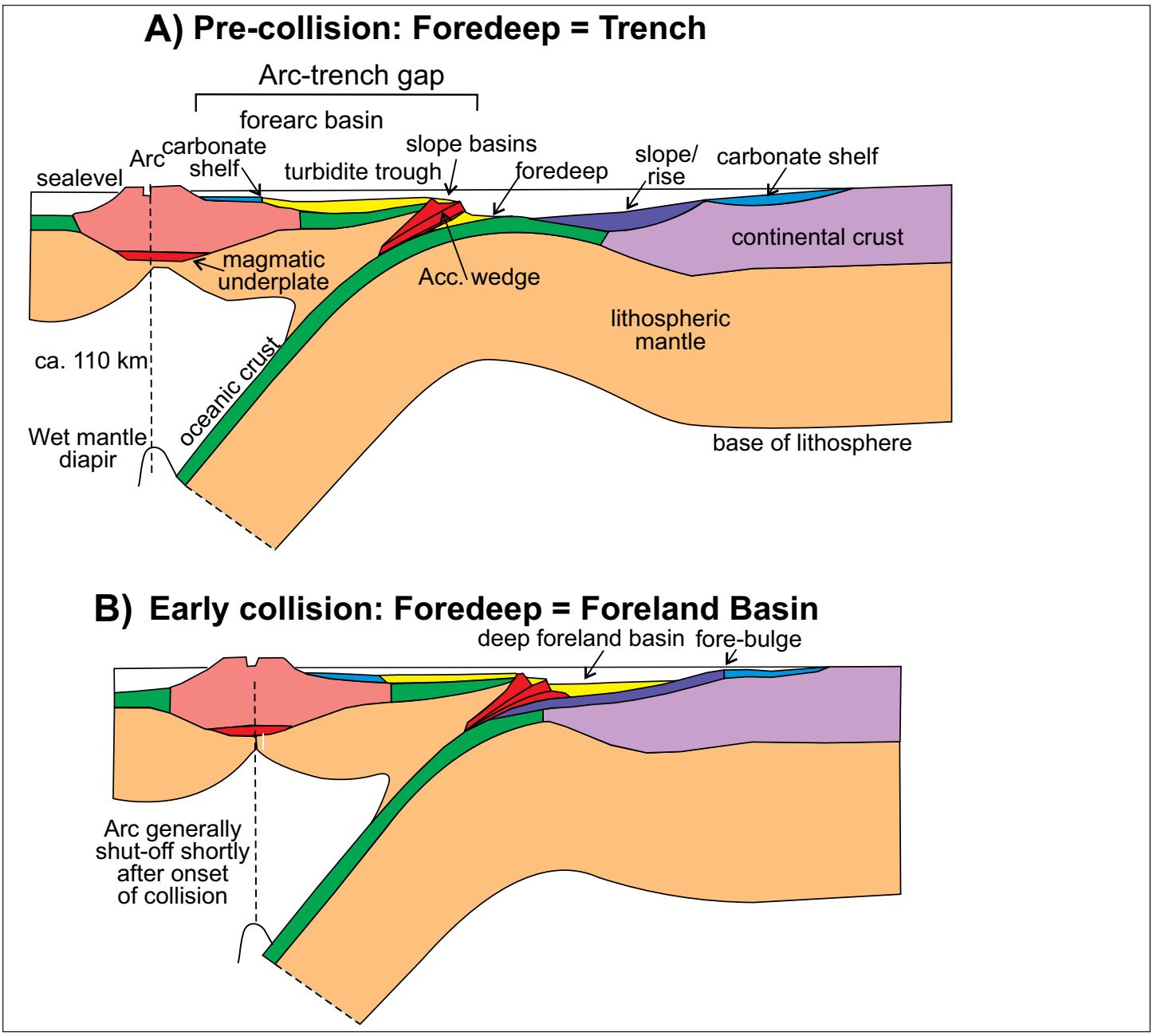

Figure 2. Diagrams showing the tectonic elements usually involved in an arc–continent collision. Collision starts when the leading edge of the approaching continent enters the trench and starts being pulled down beneath the upper plate forearc. At this stage, the foredeep (trench) becomes a foreland basin.

adjacent syn-tectonic basins (e.g. Dewey and Ryan 2016; Ryan and Dewey 2019). This qualitative definition implies that a soft collision could change into a hard collision over time. A collision could remain soft when it is rapidly (< 10 m.y.) followed by subduction step-back and/or subduction polarity reversal, releasing the compressive stresses generated in the collision zone and transferring convergence to a new outboard subduction zone (Dewey 2005). On the other hand, a collision could become 'hard' due to the entrance of progressively more buoyant crust, slowing down of convergence, and increasing coupling and compression between the plates, resulting in widening of the collisional damage zone into the overriding plate (Boutelier and Chemenda 2011; Willingshofer et al. 2013).

The use of soft and hard collision, however, varies somewhat among tectonicists. For example, Matte's (2006) use of 'soft' in his interpretation of the southern Urals was largely based on the absence or low degree of tectonometamorphism of the volcanic and sedimentary rocks of the Magnitogorsk arc and arc-adjacent basins. In contrast, Ryan and Dewey (2019) linked soft collision to the stage when the Grampian orogen in Ireland was still largely below sea level as a result of subduction of a hyperextended margin (Dewey and Ryan 2016), although this model also implies that the upper plate arc

https://doi.org/10.12789/geocanj.2020.47.161

terrane was not shortened, internally deformed and thickened at this stage. The degree and nature of the internal shortening, imbrication and burial metamorphism of the upper plate supracrustal rocks of the arc and immediately adjacent basins are thus a potential parameter that can aid in the separation of soft and hard collisions (Zagorevski and van Staal 2011).

Soft Collisions

A review of recent arc–continent collisions (see below), indicates that the early stages of a collision generally localize deformation into the supracrustal rocks of the downgoing plate and overlying, onlapping foreland basin. Together with a pre-collisional accretionary prism, if present, these rocks commonly become imbricated and folded (e.g. Saqab et al. 2017) forming the initial collisional orogenic wedge. Mélanges are common and part of the upper plate forearc terrane, including the accretionary prism, may become (re)deformed internally as a result of a growing and readjusting orogenic wedge (e.g. Westbrook 1982; Harris 2011). The suprastructure of the arc may be faulted and rifted during this stage, but as a rule, the arc is not internally shortened and thickened significantly by imbrication and/or folding. Hence, it is not metamorphosed by structural burial. In our opinion, this tectonic stage best describes a soft collision. Soft collisions are well represented in the recent geological record including segments of the Luzon arc–South China (Huang et al. 2006), Banda arc–Australia (Harris 2011), and Semail ophiolite–Arabian margin collisions (Searle and Cox 1999) as well as others, such as the Melanesian arc–Ontong Java plateau (Mann and Taira 2004), the Honshu arc–Izu-Bonin–Mariana arc (Soh et al. 1998) and Sanghile arc–Halmahera arc collisions (Pubellier et al. 1991).

The Luzon arc–South China collision (Fig. 3A) represents a transition from soft to early stages of a hard collision. This ongoing collision is propagating southward into the South China Sea but is complete in the north. In southern Taiwan, the collision is still in its early stages, parts of the forearc are preserved and there is little or no internal deformation of the Luzon arc suprastructure. The early stage collision in southern Taiwan thus could be described as soft. The initial stages of collision are dated at ca. 6 Ma, largely based on the arrival of non-volcanogenic quartz-rich turbidites derived from the uplifted and exhumed accretionary prism in the forearc and the oldest foreland basin sediments deposited on the passive margin of South China (Huang et al. 2006; Byrne et al. 2011 and references therein).

The more advanced stage collision in central Taiwan is characterized by local deformation of the arc volcanic rocks adjacent to the orogenic wedge and thus represents the start of a transition to a hard collision, although the Luzon arc is not yet pervasively deformed or metamorphosed due to structural burial. Large parts of the forearc were subducted and deformed during this stage of the collision (Tang and Chemenda 2000; McIntosh et al. 2005; Malavieille and Trullenque 2009) and the arc suprastructure became the immediate hanging wall to the orogenic wedge in central Taiwan (Byrne et al. 2011). Parts of the subduction complex (Yuli belt) are being actively exhumed in the footwall of the steeply east-dipping Longitudinal Valley fault system (Brown et al. 2015), which represents the suture between the accreted Luzon arc and the South China margin.

The south-facing Banda/Sunda arc–Australia collision (Fig. 3B) is another young (< 8 Ma) example of a diachronous collision that has reached a relatively mature stage at the longitude of Timor but has not yet taken place farther to the west where oceanic subduction is still ongoing in the Sunda trench (Harris 2011). Continuing convergence in the Banda collision zone is in part taken up by the south-dipping Wetar and Flores thrusts in the Banda Sea, which could be viewed as the initiation of a subduction polarity reversal (Silver et al. 1983; Price and Audley-Charles 1987; Hamilton 1988; Supendi et al. 2020). The Banda collision mainly involved highly deformed (imbricated) and uplifted rocks of the underthrusted Australian margin, structurally overlain respectively by tectonic mélange and a large nappe derived from the Banda forearc (Banda terrane of Harris 2011). Rutherford et al. (2001) proposed that the Banda arc–Australia collision started as early as ca. 16 Ma to explain the westward escape of the Sumba forearc block, but this is inconsistent with the stratigraphic evidence from the foreland and forearc basins. Flexural uplift of the Australian margin and analysis of the foreland basin suggest that underthrusting of the leading edge of the Australian margin beneath the Banda arc–Australia collision started at ca. 6 Ma (Saqab et al. 2017), which would equate with the onset of the soft collision stage. Harris (2011) put the onset of collision slightly earlier ca. 8 Ma), based on the age of the youngest passive margin rocks incorporated in the accretionary wedge, but neither analysis supports an older collision onset as proposed by Rutherford et al. (2001). In addition, contamination of Banda arc volcanic rocks by continental crust took place no earlier than ca. 5 Ma (Harris 2011), which also supports a Late Neogene onset of collision. Volcanism persisted until ca. 2.5–1.3 Ma. Hence, arc volcanism, unlike Taiwan, continued for some time during the advancing collision. Gravity modelling and tomography suggest that part of the forearc was subducted with the Australian lower plate (Harris 2011; Supendi et al. 2020), similar to central Taiwan, whereas part of the arc complex may have been translated to the north, suggesting that the advanced collisional stage in Timor, like in central Taiwan, records a transition from soft to hard collision.

Obduction of the relatively intact suprasubduction zone Semail ophiolite (Fig. 4) can be viewed as a Late Cretaceous collision between the infant oceanic Lasail arc and the Arabian margin (Pearce et al. 1981; Searle and Cox 1999). The onset of collision is constrained by the late Coniacian–Campanian sedimentation in the foreland basin recording underthrusting of the leading edge of the Arabian margin beneath the ophiolite (Robertson 1987). Subduction- and exhumation-related penetrative deformation and burial metamorphism are principally localized in rocks that form part of the downgoing Arabian margin. There are narrow obduction-related shear zones and serpentinite mélanges at the base of the ophiolite which is locally also imbricated and broken up in fault-bounded blocks (Searle and Cox 1999), but penetrative internal deformation and metamorphism related to overthrusting and regional

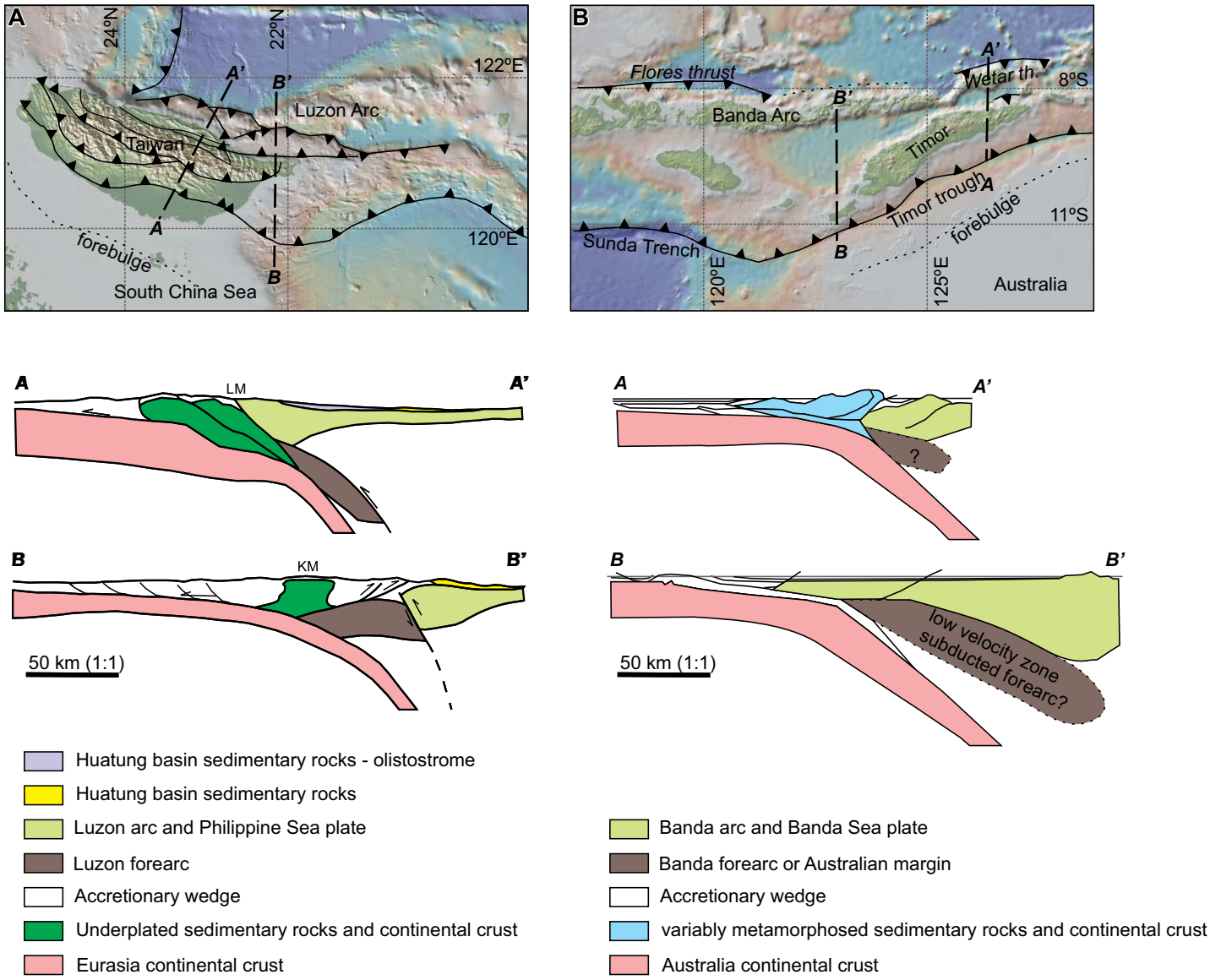

Figure 3. Maps and cross-sections showing the tectonic setting of (A) the China–Luzon arc (modified after McIntosh et al. 2005; LM – Lichi Mélange; KM – Kenting Mélange), and (B) Australia–Banda arc collisions (near surface simplified from Harris 2011, deep crust and mantle modified from Supendi et al. 2020). Background images and some plate boundaries were generated from www.geomapapp.org.

shortening is largely absent in the ophiolite. This collision thus never went beyond the soft collision stage.

Hard Collision

Orogenic belts where lower plate, forearc and significant parts of the upper plate arc and/or retro-arc hinterland are deformed and incorporated into the collisional orogenic wedge are characteristic of hard collisions. Most old orogenic belts on Earth preserve segments that have characteristics of hard collisions. This is not simply a product of deeper level of erosion, as the metamorphic histories of these orogens indicate significant thickening of the upper plate. The Scandian Caledonides in Greenland and Baltica are a good example of a hard collision that resulted in a bivergent orogenic wedge. The pro-wedge preserves Taconic deformed rocks and upper plate arc rocks in the highest east-directed nappes in western Norway (Roberts et al. 2007, 2019), whereas west-directed nappes of the retro-wedge occur in eastern Greenland (Higgins et al. 2004). The nappe stack in the Swiss–Italian Alps comprises penetratively deformed and metamorphosed rocks of both the lower European as well as the upper Adrian plates, elegantly illustrated and described in the kinematic-geometric evolutionary reconstructions made by Escher and Beaumont (1997). The geometry of the orogen with the main detachments nucleating along the interface between upper and lower crust implies a degree of decoupling of the shallow/middle crust from the lower crust and lithospheric mantle (Schmid et al. 1996). Rocks of the upper Adrian plate were also pulled down and incorporated into the evolving nappe stack, recording widening of the deformation channel into the hanging wall of the subduction zone, which was not associated with an arc. The Alps is one of the few orogens where no arc formed dur-

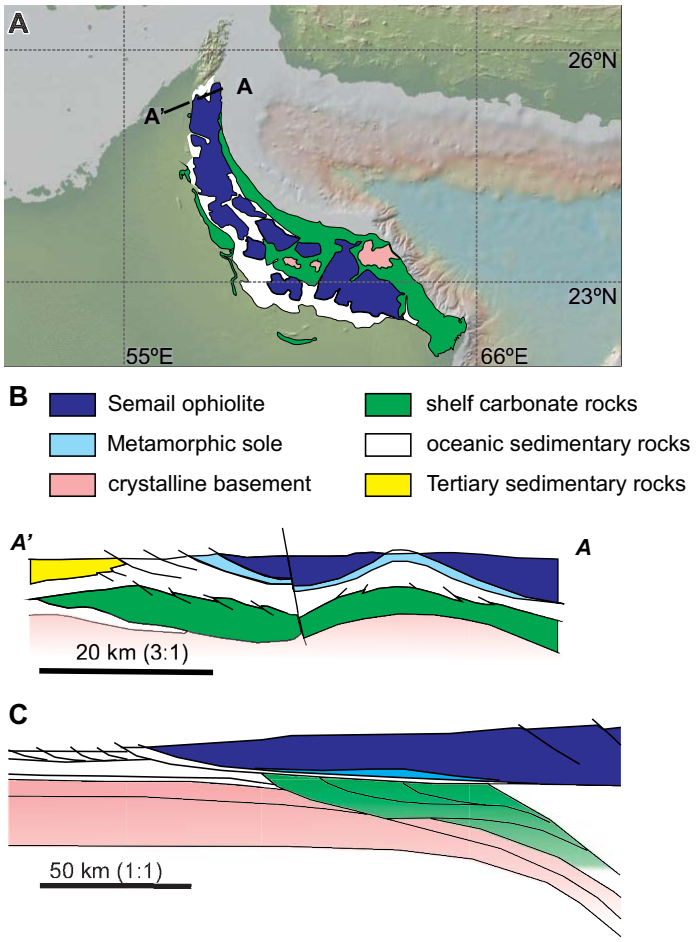

Figure 4. Simplified geological map (A) and a cross-section (B) of the Semail ophiolite and structurally underlying rocks of the Arabian margin. (C) Tectonic model of the Upper Cretaceous obduction the Semail ophiolite. Modified from Searle and Cox (1999). Background image in (A) was generated from www.geomapapp.org.

ing the slow subduction that consumed the narrow Piedmont Ocean (Schmid et al. 1996).

The Himalayan mountain belt is commonly considered as the type example of a collisional orogen (Fig. 1D; Cawood et al. 2009). Like the Alps, the geometry of the Himalaya suggests decoupling of the crust, although there is no incorporation of Eurasian upper plate rocks in the asymmetric orogenic thrust wedge, made up solely of Indian plate rocks. Nevertheless, the various phases of Paleogene–Neogene shortening, which produced foreland- and hinterland-directed thrusting in the upper plate terranes of Tibet (e.g. Lhasa and Qiangtang terranes) that can be linked mechanically to deformation in the south-directed Himalayan thrust belt formed in Indian rocks, conform to the characteristics of a hard collision. However, the gravitational potential energy stored in the thickened crust and resultant body forces in highly elevated parts of southern Tibet formed during the earlier Late Cretaceous–Paleogene collision between the Lhasa and Qiantang terranes, may have inhibited penetrative upper crustal shortening in favour of deformation localized at lower elevations in northern Tibet (e.g. Kapp et al. 2007 and references therein).

Distinction between Soft and Hard Collisions and their Relationship to Accretionary and Collisional Orogens

There are many factors that influence the tectonic style of a collision, but detailed studies of many old and young orogenic belts reveal that a distinction between soft and hard collisions are best made on the nature and tectonometamorphic characteristics of the arc and its upper plate hinterland. Soft collisions are those where the overriding arc and retro-arc hinterland were not significantly shortened and/or penetratively deformed and metamorphosed. Penetrative deformation is basically restricted to the downgoing plate and parts of the forearc of the upper plate, suggesting limited coupling between the upper and lower plates (Willingshofer et al. 2013).

Most hard collisions were preceded by a soft collisional stage(s), because closing oceans commonly contain various isolated buoyant terranes that will accrete to the upper plate before terminal closure. Strong overprint by structures related to the final hard collision may destroy evidence for earlier soft collisional stages. Hence, accretionary orogens are expected to contain the best-preserved remnants of soft or transitional collisions. Several young arc–continent collisions studied in detail, such as Taiwan and Banda, show a transitional character and preserve evidence for subduction of significant parts of the forearc beneath the arc (Fig. 3). Subduction of the forearc may be common in arc–continent collisions. Forearc subduction may explain the absence of well-preserved forearc terranes in accretionary orogens mainly formed by arc accretions (e.g. Zagorevski and van Staal 2011). In contrast, obduction of forearc and trailing arcs such as the Semail ophiolite, may occur if these are thermally immature, extensional, and hence thin (Ryan and Dewey 2019), and the downgoing margin is thin and hyperextended (Reston and Manatschal 2011). Narrower, less extended rifted margins may choke subduction early and instead cause enhanced structural thickening of the margin by inversion of the older, rift-related structures (Reston and Manatschal 2011). In general, hyperextended margins may promote development and preservation of a soft collisional stage preceding the terminal hard collision such as in the Alps and parts of the Taconic–Grampian orogen, because they may be less buoyant than normal continental lithosphere and hence are more easily pulled down and steepen the subduction zone, favouring less coupling with the overriding plate. However, the relative buoyancy of the hyperextended margin is dependent on the degree of serpentinization of the exhumed mantle and volume of mafic magmatism erupted during rifting. It is the leading edge of the downgoing hyperextended margin that is favoured to be pulled down to eclogite-facies depths and to form a complex imbricate stack of high-pressure metamorphic nappes, easily mistaken as a mélange (Beltrando et al. 2010). A hyperextended margin with a thick sequence of rift-related sedimentary rocks on the downgoing plate, on the other hand, may cause thermal blanketing, which will reduce the overall strength of the lithosphere (Reston and Manatschal 2011) and promote thickening and more distributed deformation of the crust in the downgoing plate and increased coupling with the overriding plate.

Structural thickening of the arc and/or retro-arc hinterland typify hard collisions, although such a tectonic style can also form during flat-slab subduction and/or where the upper plate and its arc advances towards the trench, such as in the Andes (Dewey 1980). Andean-style orogenic belts caught up later in a subsequent terminal collisional orogen, may therefore be difficult to separate from the later collision-related structures without careful combined structural and geochronological studies.

Mechanical Control on Orogenic Architecture

Physical analogue and numerical thermo-mechanical models (Willingshofer et al. 2013; Vogt et al. 2017) provide important insights into what controls the distribution of strain during subduction and collision, and its outward propagation from the lower plate into the upper plate (e.g. retro-wedge development); hence, what promotes soft versus hard collisions. Low plate coupling and decoupling between a strong lower and weaker upper continental crust on the downgoing plate, cold initial geotherms and high convergence rates promote formation of highly asymmetric, wide orogens and strain localization in the upper crust of the downgoing plate close to the contact with the upper plate during collision. A foreland-propagating fold and thrust belt forms in the weak upper crust of the lower plate, while the stronger lower crust subducts with the underlying lithospheric mantle (Vogt et al. 2017). Deformation in the overriding plate tends to be minimal and only a weak retro-wedge may develop, if at all (Willingshofer et al. 2013), which corresponds with the orogenic architecture produced by a soft or a transitional collision described above in young arc–continent collisions in southeast Asia (Figs. 1A–C, 3, 4). Hard collisions form where plate coupling between the plates, and the lower and upper crust of the lower plate, become stronger due to a reduced strength contrast and higher geotherms, which both may promote outward propagation of the deformation into the upper plate and formation of doubly vergent orogenic wedges. Slowing down of convergence, relaxation of geotherms and progressive thermal weakening of the orogenic wedge as a result of an ongoing prolonged collision thus could drive an early soft collisional stage to a terminal hard collision. Only short-duration collisions (< 10 m.y.), where convergence-related shortening is terminated due to a subduction polarity reversal or step-back, are settings where a hard stage may not develop.

Application of Soft/Hard Terminology in Orogenic Analysis

The 'soft versus hard' terminology has rarely been used in orogenic studies in the Americas, but can be used as a tool to identify displaced terranes in orogenic reconstructions. This utility is illustrated by the Taconic Appalachians in western Newfoundland (Fig. 5). The Taconic–Grampian orogen in the Appalachian–Caledonian mountain belt records a complex Ordovician collision between Laurentia and an outboard northwest-facing arc with its associated suprasubduction zone (SSZ) ophiolites (van Staal et al. 2007). The collision displays marked changes in tectonic style and architecture along its length (e.g. Ryan and Dewey 2019). Some segments solely preserve evidence of a soft collision, whereas others have characteristics of an earlier soft stage that is overprinted by a hard collision (van Staal et al. 1998, 2009; Dewey and Ryan 2016).

In the Canadian Appalachians, the sediment-dominated Humber margin (Fig. 5 inset) facilitated Mid Ordovician obduction of thin, young SSZ ophiolite sheets in western Newfoundland (e.g. Bay of Islands ophiolite, Cawood and Suhr 1993; Waldron and van Staal 2001) and southern Quebec (e.g. Thetford Mines ophiolite, Tremblay and Pinet 2016). This collision did not result in penetrative contractional deformation and burial metamorphism of the obducted SSZ ophiolites (Suhr and Cawood 1993). Deformation was largely restricted to the ophiolitic sole and underthrusted Humber margin strata that formed thrust sheets, mélanges and folds (e.g. Waldron et al. 2003; Pinet 2013). Metamorphism of the underthrusted Humber margin rocks was mainly low grade, and generally did not exceed greenschist facies (e.g. Castonguay et al. 2001, 2007). The Fleur de Lys Supergroup metasedimentary rocks that were deposited near the leading edge of the Humber margin are preserved in the Corner Brook Lake block (Fig. 5) and record higher grade amphibolite-facies metamorphism that was previously thought to represent Taconic tectonism. However, dating of this Barrovian metamorphism consistently showed it to be Silurian (Salinic) and younger (Cawood et al. 1994; Lin et al. 2013), hence Taconic metamorphism must have been low grade along this part of the margin, consistent with a soft collision. Localization of deformation and low grade metamorphism of the underthrusted sedimentary rocks of the pulled down continental margin, combined with the lack of penetrative deformation of the obducted SSZ ophiolites are hallmarks of a soft collision, analogous to the lack of obduction-related internal deformation of the Semail ophiolite in Oman (Pinet and Tremblay 1995).

The evidence of a soft Taconic collision in western Newfoundland and Quebec is distinctly different from the adjacent Dashwoods block (Fig. 5). The Dashwoods block is a composite terrane, comprising: (i) the Mid to Late Cambrian (509–495 Ma) Lushs Bight oceanic tract (LBOT), which is dominated by island arc tholeiitic mafic rocks and probably represent an arc ophiolite (Swinden et al. 1997), (ii) the Early to Mid Ordovician magmatic and epiclastic rocks of the ensialic first phase of the Notre Dame arc (e.g. ca. 478 Ma Brighton gabbro, Fig. 5), which intruded the LBOT (van Staal et al. 2007), and (iii) a large volume of strongly metamorphosed and deformed sedimentary rocks of various ages, into which the Early Ordovician arc plutons intruded into the oldest part (van Staal et al. 2007). The Dashwoods block is separated from the adjacent Laurentian margin by a highly attenuated narrow belt of late Cambrian (ca. 490 Ma) SSZ ophiolites of the Baie Verte oceanic tract (BVOT), such as the Advocate complex in Baie Verte Peninsula (Fig. 5, van Staal et al. 2009; Skulski et al. 2010). This tectonic boundary is generally referred to as the Baie Verte–Brompton Line (BBL), which coincides with the Cabot Fault in central and southern Newfoundland (Fig. 5). The Dashwoods block and its entrained slivers of LBOT (Fig. 5) record polyphase Taconic deformation and Barrovian metamorphism, locally up to granulite facies (Lissenberg et al. 2006;

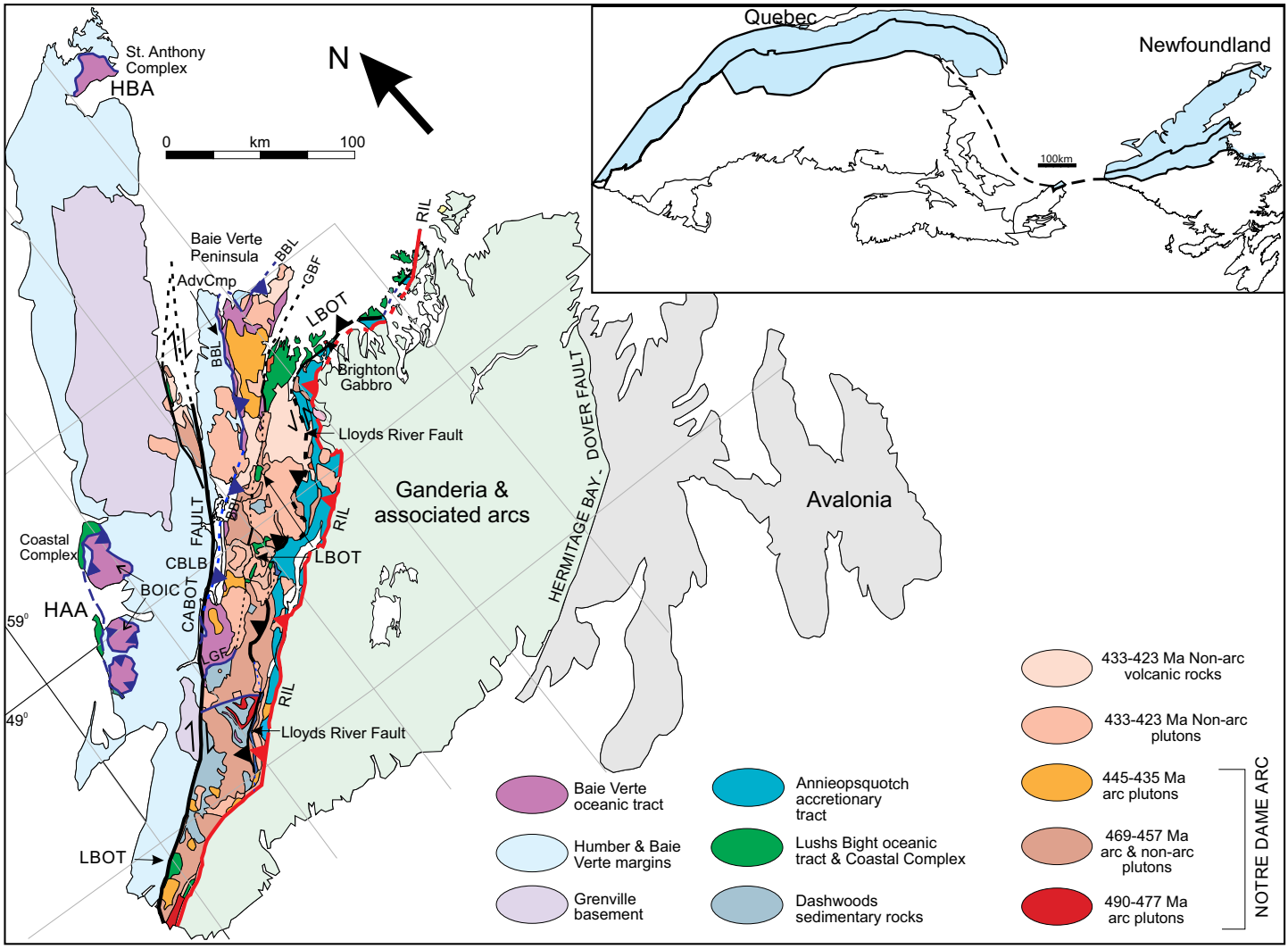

Figure 5. Geology of the Laurentian Humber and Baie Verte margins, and juxtaposed Dashwoods block (modified from van Staal et al. 2007). Note that the Lushs Bight oceanic tract (LBOT) continues as a trail of small blocks and slivers engulfed and/or surrounded by a sea of granitoid rocks (mainly tonalite and quartz diorite) of the Notre Dame arc all the way to its southern extension. Inset shows rocks of the Laurentian margin and associated offshore pericratonic terranes involved in the Taconic orogeny in Newfoundland and southern Quebec. AdvCmp – Advocate Ophiolite Complex;; BBL – Baie Verte–Brompton Line; BOIC – Bay of Island Ophiolite Complex; CBLB – Corner Brook Lake block; GBF – Green Bay fault; HAA – Humber Arm allochthon; HBA – Hare Bay allochthon; LGF Little Grand Lake Fault; LBOT – Lushs Bight oceanic tract; RIL – Red Indian Line.

van Staal et al. 2007). In contrast to the Corner Brook Lake block, the Laurentian Fleur de Lys Supergroup metamorphic tectonites on the Baie Verte Peninsula between the Cabot Fault and the irregular and curving belt of tectonized BVOT ophiolitic slivers (Fig. 4) record Taconic tectonometamorphism, including formation of eclogite, ranging in age between 483 and 460 Ma (Castonguay et al. 2014; de Wit and Armstrong 2014).

The marked contrast in tectonic style suggests the Dashwoods block and the Baie Verte Peninsula were moved from a site where the Taconic arc–Laurentia collision was hard and emplaced into their current position by strike-slip translation along the steeply dipping Cabot Fault and Baie Verte–Brompton Line system (Fig. 6). The lithosphere-cutting Cabot Fault–Baie Verte Line system (van der Velden et al. 2004) accommodated ca. 250 km of dextral displacements during the Late Paleozoic (Waldron et al. 2015) and older, poorly constrained transcurrent movements since the Middle Ordovician (Brem et al. 2007; Lin et al. 2013). The Dashwoods block and the Baie Verte Peninsula thus originated somewhere to the north of Newfoundland (Fig. 6). The site where Dashwoods collided with Laurentia, herein referred to as the Baie Verte margin, is now largely situated below sea level somewhere north of Newfoundland and so cannot be directly investigated.

The Taconic collision displays significant diachroneity along the Baie Verte and Humber margins (Fig. 6). It started between 488 and 480 Ma in the Baie Verte Peninsula and Dashwoods, based on the ages of arc magmatic rocks contaminated by continental crust, metamorphism and the Laurentian provenance of detrital zircon occurring in the Floian Kidney Pond conglomerate near the base of the Snooks Arm Group (van Staal et al. 2007, 2009, 2013; Skulski et al. 2010; Castonguay et al. 2014; de Wit and Armstrong 2014; Willner et al. 2014), at ca. 470 Ma in central Newfoundland (Waldron and

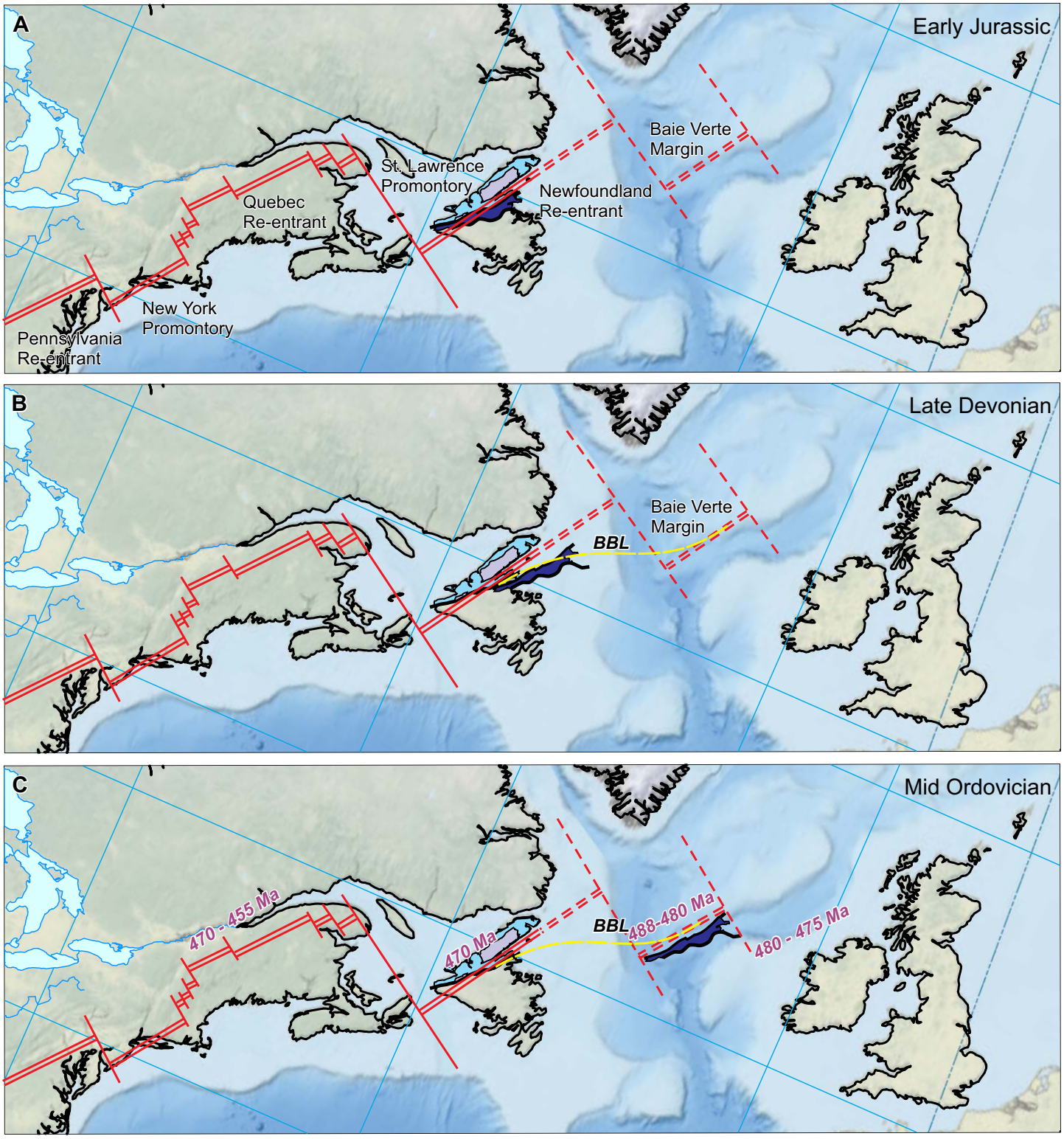

Figure 6. Superimposition of the promontories and re-entrants of Thomas (2005) and the inferred Paleozoic translations of Dashwoods on a landmass reconstruction of the Appalachian–Caledonide connection between Newfoundland and British Isles before Mesozoic opening of the North Atlantic Ocean. North Atlantic restoration includes de-stretching of areas which were subjected to significant stretching and gives an outline of shelf and deeper off-shelf areas. Restoration is based on the reconstruction of Verhoef and Roest (1993). The dashed promontory–re-entrant configuration in the North Atlantic is inspired by the pre-opening bathymetry Late Devonian position of Dashwoods, based on Waldron et al. (2015). BBL – Baie Verte–Brompton Line with its postulated trace across the pre-Atlantic opening restoration to connect with the Clew Bay suture in the west of Ireland. Ages of diachronous Taconic–Grampian arc–continent collision are indicated in (C).

https://doi.org/10.12789/geocanj.2020.47.161

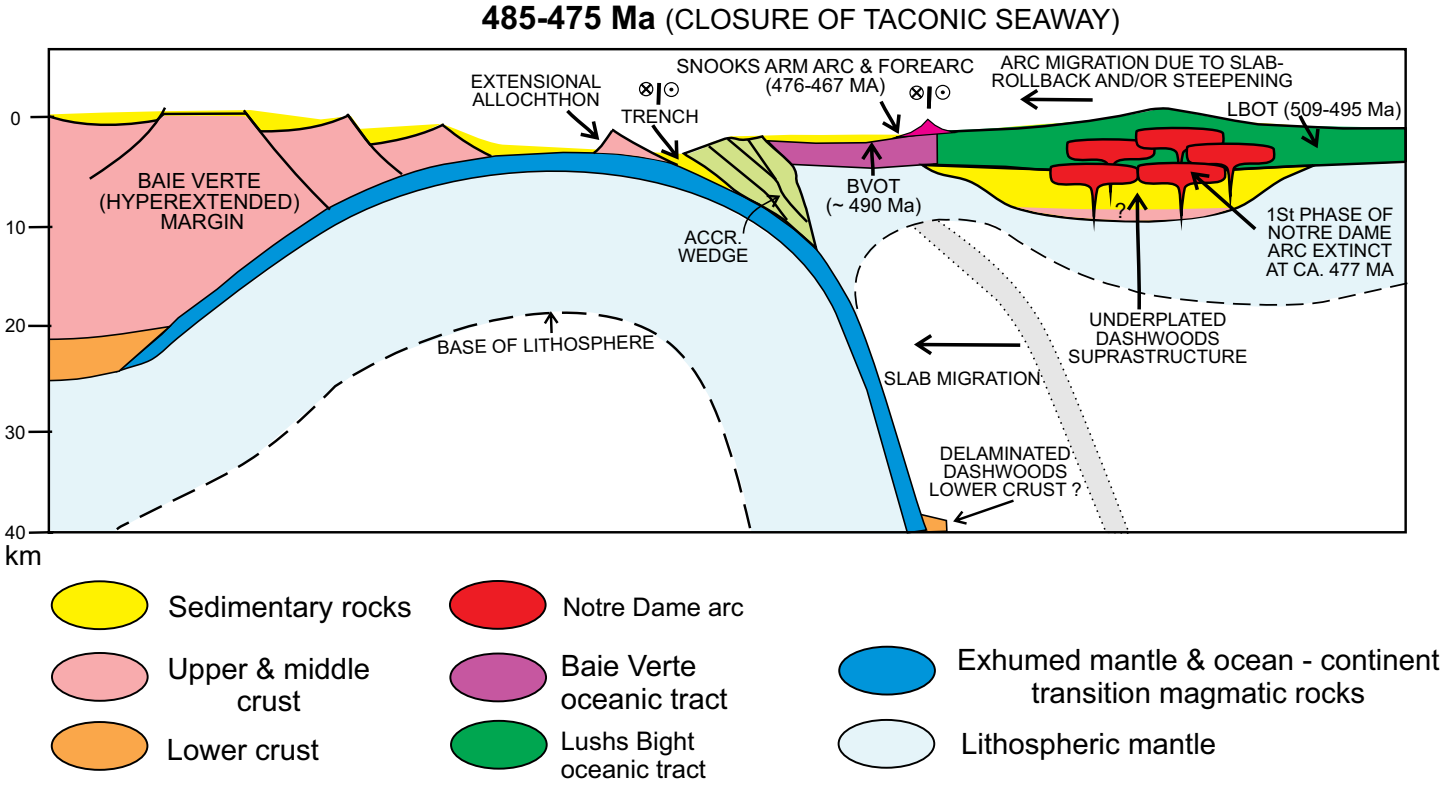

Figure 7. Closure of the Taconic seaway after Dashwoods suprastructure has been underplated to part of the Mid–Late Cambrian Lushs Bight oceanic tract (LBOT) with its lower crust (if there was any) delaminated and pulled down with the subducting plate, which in the Taconic seaway mainly comprised exhumed mantle and mafic magmatic rocks formed during hyperextension (ocean–continent transition). The Coastal Complex in Figure 5 is probably an oceanic arc correlative of the LBOT (van Staal et al. 2007), but never experienced underthrusting by Dashwoods at the latitude it formed; it has a non-exotic, relationship with the BOIC (Cawood and Suhr 1992; Suhr and Cawood 1993). Slab rollback and/or steepening of the subduction zone caused arc migration shortly after the leading edge of the hyperextended Baie Verte margin entered the trench. Figure modified from van Staal et al. (2013).

van Staal 2001) and between 470 and 455 Ma in the Quebec re-entrant (Tremblay and Pinet 2016; White et al. 2020). The hard Taconic collision preserved in the Dashwoods block occurred shortly after an earlier, Late Cambrian–Tremadocian impingement of the LBOT arc with a sediment-rich microcontinent (Dashwoods of Waldron and van Staal 2001) or isolated continental horst (Fig. 7), immediately outboard of a wide promontory in the hyperextended Baie Verte margin (van Staal et al. 2013). Evidence of this initial collision is indicated by crustal contamination of arc magmatism (Swinden et al. 1997; van Staal et al. 2007), and formation of mélanges and shear zones in the LBOT (Taconic 1 of van Staal et al. 2007). The created composite Dashwoods block and the Baie Verte margin remained separated by the Taconic seaway (Fig. 7), which was partly floored by exhumed mantle and transitional oceanic crust, but locally possibly also by highly extended continental crust, forming isolated extensional allochthons (van Staal et al. 2013).

Normal B-subduction of Iapetus lithosphere continued in the adjacent re-entrant and farther to the southwest (present coordinates) (Fig. 6). The absence of obstructing microcontinents in the re-entrants (van Staal et al. 2007) allowed SSZ ophiolite obduction (e.g. Bay of Islands ophiolite and associated Coastal Complex, Newfoundland and Thetford Mines ophiolite, Quebec) onto the narrower Humber margin during the Middle Ordovician. The continued dextral oblique convergence closed the Taconic seaway by subduction and protracted underthrusting of the thin hyperextended Baie Verte margin beneath the Dashwoods block, which culminated in an Early–Mid Ordovician hard collision and Barrovian tectonometamorphism in the upper plate Dashwoods block, including the associated BVOT. In addition, the remnants of a syn-collisional forearc basin developed above part of the BVOT and LBOT are preserved in parts of the Floian–Dapingian Snooks Arm Group and correlatives (Fig. 7; Skulski et al. 2010; van Staal et al. 2013; Castonguay et al. 2014); Snooks Arm augite-phyric diabase intruded into greenschist-facies mafic tectonites of the LBOT (Fig. 8) near Jackson's Cove, Springdale Peninsula, indicating that the LBOT and BVOT are tectonically related and both tied to Dashwoods (Fig. 7). The eastern structural boundary of the Dashwoods block (Lloyds River fault zone) accommodated Early to Mid Ordovician sinistral transpression (Lissenberg et al. 2005; Lissenberg and van Staal 2006; Zagorevski et al. 2007). Hence, the Taconic hard collision led to Mid Ordovician tectonic escape of the Dashwoods block to the southwest, towards Newfoundland.

The most proximal, correlative hard arc–Laurentia collision to northwestern Newfoundland is represented by the Grampian orogen in Ireland. The Grampian tectonites in Connemara and Tyrone resemble those in Dashwoods and the Baie

Figure 8. Undeformed and unmetamorphosed augite-phyric diabase typical of the Snooks Arm Group intruding deformed and metamorphosed Lushs Bight oceanic tract mafic rocks, close to autochthonous outcrops of the Snooks Arm Group on a peninsula immediately northwest of Jackson's Cove, Springdale peninsula, Newfoundland. Blake Hodgin for scale.

Verte Peninsula in many respects (van Staal et al. 1998). Both segments record collision with a hyperextended part of the Laurentian margin (Chew and van Staal 2014), preserve evidence of peri-Laurentian microcontinents (e.g. Waldron and van Staal 2001; Cooper et al. 2011) and have a similar Late Cambrian–Early Ordovician timing for the onset of collision, deformation and Barrovian metamorphism (Chew et al. 2010; Cooper et al. 2011; Dewey and Ryan 2016). Both areas represent a segment of the Laurentian margin with a distinct lithospheric architecture that promoted formation of sizeable syn-collisional forearc basins (e.g. South Mayo trough), but which prevented development of a notable foreland basin on the tectonically loaded margin (Dewey and Ryan 2016; Ryan and Dewey 2019). Collision between the wide hyperextended segment of the Laurentian margin in Ireland and its extension to the north of Newfoundland (Baie Verte margin) with an outboard microcontinent or isolated horst at its leading edge, and the Grampian arc and the arc preserved in the LBOT, respectively, first caused a soft collision (Ryan and Dewey 2019). Continuous convergence led to obduction of the still-active and hot arc (Dewey and Ryan 2016), including any underthrusted and underplated sedimentary rocks of the underthrusted horst and/or microcontinent, farther across the margin such that the collision progressed over time into a hard collision. This hard collision was characterized by intense deformation, Barrovian metamorphism and syn-collision magmatism formed in response to melting of the sedimentary rocks (Dewey and Ryan 2016) and/or slab break-off (van Staal et al. 2007). The Early Ordovician onset of accretion of the Grampian arc and the Dashwoods block slowed down convergence in this segment of the Grampian–Taconic orogen and caused a diachronous reversal in subduction polarity outboard of the collision zone (van Staal et al. 1998; Fig. 6). The latter formed the east-facing infant arcs of the Annieopsquotch accretionary tract in Newfoundland (Fig. 5; Lissenberg et al. 2005; Zagorevski et al. 2006) and its correlatives in Ireland (Dewey and Ryan 2016).

CONCLUSIONS

Accretion and collision of terranes to each other and to continents are basically the same process, although not when used in the sense of incorporating small bodies of sedimentary and/or volcanic rocks into an accretionary wedge by off-scraping or underplating. However, there is a distinction when used in classifying mountain belts into accretionary and collisional orogens, although most accretionary orogens will eventually terminate in continental collision (Cawood et al. 2009). Regardless, it is imperative to keep in mind that orogenic classifications are generally based on a qualitative assessment of the scale and nature of the accreted terranes and continents involved in the formation of the investigated mountain belt.

Soft collision is the stage when deformation is principally concentrated in rocks of the leading edge of the partially pulled down buoyant plate and forearc terrane of the upper plate. Several young arc–continent collisions show evidence for partial or wholesale subduction of the forearc. This process may help explain the poor preservation of forearcs in old and young mountain belts. Soft collisions generally change into hard collisions over time, except where the collision is rapidly followed by formation of a new subduction zone due to step-back or polarity reversal.

Application of the soft and hard collision terminology in comparative orogenesis can be useful, as demonstrated in western Newfoundland where soft and hard segments of the Taconic orogen were juxtaposed by significant transcurrent motions. Distinction between these two types of collision is best made on the basis whether the superstructure of the upper plate arc and retro-arc rock were subjected to contraction-related deformation and metamorphism. Where shortening-related deformation is absent or weak in the upper plate, the collision is soft or transitional; where such deformation is present, the collision is hard. Marked thickening of the arc and retro-arc part of the upper plate is thus the hallmark of a hard collision or an advancing Andean-style active margin. Strong rheological coupling of the converging plates and lower and upper crust in the downgoing continental margin promotes a hard collision. Low coupling promotes the opposite.

ACKNOWLEDGEMENTS

The first author likes to express his appreciation to Paul Hoffman and John Dewey who advanced his understanding of plate tectonics and mountain building processes in general during many discussions over the years. Jim Hibbard introduced the first author to the geology of the Baie Verte Peninsula in the early 1990s, which instigated a subsequent detailed investigation in the 2000s. Numerous fieldtrips with Paul Ryan, John Dewey and John Winchester to the Grampian orogen in the west of Ireland were instrumental in recognizing its similarities and differences to the Newfoundland Taconics. Mike Searle is thanked for showing the first author the intricacies of the Semail ophiolite obduction in Oman during a three-week fieldtrip in 1997. Participation in IGCP524 under the leadership of Dennis Brown allowed both of us to visit the various stages of the Luzon arc–South China collision in Taiwan in 2008. The first author also would like to express his gratitude to his managers (especially John McGlynn, Janet King, Murray Duke and Steve Irwin) over the 35 years he was an officer of the Geological Survey of Canada, who never ceased supporting him in his endeavours to understand formation of the Appalachian orogen and associated tectonic problems. Blake Hodgin is thanked for companionship and assistance in the field while carrying out studies in the western part of the Lushs

Bight terrane in 2018. Reviews and editing by Dave Schofield, Damian Nance, Brendan Murphy, Rob Raeside and Wouter Bleeker improved the paper.

REFERENCES

Beekman, F., Bull, J.M., Cloetingh, S., and Scrutton, R.A., 1996, Crustal fault reactivation facilitating lithospheric folding/buckling in the central Indian Ocean, *in* Buchanan, P.G., and Nieuwland, D.A., *eds.*, Modern Developments in Structural Interpretation, Validation and Modelling: Geological Society, London, Special Publications, v. 99, p. 251–263, https://doi.org/10.1144/GSL.SP.1996.099.01.19.

Beltrando, M., Rubatto, D., and Manatschal, G., 2010, From passive margins to orogens: the link between ocean-continent transition zones and (ultra)high-pressure metamorphism: Geology, v. 38, p. 559–562, https://doi.org/10.1130/G30768.1.

Boutelier, D., and Chemenda, A., 2011, Physical modeling of arc-continent collision: a review of 2D, 3D, purely mechanical and thermo-mechanical experimental models, *in* Brown, D., and Ryan, P.D., *eds.*, Arc-Continent Collision: Frontiers in Earth Sciences, Springer, p. 445–473, https://doi.org/10.1007/978-3-540-88558-0_16.

Brandon, M.T., Roden-Tice, M.K., and Garver, J.I., 1998, Late Cenozoic exhumation of the Cascadia accretionary wedge in the Olympic Mountains, northwest Washington State: Geological Society of America Bulletin, v. 110, p. 985–1009, https://doi.org/10.1130/0016-7606(1998)110<0985:LCEOTC>2.3.CO;2.

Brem, A.G., Lin, S., van Staal, C.R, Davis, D.W., and McNicoll, V.J., 2007, The Middle Ordovician to Early Silurian voyage of the Dashwoods microcontinent, west Newfoundland; based on new U/Pb and $^{40}Ar/^{39}Ar$ geochronological, and kinematic constraints: American Journal of Science, v. 307, p. 311–338, https://doi.org/10.2475/02.2007.01.

Brown, D., Wu, Y.-M., Feng, K.-F., Chao, W.-A., and Huang, H.-H., 2015, Imaging high-pressure rock exhumation in eastern Taiwan: Geology, v. 43, p. 651–654, https://doi.org/10.1130/G36810.1.

Brown, M., 2007, Metamorphic conditions in orogenic belts: a record of secular change: International Geology Review, v. 49, p. 193–234, https://doi.org/10.2747/0020-6814.49.3.193.

Brown, M., 2009, Metamorphic patterns in orogenic systems and the geological record, *in* Cawood, P.A., and Kröner, A., *eds.*, Earth Accretionary Systems in Space and Time: Geological Society, London, Special Publications, v. 318, p. 37–74, https://doi.org/10.1144/SP318.2.

Burg, J-P., 2018, Geology of the onshore Makran accretionary wedge: Synthesis and tectonic interpretation: Earth Science Reviews, v. 185, p. 1210–1231, https://doi.org/10.1016/j.earscirev.2018.09.011.

Burg, J-P., and Bouilhol, P., 2019, Timeline of the South Tibet–Himalayan belt: the geochronological record of subduction, collision, and underthrusting from zircon and monazite U–Pb ages: Canadian Journal of Earth Sciences, v. 56, p. 1318–1332, https://doi.org/10.1139/cjes-2018-0174.

Byrne, T., Chan, Y.-C., Rau, R.-J., Lu, C.-Y., Lee, Y.-H., and Wang, Y.-J., 2011, The arc-continent collision in Taiwan, *in* Brown, D., and Ryan, P.D. *eds.*, Arc-Continent Collision: Frontiers in Earth Sciences, Springer, p. 213–245, https://doi.org/10.1007/978-3-540-88558-0_8.

Calvert, A.J., 1996, Seismic reflection constraints on imbrication and underplating of the northern Cascadia convergent margin: Canadian Journal of Earth Sciences, v. 33, p. 1294–1307, https://doi.org/10.1139/e96-098.

Castonguay, S., Ruffet, G., Tremblay, A., and Féraud, G., 2001, Tectonometamorphic evolution of the southern Quebec Appalachians: $^{40}Ar/^{39}Ar$ evidence for Middle Ordovician crustal thickening and Silurian–Early Devonian exhumation of the internal Humber Zone: Geological Society of America Bulletin, v. 113, p. 144–160, https://doi.org/10.1130/0016-7606(2001)113<0144:TEOTSQ>2.0.CO;2.

Castonguay, S., Ruffet, G., and Tremblay, A., 2007, Dating polyphase deformation across low-grade metamorphic belts: An example based on $^{40}Ar/^{39}Ar$ muscovite age constraints from the southern Quebec Appalachians, Canada: Geological Society of America Bulletin, v. 119, p. 978–992, https://doi.org/10.1130/B26046.1.

Castonguay, S., van Staal, C.R., Joyce, N., Skulski, T., and Hibbard, J., 2014, Taconic metamorphism preserved in the Baie Verte Peninsula, Newfoundland Appalachians: Geochronological evidence for ophiolite obduction and subduction and exhumation of the leading edge of the Laurentian (Humber) margin during closure of the Taconic seaway: Geoscience Canada, v. 41, p. 459–482, https://doi.org/10.12789/geocanj.2014.41.055.

Cawood, P.A., and Suhr, G., 1992, Generation and obduction of ophiolites: constraints from the Bay of Islands Complex, western Newfoundland: Tectonics, v. 11, p. 884–897, https://doi.org/10.1029/92TC00471.

Cawood, P.A., Dunning, G.R., Lux, D., and van Gool, J.A.M., 1994, Timing of peak metamorphism and deformation along the Appalachian margin of Laurentia in Newfoundland: Silurian, not Ordovician: Geology, v. 22, p. 399–402, https://doi.org/10.1130/0091-7613(1994)022<0399:TOPMAD>2.3.CO;2.

Cawood, P.A., Kröner, A., Collins, W.J., Kusky, T.M., Mooney, W.D., and Windley, B.F., 2009, Accretionary orogens through Earth history, *in* Cawood, P.A., and Kröner, A., *eds.*, Earth Accretionary Systems in Space and Time: The Geological Society, London, Special Publications, v. 318, p. 1–36, https://doi.org/10.1144/SP318.1.

Chew, D.M., and van Staal, C.R., 2014, The ocean–continent collision transition zones along the Appalachian–Caledonian margin of Laurentia: Examples of large-scale hyperextension during opening of the Iapetus Ocean: Geoscience Canada, v. 41, p. 165–185, https://doi.org/10.12789/geocanj.2014.41.040.

Chew, D.M., Daly, J.S., Magna, T., Page, L.M., Kirkland, C.L., Whitehouse, M.J., and Lam, R., 2010, Timing of ophiolite obduction in the Grampian orogen: Geological Society of America Bulletin, v. 122, p. 1787–1799, https://doi.org/10.1130/B30139.1.

Cooper, M.R., Crowley, Q.G., Hollis, S.P., Noble, S.R., Roberts, S., Chew, D., Earls, G., Herrington, R., and Merriman, R J., 2011, Age constraints and geochemistry of the Ordovician Tyrone Igneous Complex, Northern Ireland: implications for the Grampian orogeny: Journal of the Geological Society, v. 168, p. 837–850, https:// doi.org/10.1144/0016-76492010-164.

Coudurier-Curveur, A., Karakaş, Ç., Singh, S., Tapponnier, P., Carton, H., and Hananto, N., 2020, Is there a nascent plate boundary in the northern Indian Ocean?: Geophysical Research Letters, v. 47, e2020GL087362, https://doi.org/10.1029/2020GL087362.

de Wit, M.J., and Armstrong, R., 2014, Ode to field geology of Williams: Fleur de Lys nectar still fermenting on Belle Isle: Geoscience Canada, v. 41, p. 118–137, https://doi.org/10.12789/geocanj.2014.41.043.

Dewey, J.F., 1980, Episodicity, sequence and style at convergent plate boundaries, *in* Strangway, D.W., *ed.,* The Continental Crust and its Mineral Deposits: Geological Association of Canada Special Paper, v. 20, p. 317–414.

Dewey, J.F., 2005, Orogeny can be very short: Proceedings of the National Academy of Sciences, v. 102, p. 15286–15293, https://doi.org/10.1073/pnas.0505516102.

Dewey, J.F., and Mange, M., 1999, Petrography of Ordovician and Silurian sediments in the western Irish Caledonides: tracers of a short–lived Ordovician continent-arc collision orogeny and the evolution of the Laurentian Appalachian-Caledonian margin, *in* MacNiocaill, C., and Ryan, P.D., *eds.*, Continental Tectonics: Geological Society, London, Special Publications, v. 164, p. 55–107, https://doi.org/10.1144/GSL.SP.1999.164.01.05.

Dewey, J.F., and Ryan, P.D., 2016, Connemara: its position and role in the Grampian orogeny: Canadian Journal of Earth Sciences, v. 53, p. 1246–1257, https://doi.org/10.1139/cjes-2015-0125.

Dorsey, R.J., 1992, Collapse of the Luzon volcanic arc during onset of arc-continent collision: evidence from a Miocene–Pliocene unconformity, eastern Taiwan: Tectonics, v. 11, p. 177–191, https://doi.org/10.1029/91TC02463.

Escher, A., and Beaumont, C., 1997, Formation, burial and exhumation of basement nappes at crustal scale: a geometric model based on the western Swiss-Italian Alps: Journal of Structural Geology, v. 19, p. 955–974, https://doi.org/10.1016/S0191-8141(97)00022-9.

Godin, L., Soucy La Roche, R., Waffle, L., and Harris, L.B., 2018, Influence of inherited Indian basement faults on the evolution of the Himalayan orogen, *in* Sharma, R., Villa, I.M., and Kumar, S., *eds.*, Crustal Architecture and Evolution of the Himalaya–Karakoram–Tibet Orogen: Geological Society, London, Special Publications, v. 481, p. 251–276, https://doi.org/10.1144/SP481.4.

Groome, W.G., Thorkelson, D.J., Friedman, R.M., Mortensen, J.K, Massey, N.W.D., Marshall, D.D., and Layer, P.W., 2003, Magmatic and tectonic history of the Leech River Complex, Vancouver Island, British Columbia: evidence for ridge-trench intersection and accretion of the Crescent terrane, *in* Sisson, V.B., Roeske, S.M., and Pavlis, T.L. *eds.*, Geology of a Transpressional Orogen Developed during Ridge-Trench Interaction along the North Pacific Margin: Geological Society of America Special Papers, v. 371, p. 327– 353, https://doi.org/10.1130/0-8137-2371-X.327.

Hamilton, W.B., 1988, Plate tectonics and island arcs: Geological Society of America Bulletin, v. 100, p. 1503–1527, https://doi.org/10.1130/0016-7606(1988)100<1503:PTAIA>2.3.CO;2.

Harris, R., 2011, The nature of the Banda arc-continent collision in the Timor region, *in* Brown, D., and Ryan, P.D., *eds.*, Arc-Continent Collision: Frontiers in Earth Sciences, Springer, p. 163–211, https://doi.org/10.1007/978-3-540-88558-0_7.

Higgins, A.K., Elvevold, S., Escher, J.C., Frederiksen, K.S., Gilotti, J.A., Henriksen, N., Jepsen, H.F., Jones, K.A., Kalsbeek, F., Kinny, P.D., Leslie, A.G., Smith, M.P.,

Thrane, K., and Watt, G.R., 2004, The foreland-propagating thrust architecture of the East Greenland Caledonides 72°–75°N: Journal of the Geological Society, v. 161, p. 1009–1026, https://doi.org/10.1144/0016-764903-141.

Huang, C.-Y., Yuan, P.B., and Tsao, S.-J., 2006, Temporal and spatial records of active arc-continent collision in Taiwan: A synthesis: Geological Society of America Bulletin, v. 118, p. 274–288, https://doi.org/10.1130/B25527.1.

Huang, C.-Y., Chien, C.-W., Yao, B., Chang, C.-P., 2008, The Lichi Mélange: a collision mélange formation along early arcward backthrusts during forearc basin closure, Taiwan arc-continent collision, *in* Draut, A.E., Clift, P.D., and Scholl, D.W., *eds.*, Formation and Applications of the Sedimentary Record in Arc Collision Zones: Geological Society of America Special Papers, v. 436, p. 127–154, https://doi.org/10.1130/2008.2436(06).

Iturralde-Vinent, M.A., García-Casco, A., Rojas-Agramonte, Y., Proenza, J.A., Murphy, J.B., and Stern, R.J., 2016, The geology of Cuba: A brief overview and synthesis: GSA Today, v. 26, p. 4–10, https://doi.org/10.1130/GSATG296A.1.

Kapp, P., DeCelles, P.G., Gehrels, G.E., Heizler, M., and Ding, L., 2007, Geological records of the Lhasa-Qiangtang and Indo-Asian collisions in the Nima area of central Tibet: Geological Society of America Bulletin, v. 119, p. 917–932, https://doi.org/10.1130/B26033.1.

Kimura, G., and Ludden, J., 1995, Peeling oceanic crust in subduction zones: Geology, v. 23, p. 217–220, https://doi.org/10.1130/0091-7613(1995)023<0217:POCISZ>2.3.CO;2.

Lin, A.T., Watts, A.B., and Hesselbo, S.P., 2003, Cenozoic stratigraphy and subsidence history of the South China Sea margin in the Taiwan region: Basin Research, v. 15, p. 453–478, https://doi.org/10.1046/j.1365-2117.2003.00215.x.

Lin, S., Brem, A.G., van Staal, C.R., Davis, D.W., McNicoll, V.J., and Pehrsson, S., 2013, The Corner Brook Lake block in the Newfoundland Appalachians: a suspect terrane along the Laurentian margin and evidence for large-scale orogeny-parallel motion: Geological Society of America Bulletin, v. 125, p. 1618–1632, https://doi.org/10.1130/B30805.1.

Lissenberg, C.J., and van Staal, C.R., 2006, Feedback between deformation and magmatism in the Lloyds River Fault Zone: An example of episodic fault reactivation in an accretionary setting, Newfoundland Appalachians: Tectonics, v. 25, TC4004, https://doi.org/10.1029/2005TC001789.

Lissenberg, C.J., Zagorevski, A., McNicoll, V.J., van Staal, C.R., and Whalen, J.B., 2005, Assembly of the Annieopsquotch accretionary tract, Newfoundland Appalachians: Age and geodynamic constraints from syn-kinematic intrusions: The Journal of Geology, v. 113, p. 553–570, https://doi.org/10.1086/431909.

Lissenberg, C.J., McNicoll, V.J., and van Staal, C.R., 2006, The origin of mafic-ultramafic bodies within the northern Dashwoods Subzone, Newfoundland Appalachians: Atlantic Geology, v. 42, p. 1–12, https://doi.org/10.4138/2152.

Liu, T.-K., Hsieh, S., Chen, Y.-G., and Chen, W.-S., 2001, Thermo-kinematic evolution of the Taiwan oblique-collision mountain belt as revealed by zircon fission track dating: Earth and Planetary Science Letters, v. 186, p. 45–56, https://doi.org/10.1016/S0012-821X(01)00232-1.

Malavieille, J., and Trullenque, G., 2009, Consequences of continental subduction on forearc basin and accretionary wedge deformation in SE Taiwan: Insights from analogue modeling: Tectonophysics, v. 466, p. 377–394, https://doi.org/10.1016/j.tecto.2007.11.016.

Mann, P., and Taira, A., 2004, Global tectonic significance of the Solomon Islands and Ontong Java Plateau convergent zone: Tectonophysics, v. 389, p. 137–190, https://doi.org/10.1016/j.tecto.2003.10.024.

Matte, P., 2006, The Southern Urals: deep subduction, soft collision and weak erosion, *in* Gee, D.G., and Stephenson, R.A., *eds.*, European Lithosphere Dynamics: Geological Society, London, Memoirs, v. 32, p. 421–426, https://doi.org/10.1144/GSL.MEM.2006.032.01.25.

McIntosh, K., Nakamura, Y., Wang, T.-K., Shih, R.-C., Chen, A., and Liu, C.-S., 2005, Crustal-scale seismic profiles across Taiwan and the western Philippine Sea: Tectonophysics, v. 401, p. 23–54, https://doi.org/10.1016/j.tecto.2005.02.015.

Nelson, K.D., and Casey. J.F., 1979, Ophiolitic detritus in the Upper Ordovician flysch of Notre Dame Bay and its bearing on the tectonic evolution of western Newfoundland: Geology, v. 7, p. 27–31, https://doi.org/10.1130/0091-7613(1979)7<27:ODITUO>2.0.CO;2.

Pearce, J.A., Alabaster, T., Shelton, A.W., and Searle, M.P., 1981, The Oman ophiolite as a Cretaceous arc-basin complex: Evidence and implications: Philosophical Transactions of the Royal Society A, v. 300, p. 299–317, https://doi.org/10.1098/rsta.1981.0066.

Pinet, N., 2013, Gaspé Belt subsurface geometry in the northern Québec Appalachians as revealed by an integrated geophysical and geological study: 2—Seismic interpretation and potential field modelling results: Tectonophysics, v. 588, p. 100–117, https://doi.org/10.1016/j.tecto.2012.12.006.

Pinet, N., and Tremblay, A., 1995, Is the Taconian orogeny of southern Quebec the result of an Oman-type obduction?: Geology, v. 23, p. 121–124, https://doi.org/10.1130/0091-7613(1995)023<0121:ITTOOS>2.3.CO;2.

Platt, J.P., Leggett, J.K., Young, J., Raza, H., and Alam, S., 1985, Large-scale sediment underplating in the Makran accretionary prism, southwest Pakistan: Geology, v. 13, p. 507–511, https://doi.org/10.1130/0091-7613(1985)13<507:LSUITM>2.0.CO;2.

Price, N.J., and Audley-Charles, M.G., 1987, Tectonic collision processes after plate rupture: Tectonophysics, v. 140, p. 121–129, https://doi.org/10.1016/0040-1951(87)90224-1.

Pubellier, M., Quebral, R., Rangin, C., Deffontaines, B., Muller, C., Butterlin, J., and Manzano, J., 1991, The Mindanao collision zone: a soft collision event within a continuous Neogene strike-slip setting: Journal of Southeast Asian Earth Sciences, v. 6, p. 239–248, https://doi.org/10.1016/0743-9547(91)90070-E.

Reston, T., and Manatschal, G., 2011, Rifted margins: building blocks of later collisions, *in* Brown, D., and Ryan, P.D., *eds.*, Arc-Continent Collision: Frontiers in Earth Sciences, Springer, p. 3–21, https://doi.org/10.1007/978-3-540-88558-0_1.

Roberts, D., Nordgulen, Ø., and Melezhik, V., 2007, The uppermost allochthon in the Scandinavian Caledonides: from a Laurentian ancestry through Taconian orogeny to Scandian crustal growth on Baltica, *in* Hatcher Jr., R.D., Carlson, M.P., McBride, J.H., and Martínez Catalán, J.R., *eds.*, 4-D Framework of Continental Crust: Geological Society of America Memoirs, v. 200, p. 357–377, https://doi.org/10.1130/2007.1200(18).

Roberts, D., Morton, A.C., and Frei, D., 2019, A Silurian age for the metasedimentary rocks of the Ekne Group, Trøndelag, Mid-Norwegian Caledonides: and inferences for a peri-Laurentian provenance: Norwegian Journal of Geology, v. 99, p. 583–595, https://doi.org/10.17850/njg99-4-3.

Robertson, A., 1987, The transition from a passive margin to an Upper Cretaceous foreland basin related to ophiolite emplacement in the Oman Mountains: Geological Society of America Bulletin, v. 99, p. 633–653, https://doi.org/10.1130/0016-7606(1987)99<633:TTFAPM>2.0.CO;2.

Rutherford, E., Burke, K., and Lytwyn, J., 2001, Tectonic history of Sumba Island, Indonesia, since the Late Cretaceous and its rapid escape into the forearc in the Miocene: Journal of Asian Earth Sciences, v. 19, p. 453–479, https://doi.org/10.1016/S1367-9120(00)00032-8.

Ryan, P.D., and Dewey, J.F., 2019, The Ordovician Grampian orogeny, western Ireland: Obduction versus "bulldozing" during arc-continent collision: Tectonics, v. 38, p. 3462–3475, https://doi.org/10.1029/2019TC005602.

Saqab, M.M., Bourget, J., Trotter, J., and Keep, M., 2017, New constraints on the timing of flexural deformation along the northern Australian margin: implications for arc-continent collision and the development of the Timor Trough: Tectonophysics, v. 696–697, p. 14–36, https://doi.org/10.1016/j.tecto.2016.12.020.

Schmid, S.M., Pfiffner, O.A., Froitzheim, N., Schönborn, G., and Kissling, E., 1996, Geophysical-geological transect and tectonic evolution of the Swiss-Italian Alps: Tectonics, v. 15, p. 1036–1064, https://doi.org/1010.1029/96TC00433.

Searle, M., and Cox, J., 1999, Tectonic setting, origin, and obduction of the Oman ophiolite: Geological Society of America Bulletin, v. 111, p. 104–122, https://doi.org/10.1130/0016-7606(1999)111<0104:TSOAOO>2.3.CO;2.

Şengör, A.M.C., and Natal'in, B.A., 1996, Turkic type orogeny and its role in the making of the continental crust: Annual Review of Earth and Planetary Sciences, v. 24, p. 263–337, https://doi.org/10.1146/annurev.earth.24.1.263.

Şengör, A.M.C., Natal'in, B.A., Sunal, G., and van der Voo, R., 2018, The tectonics of the Altaids: Crustal growth during the construction of the continental lithosphere of Central Asia between ~750 and ~130 Ma ago: Annual Review of Earth and Planetary Sciences, v. 46, p. 439–494, https://doi.org/10.1146/annurev-earth-060313-054826.

Silver, E.A., Reed, D., McCaffrey, R., and Joyodiwiryo, Y., 1983, Back arc thrusting in the Eastern Sunda Arc, Indonesia: a consequence of arc-continent collision: Journal of Geophysical Research, v. 88, p. 7429–7448, https://doi.org/10.1029/JB088iB09p07429.

Skulski, T., Castonguay, S., McNicoll, V., van Staal, C.R., Kidd, W., Rogers, N., Morris, W., Ugalde, H., Slavinski, H., Spicer, W., Moussallam, Y., and Kerr, I., 2010, Tectonostratigraphy of the Baie Verte oceanic tract and its ophiolite cover sequence on the Baie Verte Peninsula: Current research (2010) Newfoundland and Labrador Department of Natural Resources, Geological Survey Report 10-1, p. 315–335.

Soh, W., Nakayama, K., and Kimura, T., 1998, Arc-arc collision in the Izu collision zone, central Japan, deduced from the Ashigara Basin and adjacent Tanzawa Mountains: Island Arc, v. 7, p. 330–341, https://doi.org/10.1111/j.1440-1738.1998.00193.x.

Stern, R.J., 2005, Evidence from ophiolites, blueschists and ultrahigh-pressure metamorphic terranes that the modern episode of subduction tectonics began in

Neoproterozoic time: Geology, v. 33, p. 557–560, https://doi.org/10.1130/G21365.1.

Stevens, R.K., 1970, Cambro–Ordovician flysch sedimentation and tectonics in west Newfoundland and their possible bearing on a proto-Atlantic Ocean: Geological Association of Canada, Special Paper 7, p. 165–177.

Suhr, G., and Cawood, P.A., 1993, Structural history of ophiolite obduction, Bay of Islands, Newfoundland: Geological Society of America Bulletin, v. 105, p. 399–410, https://doi.org/10.1130/0016-7606(1993)105<0399:SHOOOB>2.3.CO;2.

Supendi, P., Nugraha, A.D., Widiyantoro, S., Abdullah, C.I., Rawlinson, N., Cummins, P.R., Harris, C.W., Roosmawati, N., and Miller, M.S., 2020, Fate of forearc lithosphere at arc-continent collision zones: Evidence from local earthquake tomography of the Sunda-Banda Arc transition, Indonesia: Geophysical Research Letters, v. 47, e2019GL086472, https://doi.org/10.1029/2019GL086472.

Swinden, H.S., Jenner, G.A., and Szybinski, Z.A., 1997, Magmatic and tectonic evolution of the Cambrian–Ordovician Laurentian margin of Iapetus; geochemical and isotopic constraints from the Notre Dame Subzone, Newfoundland, *in* Sinha, A.K., Whalen, J.B., and Hogan, J.P., *eds.,* The Nature of Magmatism in the Appalachian Orogen: Geological Society of America Memoirs, v. 191, p. 337–365, https://doi.org/10.1130/0-8137-1191-6.337.

Taira, A., Mann, P., and Rahardiawan, R., 2004, Incipient subduction of the Ontong Java Plateau along the North Solomon trench: Tectonophysics, v. 389, p. 247–266, https://doi.org/10.1016/j.tecto.2004.07.052.

Tang, J.-C., and Chemenda, A.I., 2000, Numerical modelling of arc-continent collision: application to Taiwan: Tectonophysics, v. 325, p. 23–42, https://doi.org/10.1016/S0040-1951(00)00129-3.

Tremblay, A., and Pinet, N., 2016, Late Neoproterozoic to Permian evolution of the Quebec Appalachians, Canada: Earth-Science Reviews, v. 160, p. 131–170, https://doi.org/10.1016/j.earscirev.2016.06.015.

van der Velden, A.J., van Staal, C.R., and Cook, F.A., 2004, Crustal structure, fossil subduction, and the tectonic evolution of the Newfoundland Appalachians: Evidence from a reprocessed seismic reflection survey: Geological Society of America Bulletin, v. 116, p. 1485–1498, https://doi.org/10.1130/B25518.1.

van Staal, C.R., Dewey, J.F., MacNiocaill, C., and McKerrow, W.S., 1998, The Cambrian–Silurian tectonic evolution of the northern Appalachians and British Caledonides: history of a complex, west and southwest Pacific-type segment of Iapetus, *in* Blundell, D.J., and Scott, A.C., *eds.*, Lyell: The Past is the Key to the Present: Geological Society, London, Special Publications, v. 143, p. 197–242, https://doi.org/10.1144/GSL.SP.1998.143.01.17.

van Staal, C.R., Whalen, J.B., McNicoll, V.J., Pehrsson, S.J., Lissenberg, C.J., Zagorevski, A., van Breemen, O., and Jenner, G.A., 2007, The Notre Dame arc and the Taconic orogeny in Newfoundland, *in* Hatcher Jr., R.D., Carlson, M.P., McBride, J.H., and Martínez Catalán, J.R., *eds.*, 4-D Framework of Continental Crust: Geological Society of America Memoirs, v. 200, p. 511–552, https://doi.org/10.1130/2007.1200(26).

van Staal, C.R., Currie, K.L., Rowbotham, G., Rogers, N., and Goodfellow, W., 2008, Pressure-Temperature paths and exhumation of Late Ordovician–Early Silurian blueschists and associated metamorphic nappes of the Salinic Brunswick subduction complex, northern Appalachians: Geological Society of America Bulletin, v. 120, p. 1455–1477, https://doi.org/10.1130/B26324.1.

van Staal, C.R., Whalen, J.B., Valverde-Vaquero, P., Zagorevski, A., and Rogers, N., 2009, Pre-Carboniferous, episodic accretion-related, orogenesis along the Laurentian margin of the northern Appalachians, *in* Murphy, J.B., Keppie, J.D., and Hynes, A.J., *eds.*, Ancient Orogens and Modern Analogues: Geological Society, London, Special Publications, v. 327, p. 271–316, https://doi.org/10.1144/SP327.13.

van Staal, C.R., Chew, D.M., Zagorevski, A., McNicoll, V., Hibbard, J., Skulski, T., Castonguay, S., Escayola, M.P., and Sylvester, P.J., 2013, Evidence of Late Ediacaran hyperextension of the Laurentian Iapetan margin in the Birchy Complex, Baie Verte Peninsula, northwest Newfoundland: Implications for the opening of Iapetus, formation of peri-Laurentian microcontinents and Taconic – Grampian orogenesis: Geoscience Canada, v. 40, p. 94–117, https://doi.org/10.12789/geocanj.2013.40.006.

Verhoef, J., and Roest, W.R., 1993, Reading the stripes: offshore discoveries in plate tectonics with examples from eastern Canada: Canadian Journal of Earth Sciences, v. 30, p. 261–277, https://doi.org/10.1139/e93-022.

Vogt, K., Matenco, L., and Cloetingh, S., 2017, Crustal mechanics control the geometry of mountain belts. Insights from numerical modelling: Earth and Planetary Science Letters, v. 460, p. 12–21, https://doi.org/10.1016/j.epsl.2016.11.016.

Waldron, J.W.F., and van Staal, C.R., 2001, Taconian orogeny and the accretion of the Dashwoods block: A peri-Laurentian microcontinent in the Iapetus Ocean: Geology, v. 29, p. 811–814, https://doi.org/10.1130/0091-7613(2001)029<0811:TOATAO>2.0.CO;2

Waldron, J.W.F., Henry, A.D., Bradley, J.C., and Palmer, S.E., 2003, Development of a folded thrust stack: Humber Arm Allochthon, Bay of Islands, Newfoundland Appalachians: Canadian Journal of Earth Sciences, v. 40, p. 237–253, https://doi.org/10.1139/e02-042.

Waldron, J.W.F., McNicoll, V.J., and van Staal, C.R., 2012, Laurentia-derived detritus in the Badger Group of central Newfoundland: deposition during closing of the Iapetus Ocean: Canadian Journal of Earth Sciences, v. 49, p. 207–221, https://doi.org/10.1139/e11-030.

Waldron, J.W.F., Barr, S.M., Park, A.F., White, C.E., and Hibbard, J., 2015, Late Paleozoic strike-slip faults in Maritime Canada and their role in the reconfiguration of the northern Appalachian orogen: Tectonics, v. 34, p. 1661–1684, https://doi.org/10.1002/2015TC003882.

Wang, T., Hong, D.-w., Jahn, B.-m., Tong, Y., Wang, J.-b., Han, B.-f., and Wang, X.-x., 2006, Timing, petrogenesis and setting of Paleozoic synorogenic intrusions from the Altai Mountains, northwest China: implications for the tectonic evolution of an accretionary orogeny: Journal of Geology, v. 114, p. 735–751, https://doi.org/10.1086/507617.

Wells, R., Bukry, D., Friedman, R., Pyle, D., Duncan, R., Haeussler, P., and Wooden, J., 2014, Geologic history of Siletzia, a large igneous province in the Oregon and Washington Coast Range: correlation to the geomagnetic polarity time scale and implications for a long-lived Yellowstone hotspot: Geosphere, v. 10, p. 692–719, https://doi.org/10.1130/GES01018.1.

Westbrook, G.K., 1982, The Barbados Ridge Complex: tectonics of a mature forearc system, *in* Leggett, J.K., *ed.*, Trench–Forearc Geology: Sedimentation and Tectonics on Modern and Ancient Active Plate Margins: Geological Society, London, Special Publications, v. 10, p. 275–290, https://doi.org/10.1144/GSL.SP.1982.010.01.18.

White, S.E., Waldron, J.W.F., and Harris, N.B., 2020, Anticosti foreland basin offshore of western Newfoundland: concealed record of northern Appalachian orogen development: Basin Research, v. 32, p. 25–50, https ://doi.org/10.1111/bre.12364.

Willingshofer, E., Sokoutis, D., Luth, S.W., Beekman, F., and Cloetingh, S., 2013, Subduction and deformation of the continental lithosphere in response to plate and crust-mantle coupling: Geology, v. 41, p. 1239–1242, https://doi.org/10.1130/G34815.1.

Willner, A.P., Gerdes, A., Massonne, H.-J., van Staal, C.R., and Zagorevski, A., 2014, Crustal evolution of the northeast Laurentian margin and the peri-Gondwanan microcontinent Ganderia prior to and during closure of the Iapetus Ocean: detrital zircon U–Pb and Hf isotope evidence from Newfoundland: Geoscience Canada, v. 41, p. 345–364, https://doi.org/10.12789/ geocanj.2014.41.046.

Windley, B., 1992, Chapter 11 Proterozoic collisional and accretionary orogens, *in* Condie, K.C., *ed.*, Proterozoic Crustal Evolution: Developments in Precambrian Geology, v. 10, p. 419–446, https://doi.org/10.1016/S0166-2635(08)70125-7.

Zagorevski, A., and van Staal, C.R., 2011, The record of Ordovician arc-arc and arc-continent collisions in the Canadian Appalachians during closure of Iapetus, *in* Brown, D., and Ryan, P.D., *eds.*, Arc-Continent Collision: Frontiers in Earth Sciences, Springer, p. 341–371, https://doi.org/10.1007/978-3-540-88558-0_12.

Zagorevski, A., Rogers, N., van Staal, C.R., McNicoll, V., Lissenberg, C.J., and Valverde-Vaquero, P., 2006, Lower to Middle Ordovician evolution of peri-Laurentian arc and backarc complexes in Iapetus: constraints from the Annieopsquotch accretionary tract, central Newfoundland: Geological Society of America Bulletin, v. 118, p. 324–342**,** https://doi.org/10.1130/B25775.1.

Zagorevski, A., van Staal, C.R., and McNicoll, V.J., 2007, Distinct Taconic, Salinic and Acadian deformation along the Iapetus suture zone, Newfoundland Appalachians: Canadian Journal of Earth Sciences, v. 44, p. 1567–1585, https://doi.org/10.1139/E07-037.

Zagorevski, A, McNicoll, V.J., van Staal, C.R., Kerr, A., and Joyce, N., 2015, From large zones to small terranes to detailed reconstruction of an Early to Middle Ordovician arc-backarc system preserved along the Iapetus suture zone: A legacy of Hank Williams: Geoscience Canada, v. 42, p. 125–150, https://doi.org/10.12789/geocanj.2014.41.054.

Received April 2020
Accepted as revised June 2020

SERIES

Igneous Rock Associations 26. Lamproites, Exotic Potassic Alkaline Rocks: A Review of their Nomenclature, Characterization and Origins

Roger H. Mitchell

Department of Geology, Lakehead University
Thunder Bay, Ontario, P7B 5E1, Canada
Email: rmitchel@lakeheadu.ca

SUMMARY

Lamproite is a rare ultrapotassic alkaline rock of petrological importance as it is considered to be derived from metasomatized lithospheric mantle, and is of economic significance, being the host of major diamond deposits. A review of the nomenclature of lamproite results in the recommendation that members of the lamproite petrological clan be named using mineralogical-genetic classifications to distinguish them from other genetically unrelated potassic alkaline rocks, kimberlite, and diverse lamprophyres. The names "Group 2 kimberlite" and "orangeite" must be abandoned as these rock types are varieties of *bona fide* lamproite restricted to the Kaapvaal craton. Lamproites exhibit extreme diversity in their mineralogy which ranges from olivine phlogopite lamproite, through phlogopite leucite lamproite and potassic titanian richterite-diopside lamproite, to leucite sanidine lamproite. Diamondiferous olivine lamproites are hybrid rocks extensively contaminated by mantle-derived xenocrystic olivine. Currently, lamproites are divided into cratonic (e.g. Leucite Hills, USA; Baifen, China) and orogenic (Mediterranean) varieties (e.g. Murcia-Almeria, Spain; Afyon, Turkey; Xungba, Tibet). Each cratonic and orogenic lamproite province differs significantly in tectonic setting and Sr–Nd–Pb–Hf isotopic compositions. Isotopic compositions indicate derivation from enriched mantle sources, having long-term low Sm/Nd and high Rb/Sr ratios, relative to bulk earth and depleted asthenospheric mantle. All lamproites are considered, on the basis of their geochemistry, to be derived from ancient mineralogically complex K–Ti–Ba–REE-rich veins, or metasomes, in the lithospheric mantle with, or without, subsequent contributions from recent asthenospheric or subducted components at the time of genesis. Lamproite primary magmas are considered to be relatively silica-rich (~ 50–60 wt.% SiO_2), MgO-poor (3–12 wt.%), and ultrapotassic (~ 8–12 wt.% K_2O) as exemplified by hyalo-phlogopite lamproites from the Leucite Hills (Wyoming) or Smoky Butte (Montana). Brief descriptions are given of the most important phreatomagmatic diamondiferous lamproite vents. The tectonic processes which lead to partial melting of metasomes, and/or initiation of magmatism, are described for examples of cratonic and orogenic lamproites. As each lamproite province differs with respect to its mineralogy, geochemical evolution, and tectonic setting there is no simple or common petrogenetic model for their genesis. Each province must be considered as the unique expression of the times and vagaries of ancient mantle metasomatism, coupled with diverse and complex partial melting processes, together with mixing of younger asthenospheric and lithospheric material, and, in the case of many orogenic lamproites, with Paleogene to Recent subducted material.

RÉSUMÉ

La lamproïte est une roche alcaline ultrapotassique rare d'importance pétrologique car elle est considérée comme dérivée du manteau lithosphérique métasomatisé, et d'importance économique, étant l'hôte de gisements de diamants majeurs. Un examen de la nomenclature des lamproïtes conduit à la recommandation que les membres du clan pétrologique des lamproïtes soient nommés en utilisant des classifications minéralogiques génétiques pour les distinguer des autres roches alcalines potassiques génétiquement non liées, de la kimberlite et de divers lamprophyres. Les noms « kimberlite du groupe 2 » et « orangéite » doivent être abandonnés car ces types de roches sont des variétés de véritables lamproïtes

Geoscience Canada, v. 47, https://doi.org/10.12789/geocanj.2020.47.162 pages 119–142

restreintes au craton de Kaapvaal. Les lamproïtes présentent une extrême diversité dans leur minéralogie qui va de la lamproïte à phlogopite et olivine, à la lamproïte à leucite et phlogopite et de la lamproïte à richtérite-diopside potassique titanifère, à la lamproïte à sanidine et leucite. Les lamproïtes à olivine diamantifères sont des roches hybrides largement contaminées par l'olivine xénocristique dérivée du manteau. Actuellement, les lamproïtes sont divisées en variétés cratoniques (par exemple Leucite Hills, États-Unis; Baifen, Chine) et orogéniques (méditerranéennes) (par exemple Murcie-Almeria, Espagne; Afyon, Turquie; Xungba, Tibet). Chaque province de lamproïte cratonique et orogénique diffère significativement par le contexte tectonique et les compositions isotopiques en Sr, Nd, Pb et Hf. Les compositions isotopiques indiquent que leur source est un manteau enrichi, ayant à long terme des rapports Sm/Nd bas et Rb/Sr élevés, par rapport à la Terre globale et au manteau asthénosphérique appauvri. Toutes les lamproïtes sont considérées, sur la base de leur géochimie, comme étant dérivées d'anciennes veines minéralogiquement complexes riches en K, Ti, Ba et ETR, ou métasomes, dans le manteau lithosphérique avec ou sans contributions ultérieures de composants asthénosphériques ou subductés récents au moment de la genèse. Les magmas primaires de lamproïte sont considérés comme relativement riches en silice (~ 50–60% en poids de SiO_2), pauvres en MgO (3–12% en poids) et ultrapotassiques (~ 8–12% en poids de K_2O) comme le montrent les lamproïtes hyalo à phlogopite de Leucite Hills (Wyoming) ou de Smoky Butte (Montana). De brèves descriptions sont données des cheminées de lamproïtes diamantifères phréatomagmatiques les plus importantes. Les processus tectoniques qui conduisent à la fusion partielle des métasomes et / ou à l'initiation du magmatisme sont décrits comme des exemples de lamproïtes cratoniques et orogéniques. Comme chaque province de lamproïte diffère en ce qui concerne sa minéralogie, son évolution géochimique et son cadre tectonique, il n'y a pas de modèle pétrogénétique simple ou commun pour leur genèse. Chaque province doit être considérée comme l'expression unique de l'époque et des caprices du métasomatisme du manteau ancien, associée à des processus de fusion partielle divers et complexes, ainsi qu'à un mélange de matériaux asthénosphériques et lithosphériques plus jeunes et, dans le cas de nombreuses lamproïtes orogéniques, à du matériel paléogène à récent subducté.

Traduit par la Traductrice

INTRODUCTION

Lamproite is a very rare potassic alkaline rock type occurring in less than 50 *bona fide* major petrological provinces on all continents. In this work, a petrological province is regarded as a discrete region of diverse lamproite magmatism of similar age and tectonic setting. Locations of particular lamproite provinces can be found in Mitchell and Bergman (1991), Fareeddudin and Mitchell (2012) or more easily by using Google Earth. Regardless of their rarity they have attained significant importance in the fields of economic geology and mantle petrology. With respect to the former they currently host major diamond mines in Australia (Argyle) and South Africa (Finsch), with the Argyle AK1 Mine being one of world's highest-grade primary diamond deposits (~30–680 ct/100 t). In terms of mantle petrology, their mineralogy and geochemistry have provided insights into metasomatic processes in the lithospheric mantle which cannot be addressed from investigations of more common magma types.

One objective of this review is to summarize recent revisions to the terminology of the lamproite petrological clan and show how these rock types can be identified correctly using petrography, mineralogy, and isotopic data. The geology of extrusive and hypabyssal lamproite bodies, which is similar to that of common magma types such as basalt, is not described in detail as summaries are given in Jaques et al. (1986), Mitchell and Bergman (1991), and Mitchell (1995a), although aspects of the geology of the most important diamondiferous volcaniclastic and pyroclastic lamproite vents are presented. Although detailed commentary is well beyond the scope of this contribution, the origins of "cratonic" and "orogenic" lamproites, and magma generation in the lithospheric mantle are briefly considered.

The mineralogy of diamonds found in lamproites is not described as, in common with those in kimberlites, these are mantle-derived xenocrysts. Also not considered here are plutonic undersaturated potassic rocks (malignite. pulaskite, missourite, shonkinite, yakutite, synnyrite, etc.) as the relationships of these rocks to lamproite, leucitite, or other potassic magmas have not been resolved. Unfortunately, many of these rocks have been incorrectly termed lamproite. For descriptions of these rock types see Mitchell (1996).

Potassic Alkaline Rocks – Classification

Rocks enriched in K relative to Na are conventionally regarded as potassic alkaline rocks. There is no generally agreed upon definition of the term alkaline, although convention considers alkaline rocks to be those in which the bulk rock alkali (Na and K) content exceeds the alkali feldspar ($NaAlSi_3O_8$ or $KAlSi_3O_8$) molecular ratio of [(Na_2O+K_2O): Al_2O_3:SiO_2] of 1:1:6, with either Al_2O_3 or SiO_2 being deficient (Shand 1922). This definition permits the recognition, with respect to silica (SiO_2), of oversaturated and undersaturated alkaline rocks. Hence, feldspathoidal (nepheline-, leucite-, kalsilite-bearing) rocks are considered to be undersaturated and alkaline, e.g leucitite, kamafugite and nepheline syenite. Silica-rich oversaturated rocks with quartz, containing Na-rich pyroxenes and amphiboles, can also be termed alkaline, e.g. peralkaline granite. Note that the presence of a high content of alkali feldspar or leucite, is usually considered as insufficient grounds for regarding a rock as alkaline. Many rocks containing leucite, such as lamproites, are alkaline by the virtue of being alumina-deficient, regardless of their silica content.

All alkaline rocks can be regarded as belonging to a sodic or potassic series in which the molar K_2O/Na_2O ratio is lesser or greater than unity, respectively. Potassic rocks are further subdivided into potassic rocks with molar K_2O/Na_2O between 1 and 3, and ultrapotassic types with K_2O/Na_2O greater than 3 (Foley et al. 1987). The relative amounts of alkalis to alumina are expressed by the peralkalinity index, i.e. molar

Table 1. ***Revised Nomenclature of Lamproites***

Historical name	*Revised name*
Wyomingite	diopside leucite phlogopite lamproite
Orendite	diopside sanidine phlogopite lamproite
Madupite	diopside madupitic lamproite
Cedricite	diopside leucite lamproite
Mamilite	leucite richterite lamproite
Wolgidite	diopside leucite richterite madupitic lamproite
Fitzroyite	leucite phlogopite lamproite
Verite	hyalo-olivine diopside phlogopite lamproite
Jumillite	olivine diopside richterite madupitic lamproite
Fortunite	hyalo-enstatite phlogopite lamproite
Cancalite	enstatite sanidine phlogopite lamproite

The term *madupitic* is used to reflect the differing *habits and compositions* of phlogopite which have *petrogenetic* significance. Rocks with phenocrystal phlogopite are termed *phlogopite lamproites* and those with poikilitic groundmass phlogopite and tetraferriphlogopite are termed *madupitic lamproites*. This texture might also be termed oikocrystic and the included minerals chadacrysts. Rocks containing both phenocrystal and groundmass mica can be referred to as transitional madupitic lamproite. Note that recently recognized lamproites in Montana, India and Australia are not given type locality names and are described using modal mineralogical criteria *e.g* the Smoky Butte lamproite (Montana) is a hyalo-olivine phlogopite lamproite; the diamond-bearing lamproites at Argyle and Ellendale (W. Australia) and Majhgawan (India) are termed pyroclastic macrocrystal phlogopite olivine lamproites; and the name *orangeite* is now replaced by lamproite *(var. Kaapvaal*) with calcite phlogopite olivine lamproite and diopside sanidine lamproite being common examples.

$[(K_2O+Na_2O)/Al_2O_3]$. If this index is greater than one, a rock is termed peralkaline regardless of the degree of silica saturation.

All lamproites described in this review, are undersaturated potassic or ultrapotassic alkaline rocks with respect to their bulk rock composition. In some instances, such as hyalo-phlogopite lavas, this approximates to parental magma liquid compositions. In contrast, the bulk compositions of alteration-free olivine lamproites, or volcaniclastic lamproites, do not represent liquid compositions because of the high content of mantle- or crustal-derived xenocrysts.

Etymology of Lamproites

The name lamproite was introduced into geological literature by Niggli (1923) and is derived from the Greek root *λάμπρος* meaning "glistening", with reference to the common presence of shiny phenocrysts of phlogopite. This term has been retained in the petrological literature regardless that many lamproites do not exhibit this particular characteristic. Currently, lamproites are regarded as a petrological clan of potassic rocks with diverse mineralogical and geochemical characteristics, which can *only* be recognized using the mineralogical-genetic classification schemes introduced by Scott Smith and Skinner (1984), Mitchell and Bergman (1991) and Woolley et al. (1996).

Unlike common rock types, lamproite and kimberlite cannot be identified by simple optical petrographic studies because of their complex mineralogy and common fine-grained textures. *They cannot be defined using non-genetic International Union of Geological Sciences modal nomenclature schemes* (Mitchell 1995a). Progress in their characterization was only made possible by the development of back-scattered electron petrography coupled with wavelength and energy dispersive X-ray spectrometry. This led to the development of mineralogical-genetic classification schemes for diverse alkaline rocks, and in particular for lamproites and kimberlites (Mitchell and Bergman 1991; Mitchell 1995a; Woolley et al. 1996; Scott Smith et al. 2018). In such schemes, rocks are classified on the basis of typomorphic assemblages of minerals whose compositions are a direct reflection of the composition of their parental magmas. *Identification of all primary minerals is required for correct characterization of a particular sample, including minerals normally considered minor or trace accessory phases*. Note that in mineralogical-genetic classifications it is *not* necessary to know the origins of the parental magmas.

The nomenclature of lamproites has been historically bedevilled by a plethora of type locality names which are unrelated and uninformative. As a result, similarities and relationships between rock types were obscured. This otiose terminology was initially rationalized by Mitchell and Bergman (1991) using a descriptive mineralogical nomenclature scheme (Table 1). *Unlike common rock types it is not possible to devise a simple definition of "lamproite" only on the basis of modal mineralogy, as compositional data for the major, minor, and trace minerals are required for correct identification (see below*). Further, lamproites exhibit an extremely wide range in their modal mineralogy owing to the large number of liquidus phases which can crystallize from compositionally diverse lamproitic magmas.

Rocks which were eventually termed lamproites (Table 1) were initially recognized in the 1890s from the Leucite Hills of Wyoming, USA (wyomingite, orendite, madupite, Cross 1897); subsequently at Almeria and Jumilla in Spain (jumillite, cancalite, verite, fortunite, Osann 1906); and in the 1920s in the West Kimberley region of Australia (cedricite, fitzroyite, mamilite, wolgidite, Wade and Prider 1940). The latter occurrence, was particularly important in that further exploration of this province in the 1970s determined that some lamproites were found to be diamond-bearing, These discoveries led to the development of the AK1 diamond mine in the Argyle pyroclastic lamproite vent as a major source of industrial and rare pink diamonds, and to the recognition of minor deposits of gem quality diamonds in olivine lamproite of the Ellendale area (Jaques et al. 1986). These discoveries prompted reclassification of "anomalous diamond-bearing kimberlites" at Prairie Creek (Arkansas, USA) and Majhgawan (India), as *bona fide* olivine lamproite (Scott Smith and Skinner 1984; Mitchell and Bergman 1991). As a historical note, diamonds were being mined at Majhgawan (formerly Panna) in the early 1800s (Franklin 1822), and this occurrence must now be recognized

as the first known primary diamond deposit in any igneous rock.

Many rocks previously classified as lamproite (*sensu lato*) are actually leucitite and related rock types (Lustrino et al. 2016, 2019), and many "kimberlites and minettes" in the Dharwar, Baster, and Singhbhum cratons of India are now reclassified as lamproite (Mitchell and Fareeduddin 2009; Fareeduddin and Mitchell 2012; Gurmeet Kaur and Mitchell 2013; Shaikh et al. 2019). Note that recently recognized lamproites are not given type locality names (e.g. Moon Canyonite, Vattikodite) and are described using mineralogical-genetic nomenclature, e.g. the Smoky Butte lamproite (Montana) is a hyalo-olivine phlogopite lamproite, and some of the Argyle diamond-bearing lamproites are xenocrystic-quartz-bearing macrocrystic phlogopite olivine lamproite tuff.

Lamproite terminological confusion has been further exacerbated by the formerly received concept that diamonds could only be found in kimberlite. Thus, the two distinct varieties of diamond-bearing rocks found in Southern Africa were initially termed "basaltic" and "micaceous kimberlites" (Wagner 1914). Although the term basaltic was eventually discarded as these rocks are totally unrelated to basalt, the micaceous variety continued to be referred to as kimberlite by Mitchell (1986). The terms Group 1 and Group 2 kimberlite were introduced by Smith (1983) and Smith et al. (1985) to distinguish between kimberlite and micaceous kimberlite primarily on their Sr–Nd isotopic signatures. Subsequently, these terms were unfortunately entrenched in petrological literature in the now otiose IUGS classification scheme of Woolley et al. (1996). However, it is now accepted that Group 1 and 2 kimberlites belong to genetically distinct parental magma types and form separate petrological clans (Dawson 1987; Mitchell 1995a; Scott Smith et al. 2018; Pearson et al. 2019). Thus, use of the term Group 1 kimberlite must be discontinued and these rocks simply referred to as *kimberlite*. Mitchell (1995a) demonstrated that Group 2 or micaceous kimberlites have close mineralogical affinities with lamproites and resurrected an older name "orangeite", as originally recommended by Wagner (1928), who recognized the mineralogical distinctiveness of these rocks. Subsequently, Mitchell (2006, 2007), Scott Smith et al. (2018) and Pearson et al. (2019) have further revised this nomenclature and considered that the southern African micaceous kimberlites are *bona fide* lamproites and represent a suite of rocks derived from ancient metasomatized lithospheric mantle. Thus, the recommended group name for orangeites is now *lamproite variety Kaapvaal*. This term is preferred as it emphasizes the common petrogenesis with lamproites *sensu lato* and eliminates any petrological confusion with petrogenetically distinct kimberlites. To avoid any further confusion and false genetic hypotheses, the term "Group 2 kimberlite" must be abandoned as these rocks are *not* kimberlites.

Although relatively rare rock types, *bona fide* lamproites, have now been recognized from all continents and occur in two distinct tectonic environments, and are currently referred to as cratonic (or anorogenic) lamproites and orogenic lamproites. The latter, also termed Mediterranean lamproites, occur primarily in a belt extending from Spain and Italy through Serbia and Turkey to Tibet. These occurrences are associated with recent subducted plate margins and diverse varieties of subduction-related potassic magmatism.

An occurrence of lamproite-like rocks associated with shoshonite has been described from Lesbos (Aegean Sea) by Pe-Piper et al. (2014), These rocks do not have the typical mineralogy of *bona fide* lamproites, especially with respect to mica composition and paragenesis, with some examples even containing plagioclase. Although isotopic data indicate derivation from light REE-enriched lithospheric mantle, this is considered to have occurred in Paleozoic times. Thus, in contrast to other peri-Mediterranean lamproites these Miocene rocks are not associated with contemporary subduction. The association with shoshonite suggests that these para-lamproites are a unique suite of rocks related to the back-arc extension of island arc volcanism as suggested by Pe-Piper et al. (2014). Mitchell and Bergman (1991) have noted that para-lamproites associated with shoshonite have much in common with island arc boninite (Crawford et al. 1989) for which a low Nd isotopic ratio has been interpreted to indicate derivation from old light REE-enriched mantle (Hickey and Frey 1982). Thus, it is considered that the Lesbos rocks are not *bona fide* lamproites.

Only cratonic varieties of lamproite have been found to be diamondiferous. The most important advance resulting from the reclassification of Group 2 kimberlites and orangeites as lamproites is the renewed emphasis on the diamondiferous character of the Kaapvaal craton lamproites. This has resulted in significant changes in the exploration philosophy used to locate these rocks, as they cannot be identified by methods used to recognize *bona fide* kimberlites, such as the use of magnesian ilmenite as an indicator mineral. Major (Finsch, Lace) and minor (Star, Roberts Victor, Bellsbank) diamond mines are now regarded as lamproite volcanic vents and dykes (a.k.a. fissure mines).

The cratonic varieties of lamproite are the easiest to identify, using the mineralogical and geochemical criteria (see below) developed by Mitchell and Bergman (1991). However, even these rocks exhibit extremely wide variations in their modal mineralogy, and it has been shown that each cratonic lamproite province has a distinct mineralogical, geochemical, and isotopic signature. This is a result of derivation of the parental magmas from modally diverse, but mineralogically similar, metasomatized lithospheric mantle source rocks with high Rb/Sr ratios and low Sm/Nd ratios. Mitchell (2006, 2007) and Scott Smith et al. (2018) have referred to cratonic lamproites as *metasomatized mantle magmas*, which can be given varietal names which reflect their underlying ancient metasomatized cratonic sources, e.g. lamproite (var. Kaapvaal), lamproite (var. Dharwar), lamproite (var. Bundelkhand). In contrast to the Mediterranean lamproites which are associated with recent subduction, cratonic lamproites, on the basis of their Sr–Nd isotope geochemistry, are now known to be derived from source regions containing a geochemical contribution from ancient subduction events (see below).

The orogenic lamproites (e.g. Cancarix, Jumilla, Orciatico, Afyon, Xungba, etc.) present significant challenges to recognition as these are found in geographic and geotectonic settings

(e.g. the Roman Volcanic Province of Italy) in association with leucitite, shoshonite, and other potassic rocks (kamafugite, tephrite, leucite phonolite) whose origins are commonly considered to be related to recent complex subduction processes. These lamproites exhibit many of the same geochemical and mineralogical features as cratonic lamproites, but their genesis is considered to have a greater contribution of recent subducted island arc or oceanic lithospheric components (Conticelli and Manetti 1995; Miller et al. 1999; Conticelli et al. 2002; Prelević and Foley 2007; Gaeta et al. 2011; Lustrino et al. 2016, 2019) compared to the ancient metasomatized mantle sources of cratonic lamproites.

Mineralogical Criteria for Lamproite Recognition

Lamproites exhibit an extraordinarily wide range in texture and modal mineralogy owing to the diverse mineralogy of their mantle sources, whether they are extrusive or intrusive, and/or the products of magmatic differentiation. Many examples of this petrographic diversity are presented in Mitchell (1997). Accordingly, it is usually necessary to examine a suite of rocks in a potential lamproite field rather than basing identification on a single specimen.

Mitchell and Bergman (1991), Mitchell (1995a) and Woolley et al. (1996) considered that typical *cratonic* lamproites might contain the following major primary minerals: titanian (2–10 wt.% TiO_2), Al_2O_3-poor (5–12 wt.%) phlogopite phenocrysts (Fig. 1); titanian (5–10 wt.% TiO_2) groundmass poikilitic tetraferriphlogopite (Fig. 2); titanian (3–5 wt.% TiO_2) potassium (4–6 wt.% K_2O) richterite (Fig. 3); euhedral, hopper and/or "dog's tooth" forsteritic olivine (see below) phenocrysts and macrocrysts; Al_2O_3-poor (< 1 wt.%) diopside (Fig. 4); non-stoichiometric Fe-rich leucite (1–4 wt.% Fe_2O_3) (Fig.4); and Fe-rich sanidine (1–5 wt.% Fe_2O_3; Fig.4). Minor and common typomorphic accessory minerals include: priderite [$(K_2(Fe^{2+},Mg)Ti_7O_{16}$–$Ba(Fe^{3+},Cr,Mg)Ti_7O_{16}$; wadeite ($K_2ZrSi_3O_9$); Sr-rich apatite; Sr-rich perovskite; titanian magnesiochromite; armalcolite [$(Mg,Fe^{2+})Ti_2O_5$]; noonkanbahite–shcherbakovite [$(K,Na,Ba)_3(Ti,Nb)_2(Si_4O_{12}$]; baotite ($Ba_4Ti_8Si_4O_{28}Cl$–$Ba_4Ti_2Fe^{2+}{}_2Nb_4Si_4O_{28}Cl$); ilmenite; and jeppeite [$(K,Ba)_2(Ti,Fe^{3+})_6O_{13}$]; and other less common K–Ba–V-titanates (haggertyite, mannardite, redledgeite, unnamed $K_2Ti_{12}O_{25}$).

Kaapvaal lamproites are unusual in that many olivine lamproites (Sover, Bellsbank, Newlands, Swartruggens) contain significant amounts of calcite or dolomite. Pearson et al. (2019) have suggested that these rocks might be termed "carbonate-rich olivine lamproite" rather than "unevolved orangeites" (Mitchell 1995a) to distinguish them from rocks that exhibit typical phlogopite lamproite characteristics (Lace, Voerspoed,, Besterskraal). However, following lamproite mineralogical genetic classifications, "calcite phlogopite olivine lamproite" and "dolomite olivine lamproite" are preferred names. Other carbonate minerals identified in lamproites

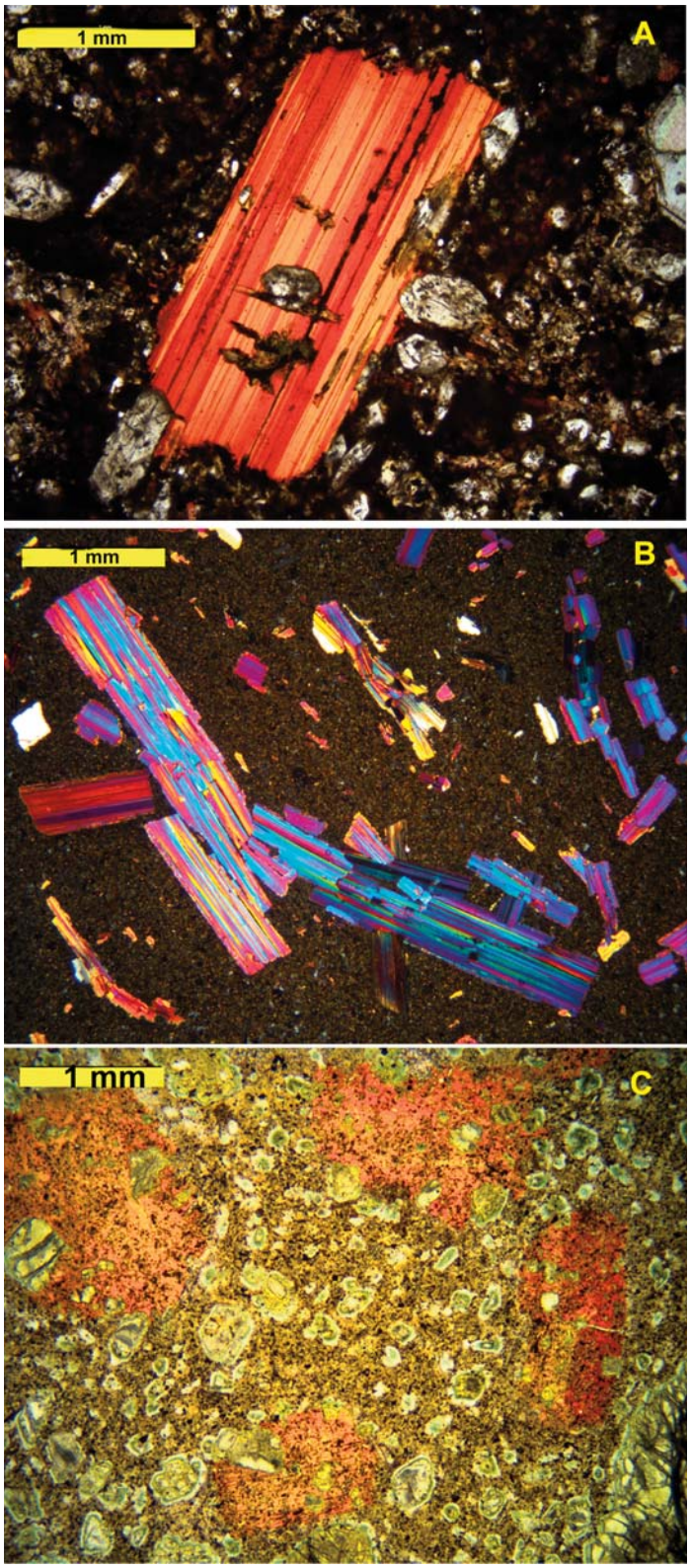

Figure 1. *(above right)* Typical appearance of titanian phlogopite in lamproites. (A) Polysynthetic twining in a phlogopite phenocryst from Mt. North (Ellendale Province) showing the characteristic lemon-yellow to orange-red pleochroism of parallel twins in different optical orientations. (B) Characteristic appearance under crossed polars of polysynthetically twinned titanian phlogopite phenocrysts from 81 Mile Vent (Ellendale Province). (C) Madupitic olivine lamproite from Prairie Creek (Arkansas) showing groundmass poikilitic (or oikocrystic) orange-red pleochroic titanian phlogopite with chadacrysts of diopside, spinel, and perovskite. Subhedral microphenocrysts are serpentinized olivine set in a groundmass of pale-yellow altered glass with spinel, diopside and perovskite.

https://doi.org/10.12789/geocanj.2020.47.162

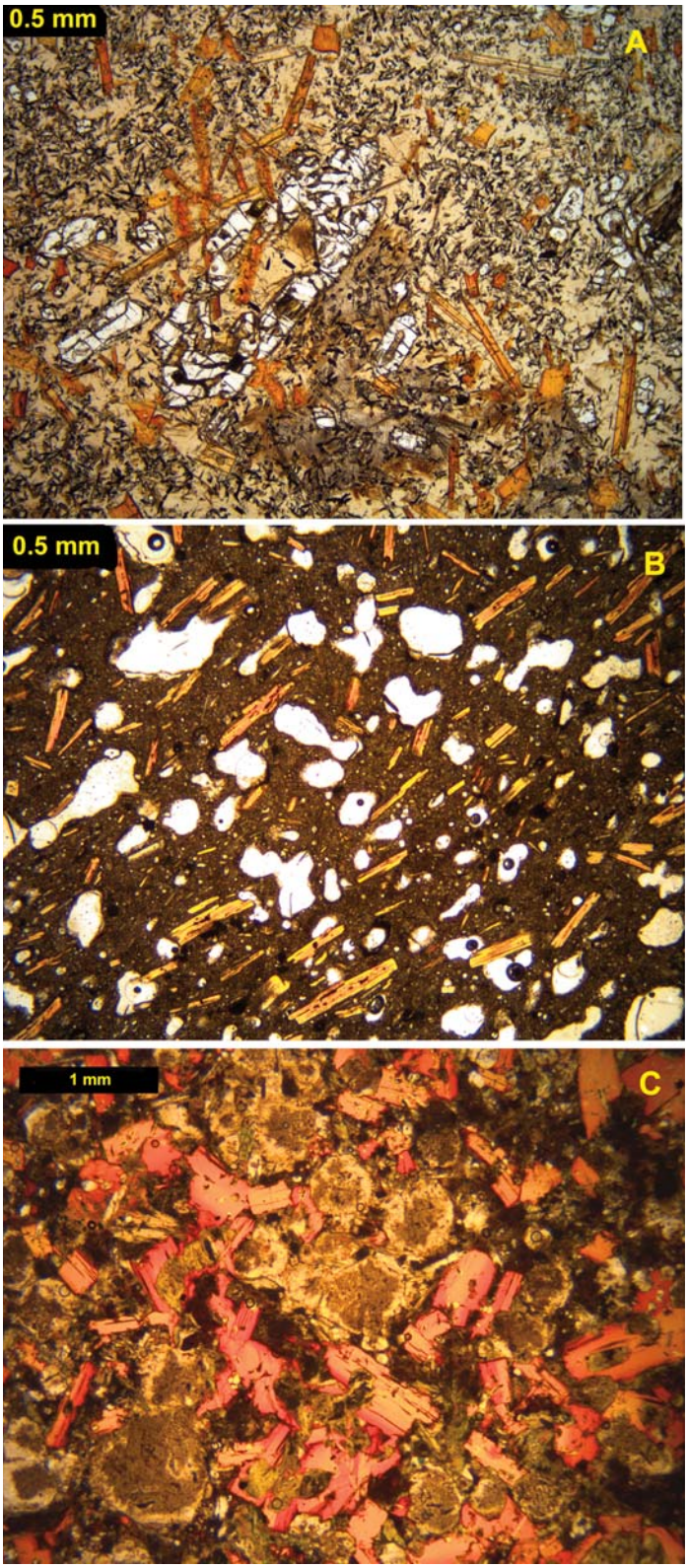

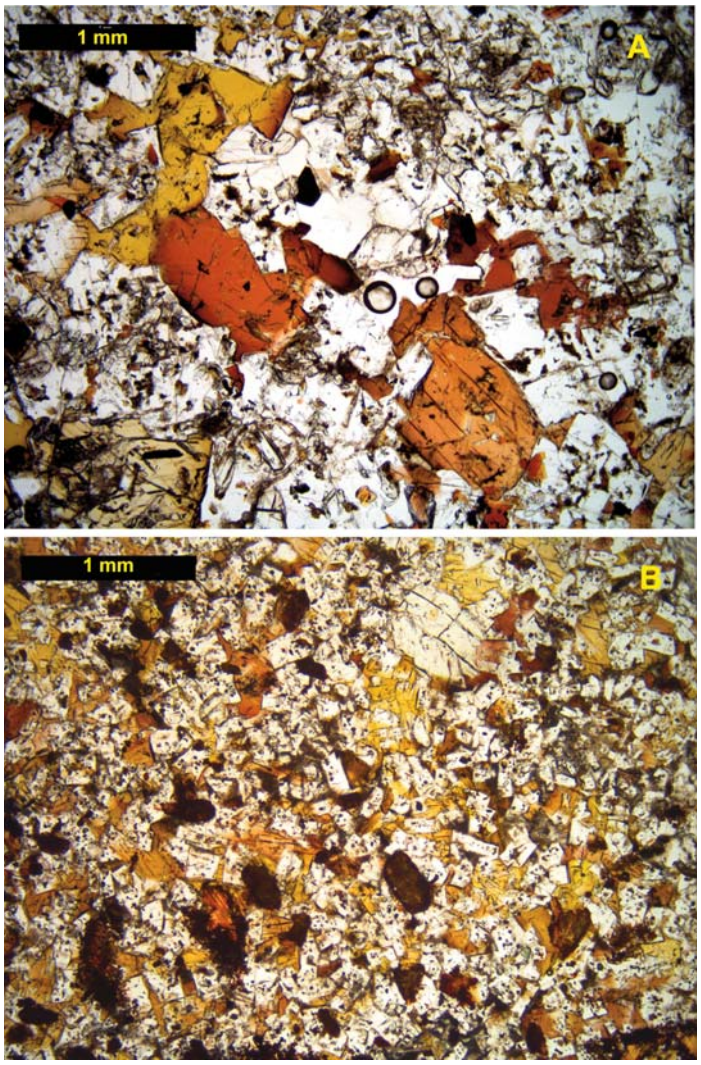

Figure 3. Examples of sanidine amphibole lamproite showing the characteristic lemon-orange to orange-brown pleochroism of groundmass poikilitic K–Ti-richterite. (A) Cancarix Sill (Murcia-Almeria Province) with colourless co-crystallizing potassium feldspar. (B) Moon Canyon (Utah) with microphenocrystal sanidine set in a matrix of K–Ti-richterite.

include witherite, ancylite, barian strontianite and norsethite. Further studies of the carbonate minerals are required.

The compositional trend of evolution from titanian phlogopite to Al-poor tetraferriphlogopite is a hallmark of lamproites and permits their discrimination from superficially similar kimberlites and minettes whose micas evolve to kinoshitalite or aluminous biotite, respectively (Mitchell and Bergman 1991).

Note that the presence of all of the above minerals in a rock is not required in order for it to be classified as a lamproite. Any one mineral might be dominant and in association with others determine the petrographic name.

Figure 2. *(above left)* Examples of phlogopite lamproite. (A) Hypabyssal hyalo-phlogopite lamproite from Smoky Butte (Montana) with resorbed phenocrysts of colourless olivine and prismatic phenocrysts of orange titanian phlogopite set in a matrix of microlitic diopside, armalcolite and pale-yellow glass. (B) Vesicular phlogopite lamproite lavas from Zirkel Mesa (Leucite Hills) with yellow-orange titanian phlogopite phenocrysts set in an optically unresolvable matrix containing diopside, altered leucite and glass. (C) Hypabyssal leucite phlogopite lamproite from Raniganj (Damodar Province) showing phenocrysts zoned from orange-yellow cores to red margins of titanian phlogopite. Former leucite is present as icosahedral phenocrysts altered to zeolite.

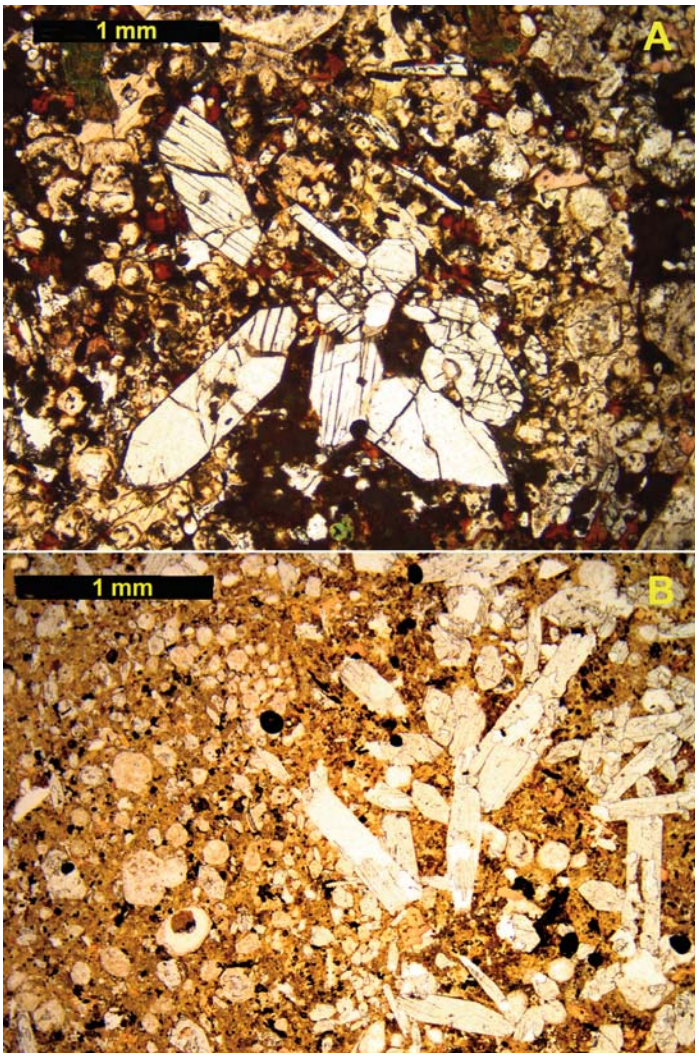

Figure 4. Examples of diopside leucite lamproite from P Hill (A) and Mt. Gytha (B), (Ellendale Province, West Kimberley) illustrating euhedral colourless diopside phenocrysts set in a matrix of altered microphenocrystal leucite with groundmass titanian phlogopite, K–Ti-richterite.

Orogenic lamproites are less easily recognized although they contain most of the major minerals listed above. In contrast to cratonic types the compositions of amphiboles tend to be more sodic, and potassium feldspars have higher Na_2O (2–3 wt.%) and Ca contents, but the latter rarely exceed 1 wt.% CaO. Typically, but not entirely, orogenic lamproites lack K–Ba-titanates, wadeite and other Ba–Ti-silicate minerals as a consequence of the relative depletion of the parental magmas in Ti, Ba, and Nb. However, many contain ilmenite and/or Ti–Cr-magnetite. Well-differentiated examples from Montecatini contain zircon, quartz, and perrierite (Conticelli et al. 1992), and at Cancarix lamproites contain dalyite, Cr–Zr-armalcolite, britholite, and roedderite (Contini et al. 1993). Further mineralogical studies are required to characterize the accessory mineralogy of orogenic lamproites. These assemblages will probably be quite variable as they depend upon the character and amount of the recent subducted material involved in their genesis.

GEOCHEMICAL CRITERIA FOR LAMPROITE RECOGNITION

Major and Trace Elements

Given the mineralogical heterogeneity of lamproites, it is not particularly useful to formulate geochemical criteria for their recognition. The bulk compositions of most lamproites, apart from glassy or fine-grained vesicular lavas, such as found in the Leucite Hills and at Smoky Butte (Table 2; compositions 1 and 2), do not represent liquid compositions. In addition, most olivine lamproites, in common with kimberlites, contain significant amounts of contamination by mantle-derived olivine xenocrysts and micro-xenoliths (Fig. 5) resulting in high Mg contents (Table 2; compositions 3–7). It is this feature, plus the presence of diamond, which has resulted in the past incorrect classification of many olivine lamproites as kimberlite. Regardless, the undersaturated, potassic nature of the magmas from which lamproite rocks crystallize confers upon their mineralogy some common geochemical characteristics. Thus, following the whole rock geochemical classification schemes of Foley et al. (1987) and Mitchell and Bergman (1991), *cratonic lamproites* are ultrapotassic (molar K_2O/Na_2O >3), commonly peralkaline [molar $(K_2O + Na_2O)/Al_2O_3$ >1] with [$Mg/(Mg + Fe^{2+})$ > 70], with low CaO (< 10 wt.%), high Ba (2000–5000 ppm), Zr (> 500 ppm) and Sr (1000–4000 ppm) contents coupled with high TiO_2 (1–7 wt.%). Note that bulk compositions are a direct reflection of mineralogy and vary within and between lamproite provinces, e.g. 3607–22102 ppm Ba versus 6600–16534 ppm Ba for West Kimberley and Smoky Butte phlogopite lamproites, respectively (Mitchell and Bergman 1991).

Orogenic lamproites are also ultrapotassic as defined by Foley et al. (1987). Compared to cratonic types they are also rich in SiO_2 (~ 48–60 wt.%) and K_2O (3–11 wt.%), and are characterized by relatively low TiO_2 (< 3 wt.%), Al_2O_3 (8–14 wt.%), and CaO (3–4 wt. %) with 0.5–4 wt.% Na_2O (Prelević et al. 2008a). In common with cratonic types they are enriched in LREE, but in contrast are also enriched in Pb (55–150 ppm) relative to cratonic lamproite (e.g. phlogopite lamproite from the Leucite Hills and Smoky Butte, 24–32 ppm and 0.2–44 ppm, respectively). These lamproites are not as enriched in Ba and Zr (< 3000 ppm) as cratonic lamproites, e.g. 1200–3055 ppm Ba and 295–1045 ppm Zr, versus 3065–24800 ppm Ba and 1250–8139 ppm Zr, for Murcia-Almeria and Leucite Hills phlogopite lamproites, respectively. Krmíček et al. (2011) have suggested that a ternary Th–Hf–Nb/2 geochemical discrimination diagram can be used to distinguish cratonic (> 100 ppm Nb) from orogenic lamproites (< 100 ppm Nb). However, in general, trace element discrimination diagrams are not especially useful for lamproite identification as in many instances there is considerable overlap with the compositions of minettes and diverse potassic rocks (Mitchell and Bergman 1991). Prelević et al. (2008b) have concluded from a study of a Turkish lamproite province, in which both cratonic and orogenic lamproites apparently coexist, that the geodynamic distinction of lamproites based only on geochemistry is questionable.

Similar reservations exist with respect to bulk rock incompatible trace element data normalized to primitive mantle com-

https://doi.org/10.12789/geocanj.2020.47.162

Table 2. Representative compositions (wt.%) of cratonic and orogenic lamproites.

	1	2	3	4	5	6	7	8	9	10
SiO_2	55.12	52.94	43.56	39.46	44.10	35.3	28.4	57.2	56.72	60.62
TiO_2	2.58	5.14	2.31	2.61	3.20	1.09	1.24	1.78	1.58	0.86
Al_2O_3	10.35	8.55	7.85	3.53	3.50	2.73	2.94	8.98	13.40	12.88
Fe_2O_3	3.27	5.65	5.57	8.78	4.50			5.89	3.34	5.51
FeO	0.62		0.85		3.09	8.56	7.60		2.42	
MnO	0.06	0.07	0.15	0.13	0.12	0.18	0.33	0.06	0.07	0.10
MgO	6.41	8.38	11.03	26.67	21.30	26.9	15.3	7.99	5.13	5.06
CaO	3.45	4.51	11.89	5.14	3.74	8.43	19.4	3.66	5.27	3.93
SrO	0.26	0.38	0.40	0.14	0.11	0.21	0.19	0.09	0.14	0.10
BaO	0.52	0.86	0.66	0.23	1.05	0.51	0.37	0.22	0.28	0.26
Na_2O	1.29	0.96	0.74	0.29	0.93	0.13	0.15	1.22	2.08	2.62
K_2O	11.77	8.84	7.19	2.56	6.51	2.73	2.66	8.72	8.02	6.23
P_2O_5	1.40	2.21	1.50	0.29	1.13	0.64	1.68	0.83	0.67	0.60
H_2O^+	1.23		2.89	7.70	3.09	5.79	6.98			
CO_2	0.20			0.21	0.28	4.64	9.46		0.02	
LOI		0.83		1.75	2.54				0.01	1.37
Total	99.06	99.32	98.68	99.49	99.19	97.84	96.7	100.09	99.15	100.14

Cratonic lamproites: 1, hyalo-phlogopite lamproite, Steamboat Mountain, Leucite Hills (Carmichael 1967); 2, hyalo-armalcolite phlogopite lamproite, Smoky Butte (Mitchell et al. 1987); 3, madupitic lamproite, Pilot Butte, Leucite Hills (Carmichael 1967); 4, olivine madupitic lamproite, Prairie Creek (Scott Smith and Skinner 1984); 5, olivine lamproite, Ellendale 9,West Kimberley (Jaques et al. 1986); 6, 7, olivine phlogopite lamproites, East Star and Wynandsfontein, respectively, South Africa (Coe et al. 2008). **Orogenic lamproites:** 8, phlogopite lamproite, Cancarix, Spain (Venturelli et al. 1984); 9, phlogopite lamproite, Mibale, Tibet (Gao et al. 2007); 10, phlogopite lamproite, Xungba, Tibet (Miller et al. 1999).

positions (a.k.a. spidergrams) as these diagrams were initially devised for whole rock compositions which approximate to melt compositions (i.e basalt) derived from mineralogically simple mantle sources (e.g. garnet lherzolite). *Hence, these diagrams cannot be applied usefully for petrogenetic purposes to magmas derived from heterogeneous multi-phase metasomatized mantle sources.* Attempts to force particular lamproites, e.g. Majhgawan, into pre-existing petrological groups such as kimberlites and "orangeites" are doomed to failure as their mantle sources are different. Hence, there can be no "transitional" magma types and the proposed re-introduction of type locality names, such as "majhgawanite" (Chalapathi Rao 2005), is regressive and petrogenetically unsound. However, these diagrams can be useful for illustrating the significant differences in lamproite geochemistry within and between provinces. Thus, Prelević et al. (2008a, b) have demonstrated that orogenic lamproites exhibit negative anomalies for Rb, Ba, Nb, Ti, Sr, and P with a significant positive Pb anomaly relative to cratonic lamproites (Fig. 6). However, interpretation of these differences requires a thorough knowledge of the tectonic regimes of emplacement.

Isotopic Variations

Isotopic studies have resulted in a better understanding of the mantle origins of lamproites and highlighted the significant differences between cratonic and orogenic types. Current petrogenetic models for lamproites rely extensively on these data. In these models it is considered that the Nd, Sr, Hf, and Pb isotopic compositions (McCulloch et al.1983; Vollmer et al. 1984; Nelson et al. 1986; Mitchell and Bergman 1991; Mitchell 1995a) of cratonic lamproites do not reflect upper crustal contamination and indicate derivation of parental magmas by single stage partial melting of lithospheric mantle sources which have undergone long term enrichment in light REE (i.e. low Sm/Nd ratios) and Rb (i.e. high Rb/Sr ratios), coupled with depletion in U. Each cratonic lamproite province has wide and distinct isotopic compositions reflecting the age and local modal mineralogy, and thus geochemistry, of their metasomatized lithospheric mantle sources. Of particular significance, is that all cratonic lamproites plot on Nd–Sr isotopic diagrams below the bulk Earth Nd composition with Sr isotopic compositions, suggesting extremely wide variations in the apparent Rb/Sr ratios of their sources (Fig. 7). The West Kimberley leucite lamproites are notable in being extremely rich in radiogenic Sr; a feature considered to reflect the high Rb/Sr ratio of their source relative to that of the Smoky Butte lamproites derived from sources with much lower Rb/Sr and very low Sm/Nd ratios (Fig. 7). Note that lamproites differ significantly with respect to kimberlites which have relatively uniform isotopic compositions (Fig.7) and are enriched in radiogenic Nd relative to bulk Earth and depleted in radiogenic Sr, suggesting derivation from REE-depleted asthenospheric sources (Pearson et al. 2019) with ancient low Rb/Sr and high Sm/Nd ratios.

Orogenic lamproites also exhibit an extremely wide range in Sr, Nd, Pb, and Hf isotopic compositions with notable differences between eastern (Serbia, North Macedonia, Turkey) and western provinces (Spain, Italy), and Tibet (Fig. 7; Miller et

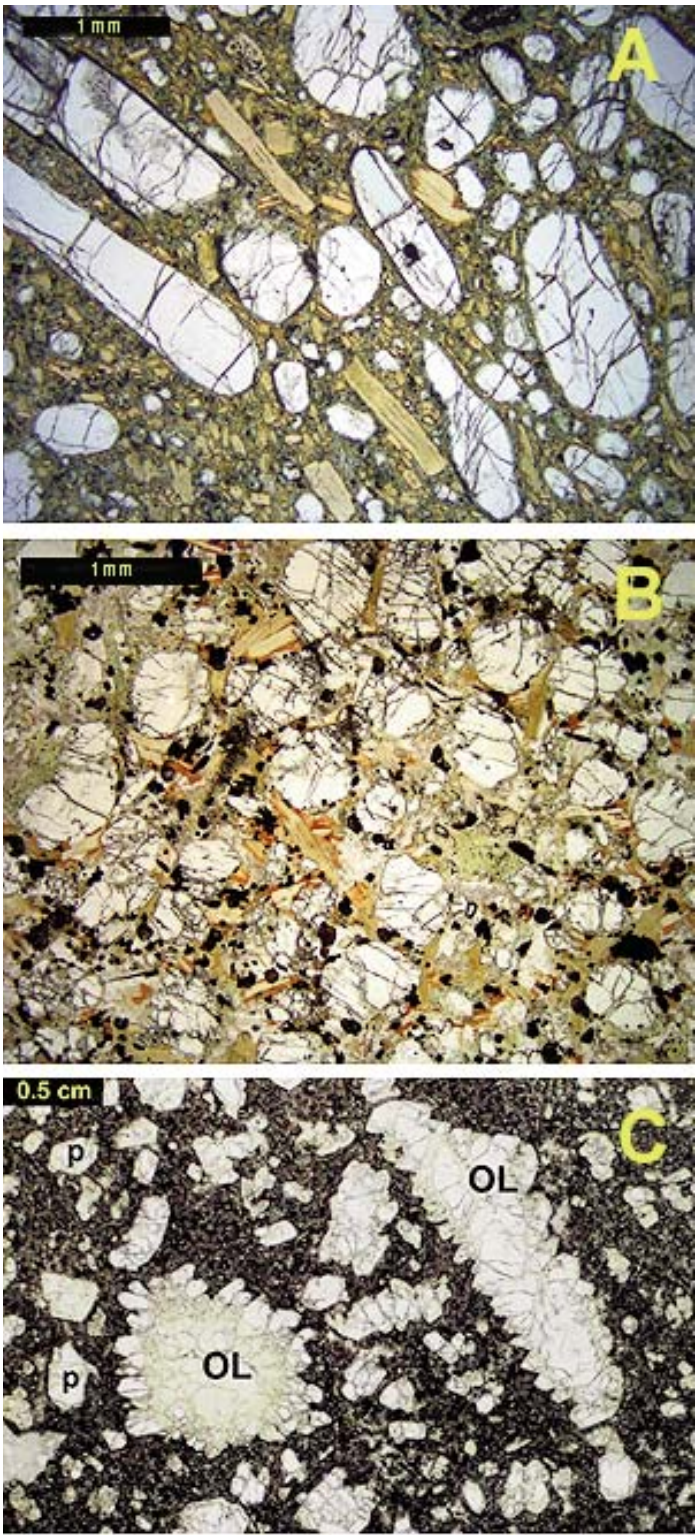

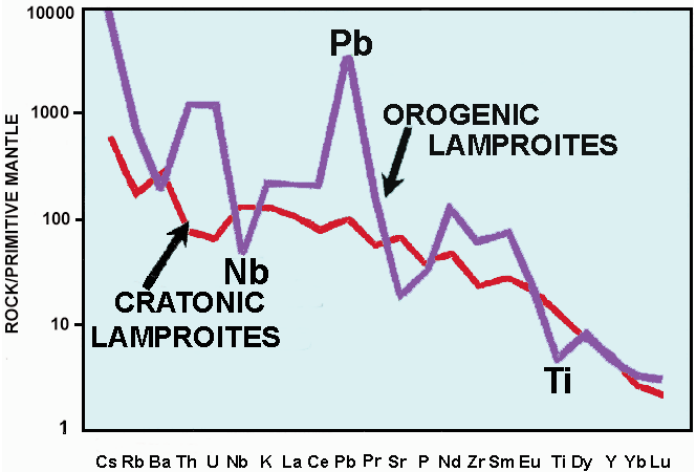

Figure 6. Typical trace element signatures of cratonic versus orogenic lamproites illustrating the characteristic positive Pb and negative Nb and Ti anomalies (after Prelević et al. 2008a).

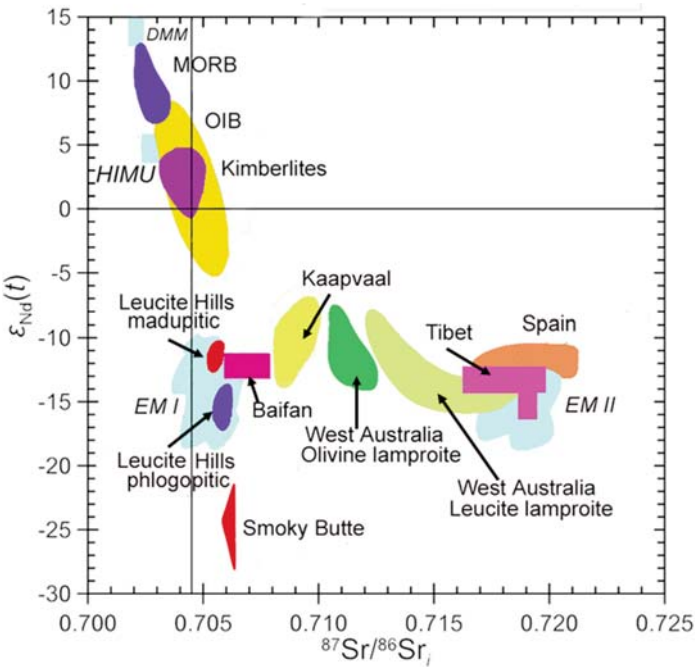

Figure 7. Sr and Nd isotopic signatures of representative cratonic and orogenic lamproites (after Xiang et al. 2020).

al. 1999; Prelević et al. 2008a, b, 2010). The differences are considered to reflect differences in the isotopic composition of the young subducted continental margin sedimentary material involved in their genesis. A major difference between cratonic and orogenic lamproites is their Pb isotopic composition (Fig. 8). The $^{207}Pb/^{204}Pb$ ratios of cratonic lamproites range from

Figure 5. *(above left)* Examples of olivine lamproite. (A) Macrocrystal phlogopite olivine lamproite from the East Star Fissure Mine (South Africa) with colourless resorbed olivine macrocrysts and pale yellow phlogopite phenocrysts set in a groundmass of phlogopite microphenocrysts, perovskite, chromite, chlorite, and minor carbonate. The margins of many of the phlogopite crystals are altered to red tetraferriphlogopite. (B) Hypabyssal olivine lamproite from Manitsoq (Greenland) with subhedral-to-anhedral olivine macrocrysts set in a matrix of yellow-to-red phlogopite-tetraferriphlogopite, together with opaque perovskite and chromite. (C) Hypabyssal olivine lamproite from Prairie Creek (Arkansas) illustrating primary olivine overgrowths on macrocrystic olivine cores forming a "dog's tooth" texture. The optically unresolved groundmass consists of diopside, phlogopite, perovskite and chromite.

https://doi.org/10.12789/geocanj.2020.47.162

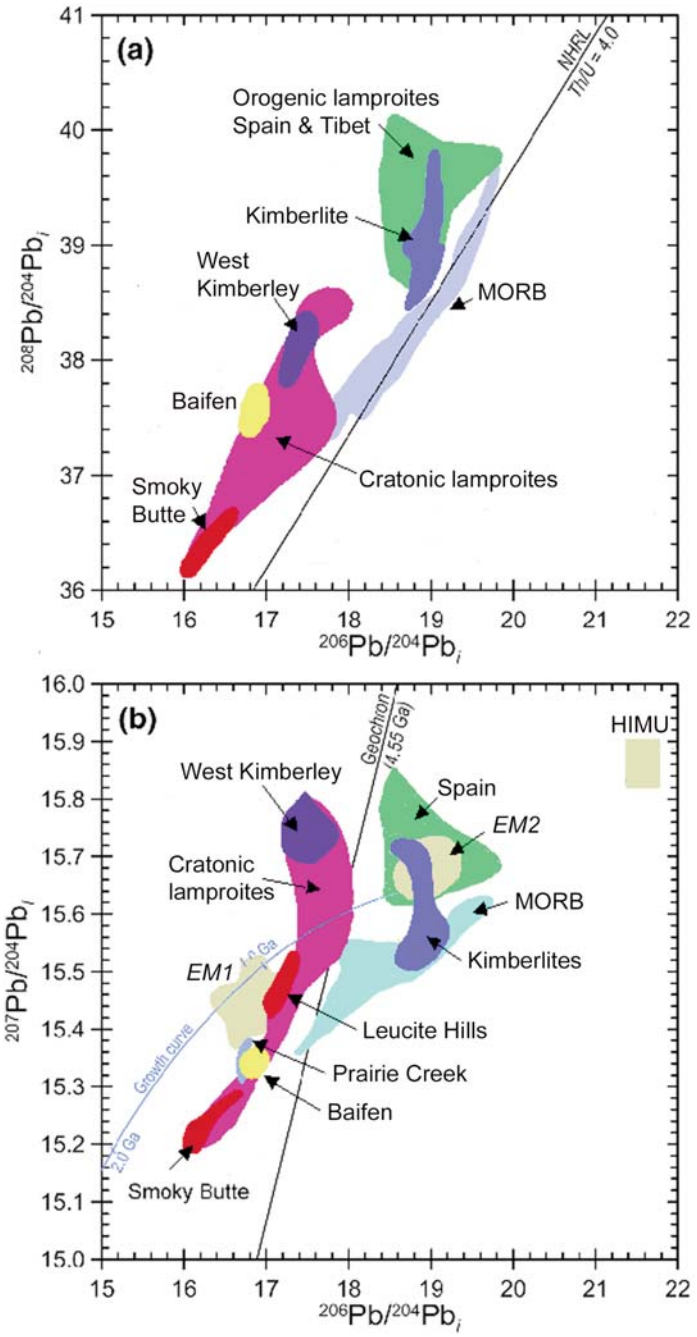

Figure 8. Pb isotopic signatures of representative cratonic and orogenic lamproites (after Xiang et al. 2020).

15.2 to 15.8 and overlap with EM1-type mantle compositions. Orogenic lamproites also exhibit high $^{207}Pb/^{204}Pb$ ratios but have a more restricted range from ~ 15.6–15.85 with overlap with EM2-type mantle. The two groups can be distinguished by the cratonic types having less radiogenic $^{206}Pb/^{204}Pb$ (< 18) and $^{208}Pb/^{204}Pb$ ratios (< 38.6) ratios relative to the more radiogenic $^{206}Pb/^{204}Pb$ (18.5–19) and $^{208}Pb/^{204}Pb$ (> 38.6) signatures of orogenic lamproites (Fig. 8).

Interestingly, the western Mediterranean lamproites have similar isotopic compositions to the West Kimberley leucite lamproites (Fig. 7) in exhibiting a very wide range in $^{87}Sr/^{86}Sr$ (0.714–0.722) at near-constant $^{143}Nd/^{144}Nd$ (~ 0.512). Regardless of this similarity, these isotopic signatures have very different origins. Whereas the West Kimberley compositions probably represent single stage partial melting of ancient metasomatized cratonic mantle, the orogenic lamproites require recent mixing of different mantle components, namely a lithospheric mantle source contaminated by subducted continental young sedimentary rocks, a convecting mantle component, and a depleted asthenospheric mantle component (Prelević et al. 2005, 2008a, b).

GEOLOGICAL RELATIONSHIPS

Lamproite magmas behave, in terms of their rheology, in a manner very similar to basaltic magmas. Detailed descriptions of the extrusive and intrusive bodies which they form is beyond the scope of this review and can be found in Mitchell and Bergman (1991) and Jaques et al. (1986). Lamproites can be found as: subaerial vesicular and glassy lava flows (Steamboat Mountain, Zirkel Mesa, Wyoming); lava lakes (Ellendale, Australia); cinder cones (Emmons Cone, Wyoming); lava tubes (Steamboat Mountain, Wyoming); diverse pyroclastic and volcaniclastic rocks (Prairie Creek, Arkansas; Majhgawan, India; Argyle, Australia); differentiated sills (Rice Hill, Australia; Cancarix, Spain); and hypabyssal dyke swarms and minor intrusions (Sisimiut and Manitsoq, Greenland; Smoky Butte, Montana; Raniganj, India). Because of the small volumes of lamproitic magmas, e.g. for the Leucite Hills it is estimated that the total volume of erupted magma is only ~ 0.66 km^3 (Lange et al. 2000), they do not appear to form large intrusions of plutonic rocks and the only known pluton is the small (2.7 x 2.5 km; 5–10 km^3) Walgidee Hills intrusion, Australia (Jaques et al. 1986, in press).

Many pyroclastic and hypabyssal olivine lamproites (Fig. 9) are diamond-bearing. Because of their economic relevance, lamproite vents and their associated pyroclastic rocks are some of the more important representatives of the lamproite clan. The principal examples are found in: the West Kimberley region of Australia (Ellendale Field, Argyle AK1 Mine); Finsch and Lace Mines (South Africa); Prairie Creek (Arkansas); Majhgawan and Atri (India); and the Kapamba Field (Zambia). Although of small volume, many of the hypabyssal Kaapvaal lamproite dykes are significant sources of diamond. Commonly referred to in South Africa as "fissure mines" the principal examples are: the Roberts Victor; Bellsbank; Sover; New Elands; Star; and Swartruggens mines (Field et al. 2008). Elsewhere, relatively poorer diamond-bearing hypabyssal lamproites include the Bobi and Seguela dykes of Côte d'Ivoire and intrusions in the Wajrakarur region of the Eastern Dharwar craton of India. In contrast to the abundance of diamond-bearing lamproites in the African and Indian cratons, lamproites in North America (Smoky Butte, Leucite Hills, Hills Pond) and Greenland (Sisimiut, Manitsoq) are typically barren with only the Prairie Creek Field carrying significant diamond.

Lamproite Vents

The nature of the country rocks into which lamproites are

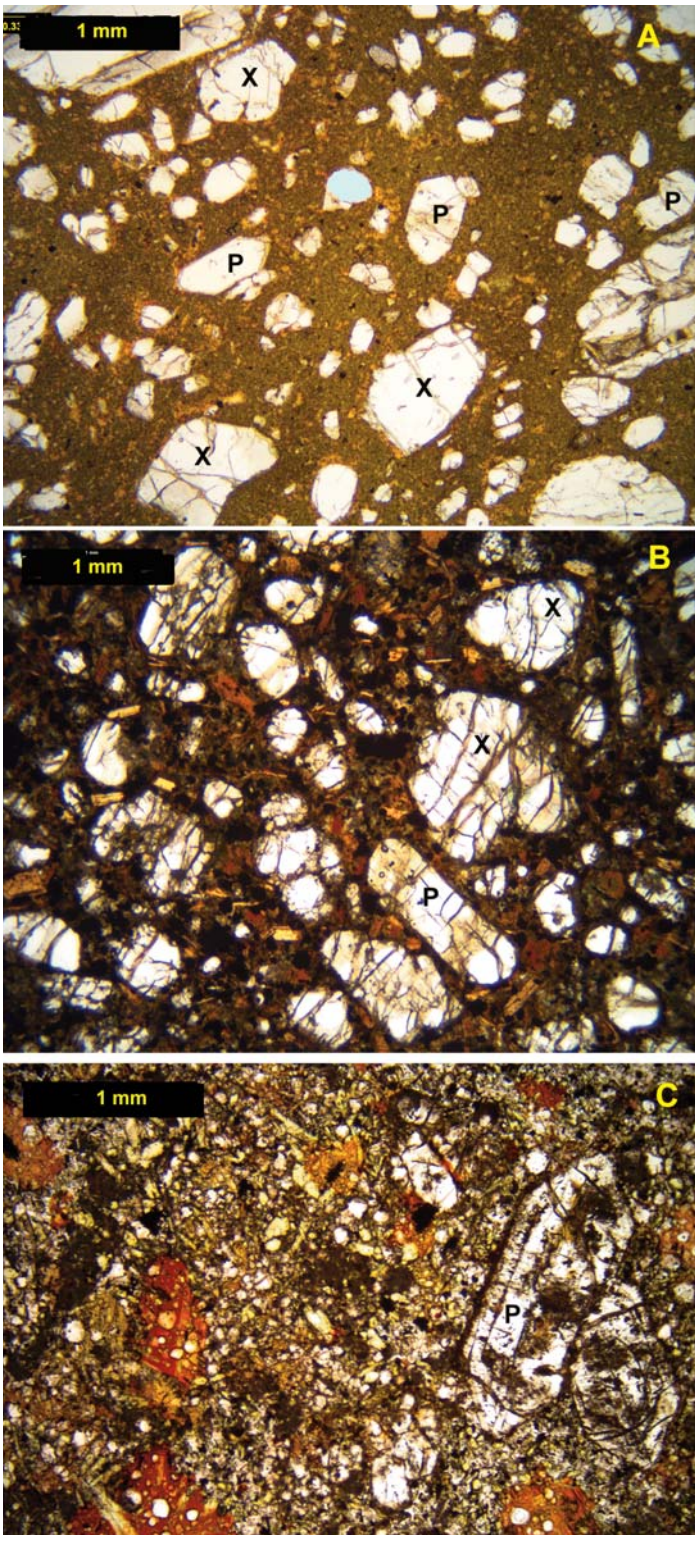

Figure 9. *(above left)* Representative olivine lamproites. (A) Ellendale olivine lamproite with macrocrysts, or xenocrysts (X) of anhedral olivine with minor euhedral primary olivine microphenocrysts (P). The optically, essentially unresolvable, groundmass contains fine-grained diopside, priderite and chromite with poikilitic yellow Ti-phlogopite. (B) Sisimiut olivine lamproite (West Greenland) with olivine macrocrysts/xenocrysts (X) and primary olivine (P) and microphenocrysts of yellow Ti-phlogopite set in a groundmass with diopside microlites and red Ti-phlogopite-tetraferriphlogopite. (C) Madupitic olivine lamproite from Majhgawan (India) with mantled primary olivine phenocrysts (P) set in groundmass with microlitic diopside, altered leucite, chromite in poikilitic red–yellow pleochroic Ti-phlogopite.

intruded plays a significant role in the style of lamproite magmatism. Lamproite vents with abundant pyroclastic or volcaniclastic rocks are found primarily where the magmas have intruded weakly consolidated sedimentary sequences and where there are significant aquifers. Emplacement in other geological environments results in lavas and/or dykes without pyroclastic sequences. Thus, the major Leucite Hills lamproite province of Wyoming does not contain any pyroclastic or volcaniclastic vents and their expression is as subaerial lavas, monogenetic cinder cones and minor hypabyssal dykes and plugs (Carmichael 1967). Lamproites emplaced in basement crystalline metamorphic rocks typically form dyke swarms, as at Sisimiut and Manitsoq (Greenland).

Although lamproite pyroclastic and phreatomagmatic vents are unlike diatremes formed by Kimberley-type pyroclastic kimberlites they do bear a resemblance to vents formed by the Fort à la Corne-type pyroclastic kimberlites (Scott Smith 2008) as a result of the significant hydrovolcanism involved in the formation of the latter. Because of their economic significance brief descriptions of representative examples of diamond-bearing lamproite occurrences are presented below to illustrate the common factor of phreatomagmatism in their emplacement and the complexities of the geology of these vents.

Argyle AK1 Diamond Deposit, West Kimberley, Australia

The 1180 Ma diamondiferous (30–680 ct/100 t) Argyle AK1 vent was emplaced in Paleo- and Mesoproterozoic sandstone, siltstone, and shale within the Halls Creek orogen at the southeastern margin of the Kimberley craton. Subsequent to emplacement the lamproites were subjected to major and minor faulting. The bulk of this elongate steep-sided NNE-trending deposit (~ 47 ha) consists of pyroclastic or volcaniclastic olivine lamproite intruded by minor late-stage olivine lamproite dykes.

Exploration and mining (Jaques et al. 1986; Boxer et al. 1989; Rayner et al. 2018) have shown that AK1 is a composite body consisting of a large Southern Vent (or diatreme) with two feeder zones, a smaller two phase Northern Vent, and a small elongated unit known as the Southern Extension (or Tail). In outcrop (Fig. 10), the lamproites of the Northern Vent narrow southwards from 500 m in the north to a width of ~ 150 m where they are offset from the Southern Vent by the major sinistral NNW-trending Gap Fault system. South of this fault the main part of the deposit consisting of the Southern Vent(s) extends a further ~ 750 m until it is terminated by the Razor Ridge Fault. This dextral fault has displaced the lamproites to the west as the 400 m x 50 m Southern Extension unit.

The AK1 deposit consists of volcaniclastic olivine lamproites, commonly referred to as "sandy tuffs" and "non-

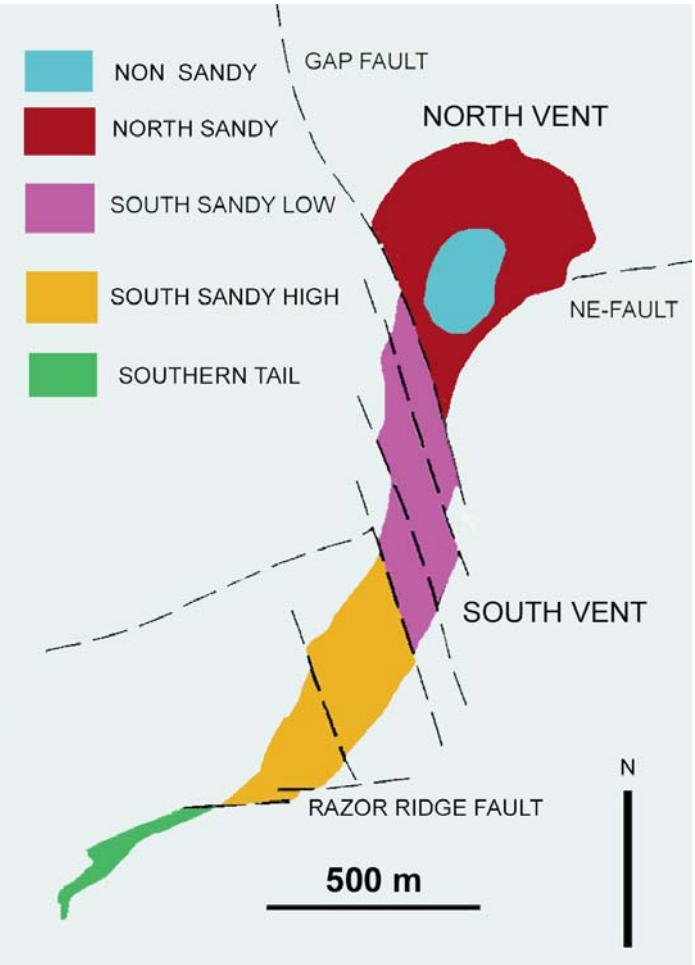

Figure 10. Outcrop map of the Argyle AK1 lamproite showing the mining domains (after Roffey et al. 2018).

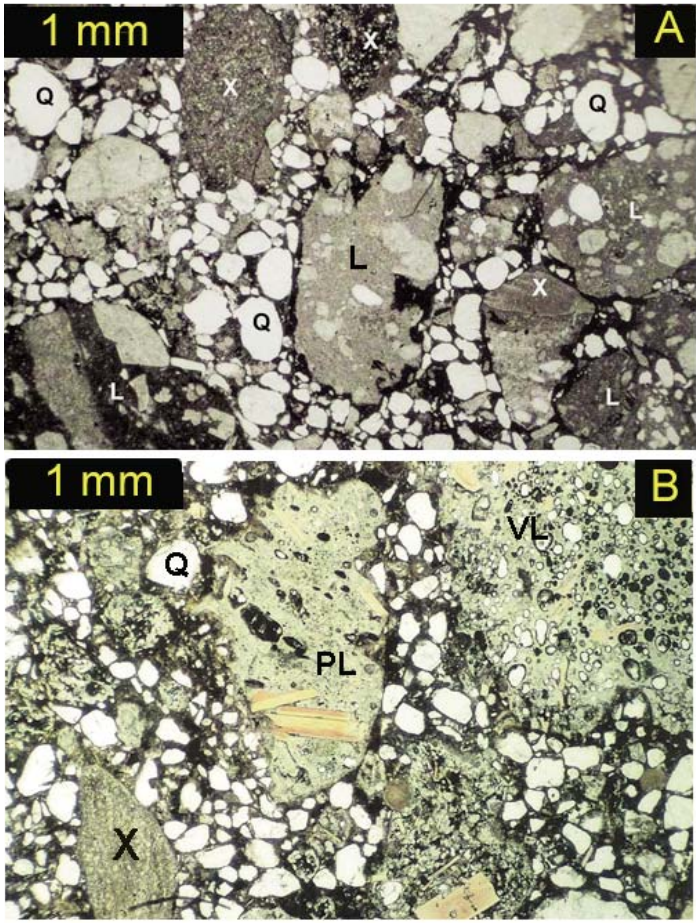

Figure 11. Representative examples of "sandy tuffs" or volcaniclastic phlogopite olivine lamproites from Argyle AK1 (A) and Ellendale Seltrust Pipe 3 (B). Q = quartz xenocryst; X = country rock xenoliths; L = olivine lamproite clasts; PL = phlogopite olivine lamproite clasts; VL = vesicular olivine lamproite clast. Note that the quartz xenocrysts are rounded, a morphology suggesting that the sandstone was not consolidated at the time of intrusion.

sandy tuffs", on the basis of the presence or absence of xenocrystic quartz derived from poorly consolidated country rocks. The bulk of the deposit (Southern Vent, Southern Extension, most of the Northern Vent), consists of sandy tuffs (Fig. 11A) which are correctly termed quartz-rich volcaniclastic olivine lamproite in modern terminology by Rayner et al. (2018). Figure 10 illustrates that the current mining domains of the Southern Vent are divided into low (< 10 ct/t) and high grade (> 10 ct/t) lamproites, representing different episodes of volcanism. The sandy tuffs of the Northern Vent (< 5 ct/t) have been intruded by lapillar and devitrified lapillar tuffs (non-sandy tuffs) consisting of juvenile lapilli and ash of olivine lamproite.

With respect to the sandy tuffs, four main lithological units are recognized: bedded quartz-rich lapilli tuffs, bedded quartz-rich ash tuffs, bedded quartz-rich fine ash tuffs, and massive quartz-rich lapillar tuffs. Detailed descriptions of these units are given by Rayner et al. (2018). The sandy tuffs show extensive variation in components, texture and bedding, but have common characteristics of formation as multiple small volume maar-type eruptions in a phreatomagmatic environment (Jaques et al. 1986; Boxer et al. 1989).

In common with other lamproite vents, initial phreatomagmatism resulted from ascending magma interacting with water-saturated sedimentary units in a fault zone. Maar-type volcanism probably occurred at progressively deeper levels leading to crater formation and coalescence of vents along the main fracture zone. Collapse of rim pyroclastic deposits into the vents resulted in interbedded resedimented and primary volcaniclastic olivine lamproite. The current presence of bedded pyroclastic layers at deep levels (1200 m) in the AK1 vents suggests that continuous subsidence of the vent fill occurred. During the final stages of activity, olivine lamproite magma was erupted into the Northern sandy tuffs. The textures and alteration of the olivine lamproite lapilli forming these non-sandy tuffs resemble those of hyaloclastite, suggesting eruption into a crater lake (Boxer et al. 1989). In contrast to the Ellendale Field (see below), lava lakes were not formed at Argyle, this being a direct consequence of the differences in the character of the country rocks.

Ellendale Field, West Kimberley Province, Australia

The 45 lamproite volcanic centres of the 22–20 Ma Ellendale

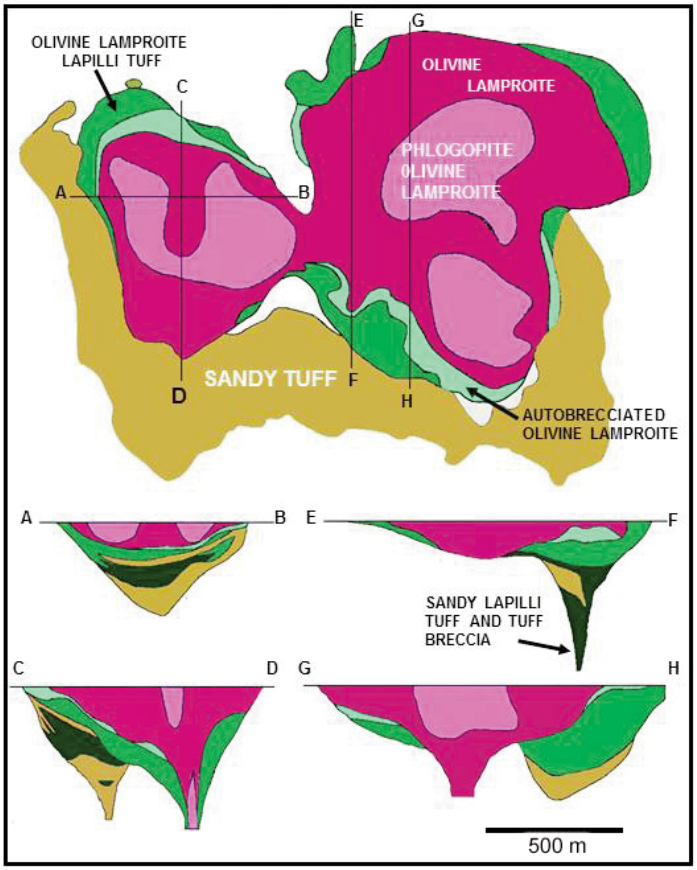

Figure 12. Morphology of a typical lamproite phreatomagmatic vent (Ellendale 4, West Kimberley Province) with subaerial pyroclastic "sandy tuffs" of phlogopite olivine lamproite and the vent filled by holocrystalline magmatic olivine lamproite as lava lakes (after Jaques et al. 1986).

Lamproite Field (Jaques et al. 1986) range from single vents (81 Mile Vent, Ellendale 9) to complex multiple vents (Ellendale 4; Fig. 12). The intrusions in this field exhibit a wide range of morphology and mineralogy ranging from unexposed diamondiferous (< 1–14 ct/100 t) olivine lamproite through phlogopite lamproite as columnar-jointed eroded vents (Mt North) to leucite K-richterite diopside lamproite forming differentiated sills (Rice Hill). The field includes the highly evolved Waldigee Hills pluton characterized by the presence of abundant coarse-grained K–Ti-richterite, noonkanbahite, wadeite, priderite, jeppeite, haggertyite, apatite, Sr-perovskite (Jaques et al. in press).

The vents originate where dykes intruded poorly consolidated sedimentary rocks and aquifers of the Lower Permian Grant Group sandstone. An initial explosive phase produced laminated and bedded olivine lamproite tuffs (Fig. 11B) similar to the sandy tuffs found at Argyle AK1 (Fig. 11A). However, phreatomagmatism was not prolonged, as at Argyle, due to the smaller amount of poorly consolidated sedimentary rocks present in this area. The laminated tuffs consist principally of fractured quartz grains, ash-sized lamproite clasts, phlogopite flakes, and interstitial very finely comminuted lamproite ash (Fig. 11B). The bedded tuffs are airfall deposits similar to those

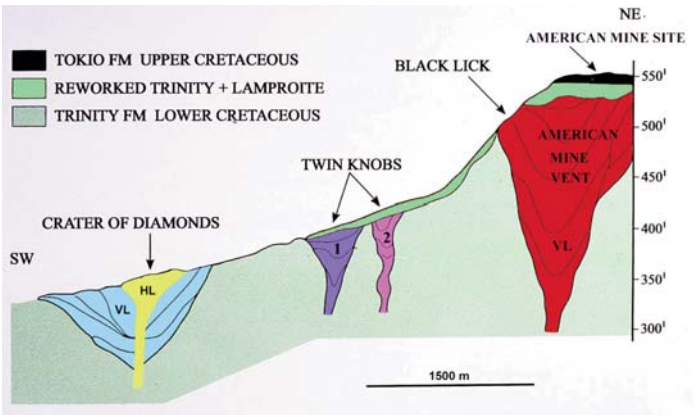

Figure 13. Cross-section of lamproite vents in the Prairie Creek Province (Arkansas) illustrating the differential exposure of four volcaniclastic phreatomagmatic vents (VL) as a result of post-emplacement erosion. Hypabyssal olivine lamproite (HL), emplaced in lamproite breccia, is exposed only adjacent to the Little Missouri River system in the Crater of Diamonds vent at the southwestern margin of the field. Vents with lesser degrees of erosion of the Lower Cretaceous country rocks are either hidden under later deposited Upper Cretaceous sedimentary rocks (Twin Knobs) or poorly exposed (Black Lick) at the southern margins of the large essentially un-exposed American Mine vent system. The American Mine was originally worked as scattered exposures in the overlying Tokio Formation. Note that the vertical scale is in feet.

associated with maar-type phreatomagmatic volcanism and consist of rounded quartz grains together with shale and lamproite clasts. The subsequent stages of activity in many of the occurrences are marked by intrusion of holocrystalline hypabyssal-like phlogopite, leucite and olivine lamproites into the tuffs with, in some instances, the formation of lava lakes in former craters.

Prairie Creek Field, Arkansas, USA

The 106–97 Ma Prairie Creek lamproite field (~13 ct/100 t) consists of several lamproite vents emplaced along a northeast–southwest-trending fracture zone into nearly flat-lying Carboniferous–Cretaceous sedimentary rocks (Meyer 1976; Mitchell and Bergman 1991; Dunn 2002). The field includes the Prairie Creek intrusion, also known as the Crater of Diamonds, the only known North American source of lamproite-derived diamonds. All vents contain pyroclastic rocks and hypabyssal olivine lamproite. Figure 13 illustrates how these lamproite vents, belonging to the same magmatic event, appear when subjected to various degrees of erosion. Significant erosion by the Little Missouri River has exposed the lower part of a vent, now represented by the Crater of Diamonds, exposing hypabyssal olivine lamproites (Fig. 1C) and diverse tuff breccias. In contrast, the upper levels of vents, characterized by diverse pyroclastic rocks, are preserved where there has been less erosion. The pyroclastic rocks are typically bedded (Fig. 14) with well-sorted and graded intervals of lithic tuff, and tuff breccia composed of fragments of country rock and juvenile phlogopite, and/or olivine lapilli set in a chloritic matrix with abundant xenocrystic quartz (Fig. 15). The abundance of quartz indicates eruptive disaggregation of the poorly consolidated country rock of the Jackfork sandstone, a member of the Trinity Formation, at depth.

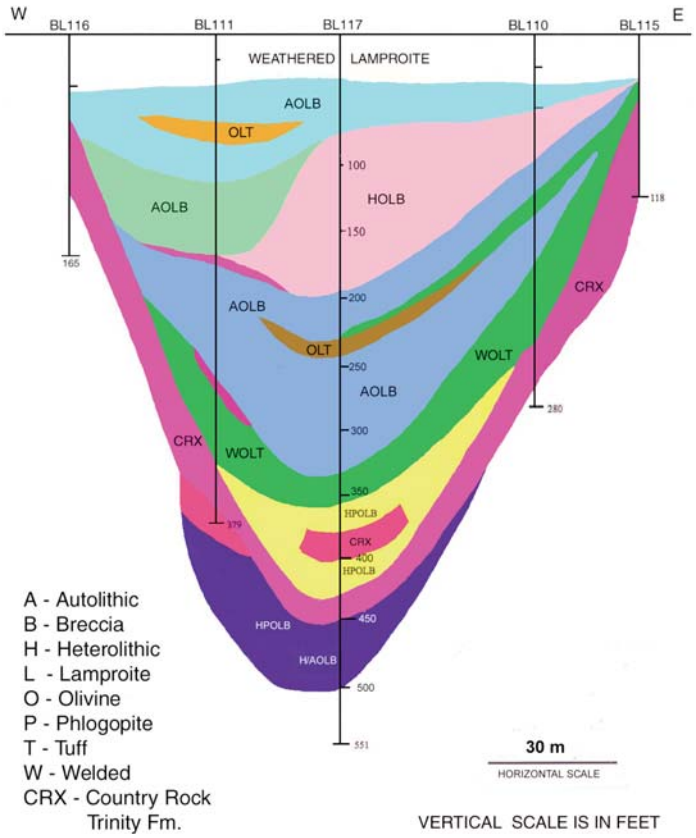

Figure 14. Geological cross-section of the Black Lick-American Mine pyroclastic vent (Prairie Creek Province) illustrating the complexity of the pyroclastic olivine lamproite tuff and breccia sequences. Each unit differs with respect to the abundance of country rock xenoliths, quartz xenocrysts, texture and style of alteration of olivine lamproite clasts. At this structural level hypabyssal lamproites are not present, although a feeder dyke is inferred on the basis of Figure 13 to occur at depth. (data courtesy of Star Resources and Iain F. Downie).

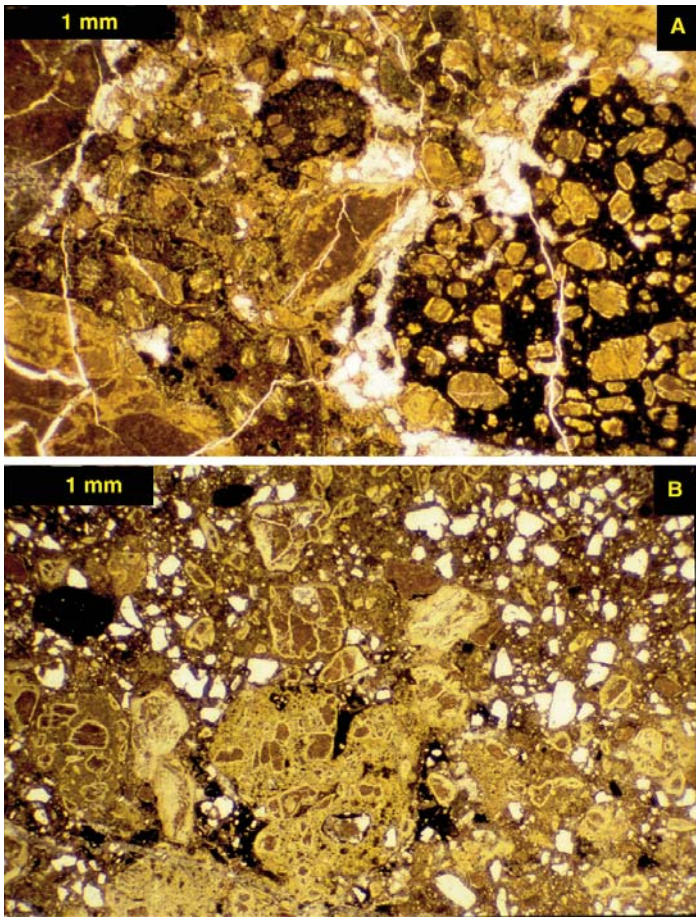

Figure 15. Volcaniclastic olivine lamproite tuffs from the Black Lick Vent (Prairie Creek Province). (A) heterolithic olivine lamproite tuff/breccia with relatively fresh olivine lamproite clasts. (B) quartz-bearing heterolithic olivine lamproite breccia ("sandy tuff") with extremely altered olivine lamproite clasts.

Finsch Mine, Northern Cape Province, South Africa

The 118 Ma diamond-bearing (~ 37 ct/100 t) rocks forming the cluster of dykes (Smuts, Botha and Bonza) and vents (Finsch, Shone, Bowden) were for many years considered to be kimberlite but are now recognized as *bona fide* lamproite. Unfortunately, the designation as Group 2 kimberlite persists in many publications concerned with diamond deposits (e.g. Field et al. 2008). The lamproites were intruded into the Proterozoic Griqualand West dolomite, banded iron formation, and shale. The Finsch mine occurs as a vent on the northeast-striking Smuts Dyke and consists of eight (F1–F8) main lamproite types (Clement 1982). Ekkerd et al. (2006) have described the sequence of emplacement and presented representative descriptions of the individual intrusions. The Finsch vent (Fig. 16) consists principally of phlogopite lamproite and diopside phlogopite lamproite breccia containing xenoliths of Karroo basalt and Griqualand West sedimentary rocks which have been intruded by hypabyssal phlogopite lamproite as a central body and as internal dykes and sills. Karroo-age rocks were present at the time of emplacement but have subsequently been removed by erosion.

Finsch hypabyssal lamproites are olivine phlogopite lamproites with serpentinized rounded olivine crystals set in a matrix of phlogopite laths, in turn set in a matrix of mica plates, microlitic diopside. perovskite, apatite, and spinel of various compositions. The Finsch F1 volcaniclastic lamproite is the most abundant unit and of similar mineralogy to the hypabyssal units**,** apart from the presence of abundant xenolithic material. The F8 lamproites are unusual in that large round lamproite magmaclasts similar to those occurring in the Pilot Butte lamproites and some Kimberley-type pyroclastic kimberlites (Mitchell 1997) are present.

Majhgawan, Madhya Pradesh, India

The diamondiferous Majhgawan volcaniclastic lamproites (ca. 7–19 ct/100 t) were intruded (ca. 1080–1067 Ma) into sandstone and shale of the Proterozoic Vindhyan Supergroup which were deposited at the southeastern margin of the Archean Bundelkhand Craton. At the current level of erosion the Majhgawan vent is exposed in the Kaimur Group sandstone and the overlying Rewa and Bhander groups, which are considered to have been present at the time of intrusion, and now found as xenoliths in the lamproite (Fareeduddin and Mitchell 2012).

The Majhgawan vent has been interpreted as a downward tapering cone-shaped body with a pear-shaped outcrop meas-

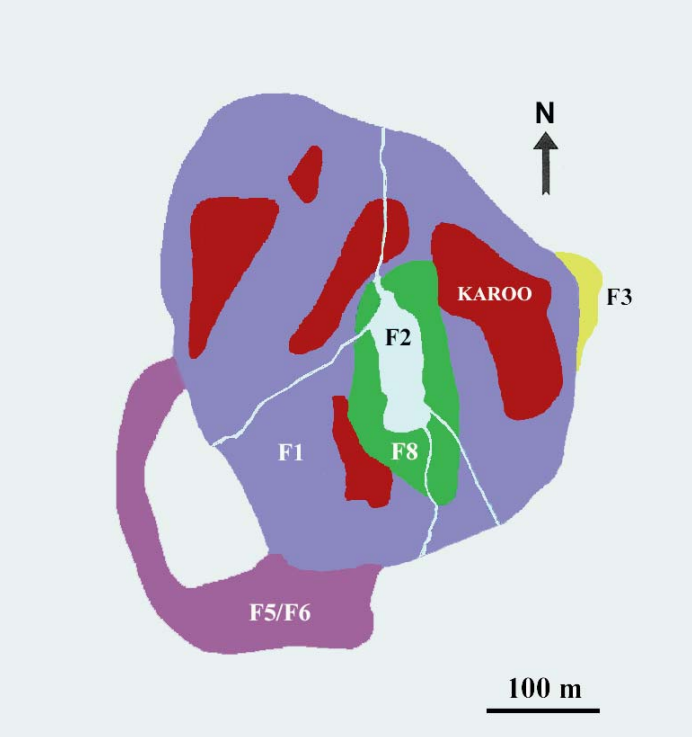

Figure 16. Plan view of the Finsch Mine lamproite, South Africa at the 510 m level showing the distribution of the diverse petrographic varieties of the lamproite and the presence of megaxenoliths of Karroo age sedimentary rocks (after Ekkerd et al. 2006).

uring 530 x 320 m. Recent drilling has shown that the vent is reduced in cross-section to about 125 m at depth of 330 m, suggesting that the volcaniclastic rocks originated from a hypabyssal feeder dyke emplaced in the Bundelkhand granite. The smaller (200 x 180 m) adjacent Hinota vent is considered to have been formed by a branch of this feeder dyke. The geology and mineralogy of this satellite vent is not well characterized as it appears to have no economic potential.

Regardless of the antiquity of mining, the geology of the Majhgawan vent is not well-understood, in part, due to the paucity of exploration drilling and the intermittent character of mine operations. Models presented by Mathur and Singh (1971) and Rao (2007) have suggested the vent consists of concentric bands of volcaniclastic rocks all of which taper to a common focal point at unknown depth. Given the complexities of other lamproite vents, in particular the Atri Pipes (see below; Das et al. 2018), revealed by recent studies, such a model is highly improbable and should be re-evaluated. The vent fill consists of diverse heterolithic olivine lamproite breccias distinguished on the basis of colour, grain size, content of xenoliths, and abundance of mica (Fig. 17). The margins of the vent on the east and west sides are different varieties of breccia, and the finer grained core is an intensely brecciated mica-free lamproite. The breccias contain clasts of vesicular pyroclastic lamproite (see below).

Interpretation of the geology and petrology of the vent has been hampered by the incorrect designation as "kimberlite", "transitional kimberlite", "orangeite", or "majhgawanite"

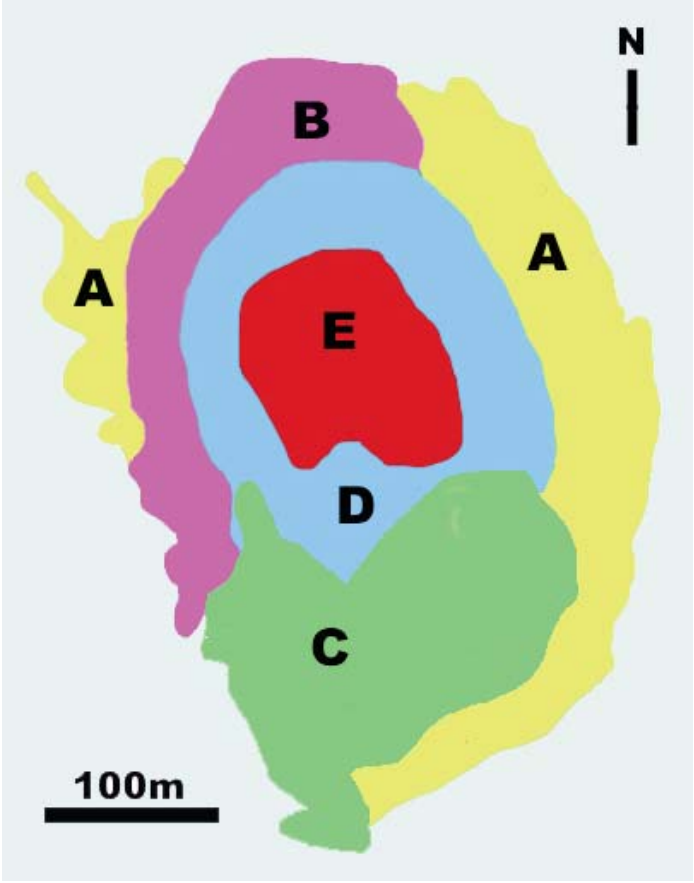

Figure 17. Outcrop plan of the Majhgawan lamproite illustrating the disposition of the pyroclastic units (after Mathur and Singh 1971; Rao 2007). A = yellow-green heterolithic pyroclastic breccia; B = yellow-brown heterolithic pyroclastic breccia; C = heterolithic breccia; D = mica-rich pyroclastic breccia; E = mica-free breccia. Note that these units require re-investigation and reclassification (see Fig. 18).

(Chalapathi Rao 2005), regardless of the correct classification as lamproite by Scott Smith (1989). This study was the first detailed investigation of the breccias and revealed the presence of glassy and vesicular juvenile lapilli (Fig. 18), and the presence of olivine lamproites similar to those found elsewhere. The mineralogy and texture of lapilli forming the breccias are typical of olivine phlogopite lamproites in general with mica phenocrysts set in a groundmass of Al-poor mica, Ti-spinel, rutile, perovskite, and a wide variety of secondary minerals (Fig. 18). As the mineralogy and petrology of the vent rocks are not well understood a complete re-investigation of the Majhgawan lamproites by modern methods is required. What is evident from the limited studies is that most of the vent rocks are pyroclastic in origin and similar to pyroclastic lamproites occurring in the nearby Atri Pipes (see below). Thus, the geology and economic evaluation should be interpreted using airfall eruptive and phreatomagmatic models similar to those proposed for the Atri, Argyle and Ellendale pyroclastic lamproites.

Saptarshi Lamproites and the Atri Pipes, Madhya Pradesh, India

The Saptarshi Lamproites, discovered in 2004 by Rio Tinto's

https://doi.org/10.12789/geocanj.2020.47.162

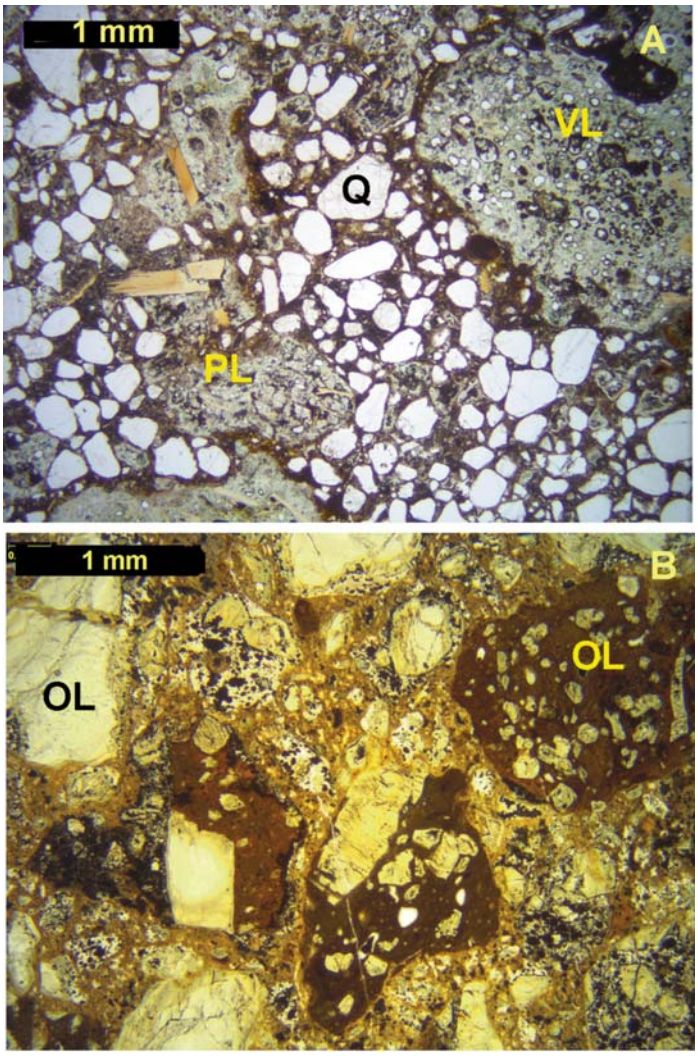

Figure 18. Volcaniclastic lamproites from Majhgawan Mine (India). (A) Quartz-rich tuff (or "sandy tuff") with vesicular juvenile lamproite clasts (VL) and fine-grained phlogopite lamproite (PL) clasts. Note the close petrographic similarity of this lamproite to the Seltrust Pipe 3 lamproite illustrated in Figure 11B. (B) Olivine lamproite tuff-breccia with clasts of altered hypabyssal olivine lamproite. Note the close similarity of this lamproite to the olivine lamproite tuff-breccia from the Black Lick vent (Arkansas) illustrated in Figure 15A. These similarities indicate that the Majhgawan tuffs are typical lamproite phreatomagmatic volcaniclastic rocks similar to those occurring at Argyle AK1 and Atri, and are not kimberlites.

Bunder Diamond Project (Das et al. 2018) are a cluster of seven lamproite vents and dykes located 80 km west-southwest of Majhgawan. The lamproites were emplaced in Vindhyan Kaimur Group supracrustal sedimentary rocks contemporaneously with the 1080–1067 Ma Majhgawan-Hinota vents. The major occurrence is the 1079 ± 6 Ma, Atri Pipe (18.5 ha) which consists of at least two irregular downward-tapering vents (Atri North and South) of diamondiferous pyroclastic/volcaniclastic lamproite (44 Mt @ 0.7 ct/t) which have coalesced near the present surface where Atri North cross-cuts Atri South (Fig. 19).

Five distinct lamproite pyroclastic or volcaniclastic units are present in the South pipe and three in the North pipe. These lamproites, described in detail by Masun et al. (2009)

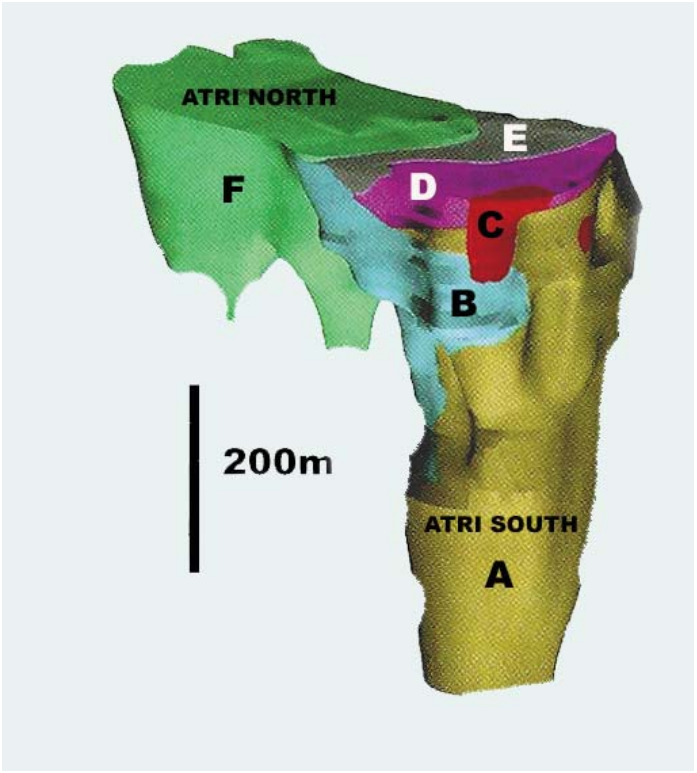

Figure 19. Model of the geology of the Atri lamproite vent looking northeast (after Das et al. 2018), showing the disposition of pyroclastic units in the South (A–E) and North (F) lamproites. Individual units in the northern vent are not delineated, and this vent is interpreted by Das et al. (2018) to have several feeders.

and Das et al. (2018), consist of diverse melt-bearing olivine phlogopite pyroclasts with country rock clasts and rarer autolithic clasts. Individual units (Fig. 19) can be easily distinguished on the basis of texture, colour, xenolithic, and primary mineral constituents. The rocks are similar to the Majhgawan lamproites and contain many vesicular pyroclasts. Mica compositions follow the lamproite trend of compositional evolution from phlogopite to tetraferriphlogopite with Ti- and Al-depletion coupled with Fe^{3+} enrichment (Das et al. 2018).

Unfortunately, regardless of the mineralogical and petrological evidence, Das et al. (2018) have incorrectly classified the Atri Pipes as "transitional kimberlite-orangeite-lamproite" or "majhgawanite". As noted above this nomenclature is petrogenetically impossible and should be discontinued. Both the Bunder and the Majhgawan pyroclastic/volcaniclastic rocks are *bona fide* lamproites derived from metasomatized lithospheric mantle, which can also be termed lamproite (*var.* Bundelkhand) following Mitchell (2006).

Das et al. (2018) considered that the Atri vents are composed predominantly of pyroclastic rocks with the low modal abundances of country rock xenoliths suggesting that pipe excavation preceded vent in-filling. The products of these events are not preserved at the current level of erosion. At Atri North several airfall pyroclastic eruptions of varying intensity and volume occurred, which included the formation of graded beds. The Atri South vent represents a change in locus of eruption and eruptive products and included the formation of units with graded beds, cross-beds, and soft sediment defor-

mation. The lamproites are finer grained and probably represent a phreatomagmatic style of eruption.

PETROGENESIS

A comprehensive review of the petrogenesis of lamproites is well beyond the scope of this work as it would require a detailed discussion of metasomatism and the mineralogy of the lithospheric mantle; how experimental petrology and isotope geochemistry has led to an understanding of differences in the formation of the sources of lamproites; the relative roles of mantle metasomatism and/or ancient and recent subduction; depth, causes and styles of melting leading to lamproite magmatism; and the tectonic history of particular cratons and orogenic belts containing lamproites. Summaries of these topics can be found in Mitchell and Bergman (1991) and Mitchell (1995a).

As each lamproite province is mineralogically and geochemically different, and lamproite magmas are neither common nor abundant, it is evident that there cannot be a single simple petrogenetic scheme applicable to all lamproites, although all have in common origins from metasomatized lithospheric mantle sources. Unlike common magma types, their genesis and composition are not repeated uniformly in time and space. *Thus, the formation of each lamproite province must be regarded as a singular event without the possibility of re-occurrence or formation of another province of identical character*. The rarity of lamproites also suggests that processes leading to their formation are also very rare and require particular tectonic environments and melting regimes. Thus, apart from the general observation that cratonic and orogenic lamproites appear to have different origins, the genesis of each lamproite province must be evaluated on its own merits. For details of many of these aspects of lamproite genesis see: Mitchell and Bergman (1991); Foley (1992a, b); Conticelli and Peccerillo (1992); Mitchell (1995a); Conticelli et al. (2002); Prelević et al. (2010); Krmíček et al. (2016); and Helmstaedt (2018).

The most important process in the petrogenesis of lamproites is the development of their lithospheric mantle sources. The initial stage appears to be formation of harzburgitic depleted mantle by extraction of large volumes of basic magma. A second stage requires the addition of incompatible elements to this substrate (Foley 1992a, b). This process is one of the more speculative aspects of lamproite genesis as it is not resolved as to whether incompatible element-rich fluids or melts originate from the asthenosphere, are introduced by partial melting of subducted material, or result from a combination of these processes. From isotopic data, experimental studies of lamproites at high pressure, and the mineralogical character of mantle xenoliths such as the MARID suite (mica–amphibole–rutile–ilmenite–diopside rocks, Dawson and Smith 1977) and metasomatized harzburgite, it is clear that harzburgite substrates must contain modally significant quantities of minerals that can sequester significant amounts of incompatible elements rather than these occurring as trace elements in common mantle minerals (i.e. cryptic metasomatism). The development of these new mineral assemblages is termed patent metasomatism and results in the formation of modally diverse veins in the harzburgite substrate (Foley 1992a, b).

The mineralogy of the metasomatic veins, or metasomes (Haggerty 1989), is considered to be dominated by minerals which can sequester K, REE, Ti, Ba, Sr, Zr, Nb, P, and volatile elements. The major components are probably titanian phlogopite and K-titanian richterite, the principal components of MARID xenoliths, both of which are stable throughout the lithospheric mantle and also at depths of up to 300 km. Other potential phases that have been recognized from mantle-derived xenoliths are: diopside; Nb-rutile; Cr–Mg-ilmenite; lindsleyite–mathiasite, yimengite–hawthornite; hollandite group K–Ba–V titanate minerals (priderite, redledgite, mannardite); and wadeite (Haggerty 1995). Experimental studies of the crystallization of potential primary lamproite magmas at lithospheric mantle pressures (4–8 GPa) suggest the presence of Zr-bearing $K_4(Si,Ti)_9O_{20}$, K–Ba-phosphate, Sr-apatite, and K-feldspar in the metasomes (Mitchell 1995b). The presence of apparently primary calcite in the Kaapvaal and Raniganj lamproites is unusual and its source from asthenospheric melts, pre-existing lithospheric primary carbonate or subduction is unknown. Although some carbonate-bearing lamproites are also known from West Kimberley, the primary source of this carbonate appears to be contamination by local limestone country rocks but it is possible that late calcite veins in the centre of the Walgidee Hills are deuteric (Jaques et al. 1986).

It is to be expected that the mineralogy of metasomatically enriched mantle will not everywhere be identical and that modal variations will lead on a long-term basis (gigayears) to the different isotopic compositions reported for lamproites (Figs. 7 and 8). Apart from the inherent modal variations of the veins, melting in harzburgite substrates according to the vein–wall rock partial melting models of Foley (1992b), will also give rise to unique magma compositions depending on the ratio of vein (V) to wall rock components introduced as melts (W) or xenocrysts (WX). Mitchell and Bergman (1991) and Mitchell (1995a, b) considered that silica-rich erupted phlogopite lamproites, such as occur at North Table Mountain and Steamboat Mountain (Leucite Hills) or Smoky Butte (Montana), represent the closest approach to primary magmas (Table 2) and represent partial melts in which vein components are dominant with V/(W +WX) ratios greater than 50%. Similar high vein contributions can be postulated for other unevolved silica-rich phlogopite lamproites such as found at the Ellendale 81 Mile Vent (Table 2). Following eruption of these magmas, differentiation by crystal fractional of liquidus phases leads through lamproites with leucite and diopside phenocrysts to evolved lamproites with groundmass tetraferriphlogopite, K–Ti-richterite and K-feldspar. In contrast, olivine lamproites are demonstrably hybrid rocks contaminated by wall-rock-derived olivine. Initial melts must have had low V/(W+WX) ratios (< 5%) with olivine apparently dominating the WX fraction. The absence of orthopyroxene xenocrysts is unexpected for partial melts derived from a harzburgite substrate and is a feature in common with kimberlites contaminated by mantle material (Mitchell 1997; Mitchell et al. 2019). Only a few silica-rich lamproites from Spain (Fortuna, Cancarix) and the Leucite Hills (Emmons Cone) contain orthopyroxene. These are typically Fe-rich relative to harzburgite orthopyroxene and consid-

ered to be xenocrysts or bronzite–mica microxenoliths (Mitchell and Bergman 1991). Not surprisingly olivine lamproites do contain mantle-derived orthopyroxene-bearing xenoliths of garnet lherzolite and harzburgite (Jaques et al. 1986; Dunn 2002). The typical absence of orthopyroxene in olivine lamproites can be explained by its incongruent melting which produces silica-rich liquids plus crystallization of the current liquidus phase, which in these melts is probably olivine and/or phlogopite. Hence, again in common with kimberlites, some olivine crystals are interpreted to be xenocrysts whereas others are primary phases. The combination of these parageneses can be seen in the formation of "dog's tooth"-textured olivine (Fig. 5C) in some olivine lamproites. Note that the sequence of crystallization of the groundmass of olivine lamproites leads to mineral assemblages similar to those observed in evolved lamproites implying that even initial melts with low V/(W+WX) ratios were also incompatible element- and silica-rich. Given that only olivine lamproites contain xenocrystic diamond it is not a coincidence that they are also the only lamproite magmas extensively contaminated by lithospheric mantle. These magmas might be melts formed in parts of the mantle containing few metasomatic veins or are initial melts in peripheral regions of extensively modified mantle. What is certain is that they are not primary magmas to phlogopite lamproites and their evolved derivatives.

As noted, the origins of enriched metasomes in many instances have not been conclusively identified and diverse hypotheses have been advocated for both these and the tectonic factors leading to the initiation of partial melting of the mantle for individual lamproite provinces. Although detailed discussion is well beyond the scope of this work some examples illustrating the diversity of opinion are given below.

Leucite Hills Province

The 3.0 to 0.89 Ma Leucite Hills lamproites (Carmichael 1967) are typical of cratonic lamproites in being emplaced near the margin of the Archean Wyoming craton about 100 km north of the surrounding Cheyenne mobile belt which separates the craton from the Colorado Plateau. The genesis of the province initially involved Archean craton formation resulting in a residual harzburgite lithospheric mantle which underwent subsequent metasomatism. The origins and age of this metasomatism have not been constrained and are considered to range from the Archean (3.2–2.5 Ga) to several Proterozoic events ranging from 2.5–1.0 Ga (Vollmer et al. 1984; Mirnejad and Bell 2006). The presence of negative Nb, Ti, and Ta anomalies in the trace element distribution patterns and the isotopic composition of the lamproites are considered by Mirnejad and Bell (2006) to indicate involvement of subduction in these events rather than any sub-lithospheric sources. Subsequently, the metasomes remained closed systems, for at least 1 Ga, until they were re-metasomatized by volatile-rich material derived from asthenospheric mantle upwelling. Complete partial melting of veins without involvement of the harzburgite substrate resulted in silica-rich melts which were erupted without differentiation during transit through the lithosphere or pooling in the crust. Lange et al. (2000) considered that the time of eruption was closely related to time of melting.

The initiation of the Quaternary lamproite magmatism has been attributed to the peripheral thermal effects of the Yellowstone plume (Mitchell and Bergman 1991); back-arc extension and lithospheric thinning associated with the northwest subduction of the Farallon oceanic plate; or uplift of the Colorado Plateau related to delamination of the lower crust by lithospheric downwelling, together with passive upwelling of the asthenospheric mantle (Levander et al. 2011). Although any relationships with the Yellowstone plume have been effectively ruled out by Lange et. al. (2000) and Mirnejad and Bell (2006), details of the relationships of the Cenozoic lamproite and other magmatism with the subducted Farallon Plate and Colorado Uplift remain unsettled. All models acknowledge the importance of the northwesterly low angle subduction of the Farallon oceanic plate in removal of lithospheric mantle and heating of the base of the Wyoming craton by upwelling asthenosphere (Levander et al. 2011; Hernández-Uribe and Palin 2019).

The Leucite Hills form an isolated province geographically isolated from other alkaline rocks although the genesis of the 40–13 Ma Francis (Moon Canyon) lamproites, located 250 km to the southwest at the margin of the Wyoming craton is also probably related to Colorado Plateau uplift. Minette intrusions are common within the Colorado Plateau and Montana although these are considered to have different sources and genesis to lamproites (O'Brien et al. 1995). Kimberlites are absent from the Leucite Hills Province but do occur in western Colorado, although these are not related genetically, and in addition are of Devonian age.

Kaapvaal Lamproites

The Kaapvaal cratonic lamproites are located in two principal clusters: 165–145 Ma intrusions in the centre, and 125–110 Ma intrusions at the southwestern margin of the Kaapvaal craton, suggesting two discrete episodes of magmatism. Many of the older petrogenetic hypotheses for Kaapvaal lamproites are now regarded as untenable as the lamproites were considered to be part of a broader spectrum of "kimberlite" magmatism. Regardless, most of these hypotheses (e.g. Becker and le Roex 2006; Coe et al. 2008) require for their genesis the formation of ancient enriched metasomes with phlogopite and amphibole at the base of the lithosphere (150–200 km). Recently, Giuliani et al. (2015) have focussed upon the similarity in composition of lamproites and the MARID xenoliths which have been found in both lamproites and kimberlites in southern Africa, and have suggested that MARID suite rocks form the metasomes.

Formation of enriched lithosphere is ascribed to late Proterozoic subduction under the Archean Kaapvaal craton and the accretion of adjacent 1.1 Ga Proterozoic Namaqua-Natal mobile belt with fluids or melts carrying a calc-alkaline geochemical signature into the subcontinental lithospheric mantle (Becker and le Roex 2006; Coe et al. 2008). These metasomes remained closed systems until the break-up of Gondwana (150–144 Ma) by one or more mantle plumes (Becker and le Roex 2006) resulted in partial melting. In contrast to this model, Giuliani et al. (2015) have suggested that the meta-

somes were formed by, and during, earlier (~ 180 Ma) Karroo asthenospheric magmatism. This hypothesis obviates any need for any subducted component in their genesis, although eclogite representing subducted material is common as xenoliths in these lamproites. A problem with this hypothesis is that the time between metasome formation and lamproite genesis might be insufficient to generate the observed isotopic signatures.

Regardless of the causes, partial or complete melting of metasomes, with or without wall rock contributions, following the Foley (1992b) models, resulted in the genesis of olivine lamproites or silica-rich types, respectively. In addition, the formation of Kaapvaal olivine lamproites requires a carbonate component which must be either added to some, but not all, parts of the metasomes during partial melting, or by contamination in the mantle during ascent of particular batches of melt. The origin of this carbonate remains an unresolved problem.

Most earlier studies of the Kaapvaal craton suggested the presence of a thick craton with a "smooth" keel (see Mitchell 1986; Haggerty 1989) and the location of subducted material at the lithosphere–asthenosphere boundary. In contrast, recent geophysical studies (Celli et al. 2020) have shown this simple picture does not describe the current configuration of most African cratons, and that much of the of original Kaapvaal craton, including any subducted components, has been removed by sub-lithospheric erosion. The 180 Ma Karroo large igneous province, the 150–110 Ma lamproites, and the ~ 90 Ma kimberlites, are all now situated over an eroded thinned part of the craton. Erosion and magmatism might be related to a fixed region of asthenospheric upwelling rather than associated with migrating hot spots, as suggested by Becker and le Roex (2006). In such a scenario partial melting of ancient metasomes could be due to melt/fluid influx associated with lithospheric thinning. However, appeal to such Maxwell's Demons is not a satisfactory solution to the problem as the temporal and tectonic relationships between the lamproites, kimberlites, and the earlier Karroo magmatism are not resolved. Clearly, two temporally distinct partial melting events are involved in Kaapvaal lamproite genesis, perhaps involving mineralogically distinct metasomes in different parts of the craton. In addition, many ancient metasomes might have been destroyed and assimilated during craton erosion and the genesis of the Karroo magmas, perhaps accounting for the relatively restricted occurrence of lamproites in contrast to the widespread distribution of younger asthenospheric kimberlites in southern Africa. Recent subduction or rifting is not considered to have played any role in the genesis of Kaapvaal lamproites.

Tibetan Lamproites

Lamproite lavas occur in eight distinct fields in the western region of Lhasa Block (Chen et al 2012) located at the southwestern margin of the Tibetan Plateau. These lamproites were emplaced in an area of active tectonism and illustrate well the complexities of orogenic ultrapotassic magma genesis as, in common with the Spanish and Italian lamproites, they are associated with abundant less potassic rocks, and minor felsic magmas (Miller et al. 1999; Mo et al. 2006; Gao et al. 2007; Xia et al. 2011; Chen et al. 2012; Guo et al. 2015; Zhang et al. 2017). The lamproites and other potassic rocks represent post-collisional magmatism with emplacement ages of 25–18 Ma and 13–8 Ma, respectively (Miller et al. 1999; Gao et al. 2007). Individual lamproite fields have distinctive geochemical characteristics with high Pb abundances, low Ce/Pb ratios, and Pb isotopic ratios indicative of binary (or ternary) mixing, implying contributions to their genesis from diverse subducted materials and mantle components. Lamproite sources are also geochemically distinct from those of the more widespread potassic volcanism in the Lhasa and Qiangtang Blocks of the Tibetan Plateau (Guo et al. 2015).

Petrogenetic hypotheses for the lamproites are complicated by the diversity of hypotheses proposed for the geodynamic evolution of the Tibetan Plateau which include convective removal of the subcontinental lithospheric mantle, subducted slab roll-back and break-off, and intra-continental subduction. There is an extensive literature on these topics. For recent summaries of the tectonics of the India–Asia collision see, among many others, Ge et al. (2012), Hyndman (2019) or Xiao et al. (2020). As the components and extent of the Indian plate underthrusting and paleothermal regime under Tibet are not well-constrained, lamproite petrogenetic models are at best speculative.

In common with other models of lamproite genesis it has been suggested by Miller et al. (1999) that the Tibetan lithospheric mantle was enriched by a complex multi-stage metasomatism from > 2.2 Ga to 1.3 – 1.9 Ga and remained isolated until recently. The origins of the enriched sources are not well-characterized by Miller et al. (1999). The potassic and lamproitic magmatism is interpreted as the product of partial melting resulting from either convective thinning of the lithosphere with diverse magmas derived from distinctive sources or subducted oceanic plate break-off resulting in the uprise of hot asthenosphere causing thermal perturbations and melting of heterogeneous domains in the lithospheric mantle. In contrast, Gao et al. (2007) claimed that such isolation is unlikely given the complex Phanerozoic tectonic and magmatic evolution of Tibet, and suggested that metasomatism by partial melts from isotopically evolved old sedimentary material subducted with the Tethyan slab can explain the apparent Precambrian Nd and Pb model ages reported by Miller et al. (1999).

Guo et al. (2015) have shown that the Sr–Nd–Pb isotopic compositions of Tibetan lamproite and potassic volcanic rocks define linear trends between depleted MORB, source mantle (DMM) and Indian continental crust. The enrichment of the upper mantle below southern Tibet is considered to result from the addition of material derived from subducted Indian continental crust to the overlying mantle wedge during the northwestern underthrusting of the Indian plate at 55 Ma. In contrast to most lamproite petrogenetic models the post-collisional lamproites are considered to be generated by partial melting of pyroxenite in a mantle source created by reaction of hydrous fluids and silica-rich melt derived from subducted granulite–eclogite facies Indian continental crustal with surrounding peridotitic mantle. Slab roll-back and detachment then induces partial melting of pyroxenite.

https://doi.org/10.12789/geocanj.2020.47.162

Although the Tibetan lamproites are well-characterized in terms of their mineralogy, trace element and isotope geochemistry, it is evident that a geological solution to their genesis remains elusive. This is because of the complexity of the tectonic evolution of the sub-Tibetan lithospheric mantle coupled with underthrusting of the Indian plate which precludes both definitive characterization of potential enriched sources and mechanisms of partial melting. Interpretation of genetic models in terms of the evolution of the Tibetan Plateau according to the tectonic and thermal model of Hyndman (2019) is required. The geophysical studies of Xiao et al. (2020) indicate significant underthrusting of the Indian lower crust coupled with destruction of the Asian lithosphere under the western parts of the Tibet Plateau together with the presence of a steep down-dipping slab of Indian lithosphere. In Hyndman's (2019) model, the presence of a pre-collision hot back-arc is considered to weaken the lithosphere and is considered as a pre-collision requirement for orogenic deformation and crustal thickening rather than a consequence of orogeny. How these concepts will affect pre-exiting metasomes is not as yet understood.

Indian Lamproites

Apart from the complexities of their tectonic setting, studies of the petrogenesis of Indian lamproites have been hindered by problems in terminology resulting from resistance to using modern mineralogical-genetic classification schemes and undue reliance upon bulk rock geochemical studies. Many rocks previously described as "kimberlites" have now been reclassified as *bona fide* lamproites (Fareeduddin and Mitchell 2012; Gurmeet Kaur and Mitchell 2016). The numerous occurrences of "para-kimberlites" have not been investigated using detailed mineralogical studies and are probably varieties of olivine lamproite, e.g. the Tokapal epiclastic/pyroclastic vent which is typical of a lamproite volcano and not a kimberlite diatreme (Fareeduddin and Mitchell 2012). It is possible that archetypal kimberlites are absent from eastern and central India. Figure 20 shows that the known lamproites are emplaced in four Archean cratons, isolated from each other by Proterozoic mobile belts and rifts, which differ in geology, age, and genesis. A notable aspect of the distribution of most of the para-kimberlite and lamproite fields is that they form a SW–NE trending zone parallel to a zone of deformed undersaturated alkaline complexes emplaced within the Proterozoic polyphase granulite terrane of the Eastern Ghats Mobile Belt (Burke and Khan 2006). Exceptions are the Bunder and Majhgawan lamproites which are emplaced at the southern margins of the Bundelkhand craton adjacent to a different Proterozoic mobile belt. Lamproites are notably absent, or have not yet been discovered, from the Western Dharwar and Aravalli cratons. In the Eastern Dharwar craton, several lamproite provinces range in age from ~ 1350 Ma (Chelima) to ~ 1090 Ma (Wajrakurur) with most of the activity occurring at about 1.1 Ga. In the Bastar craton lamproites range in age from ~616 Ma (Tokapal) to 62–65 Ma (Kodomali, Bahradih). In the Singbhum Craton lamproites were intruded into the Gondwana supracrustal sediments of the Damodar Valley Basins at

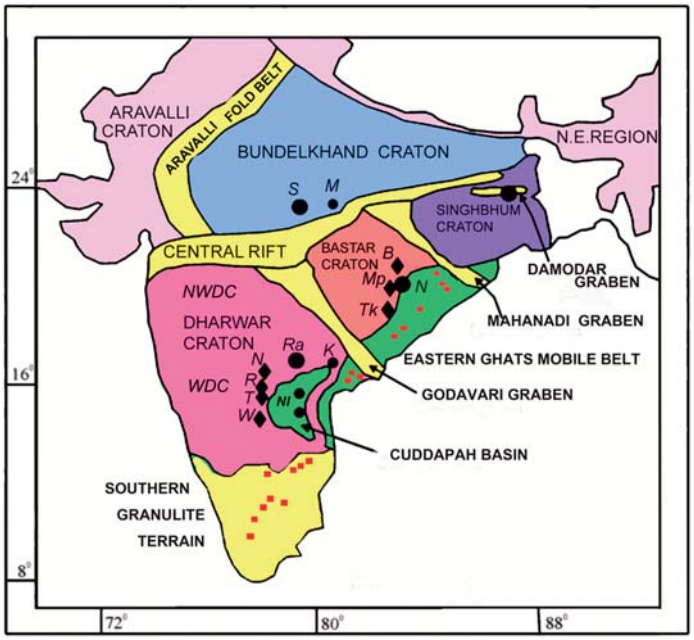

Figure 20. Distribution of lamproites (black circles: S - Saptarshi; M - Majhgawan; D - Damodar; Na - Nawapara; Ra - Ramadugu; K - Krishna; NI - Nallamalai-Chelima;), and lamproite-"para-kimberlite" fields (black labelled diamonds: B - Basna; Mp - Mainpur; Tk - Tokopal; N - Narayanpet; R - Raichur; T - Tungabhadra; W - Wajrakarur) in the cratons of the Indian subcontinent together with the locations of deformed Proterozoic alkaline rocks and carbonatites (red squares) in the Eastern Ghats Mobile Belt and Southern Granulite Terrain (after Gurmeet Kaur et al. 2018). Note that much of the northwestern part of the Dharwar craton (*NWDC*) is covered by Deccan Trap basalts which might account for the apparent absence of lamproites in that region but not the area (*WDC*) due west of the Narayanpet-Wajrakurur belt of lamproites of the Eastern Dharwar craton. Their absence might be related to the Archaean-Proterozoic paleo-subduction and origins of the Eastern Ghats Mobile Belt and formation of metasomes only within the eastern parts of the craton.

117–110 Ma and thus are of the same age as many of the Kaapvaal lamproites.

Each of the Indian lamproite provinces differs in mineralogy and age. Within each province there are typically several subfields consisting of para-kimberlites and lamproites of differing mineralogy, e.g. the Bokaro, Jharia, and Raniganj subfields of the Damodar Province, or the hypabyssal Wajrakurur Province which consists of the Wajrakurur, Lattavaram, Timmasamudram, and Chigicherla subfields. This observation implies that magmatism involves slightly different vein or wall-rock melting regimes within and between provinces, in some instances producing olivine lamproites, e.g. Lattavaram Pipe 3, or in others, more silica-rich lamproites, e.g. Wajrakurur P2-west (Fareeduddin and Mitchell 2012; Gurmeet Kaur and Mitchell 2013). In some provinces, differentiation of olivine phlogopite lamproite to leucite -K-feldspar lamproite is evident, e.g. Raniganj Province (Mukherjee 1961; Mitchell and Fareeduddin 2009). Shaikh et al. (2019) have concluded from an investigation of the trace element compositions of olivine in Wajrakarur (dykes CC2 and P13) and the Kodomali-Behradih lamproites that a hotter paleogeotherm existed in the lithospheric mantle beneath the Eastern Dharwar craton at ~ 1100 Ma than beneath the Bastar craton at ~ 65 Ma. In addition, it is proposed that the Eastern Dharwar craton experi-

enced a greater degree of metasomatism relative to the Bastar craton.

The initiation of partial melting of the metasomatized sources, which have been proposed for the diverse Indian lamproites, ranges from peripheral thermal effects of mantle plumes to regional asthenospheric upwelling and/or combinations of these processes. It is notable that the lamproites of the Eastern Dharwar craton have the same age as the Bunder-Majhgawan lamproites. However, as these lamproites are separated by 600 km, it is considered that hot spot magmatism could not have been involved in their simultaneous genesis (Helmstaedt 2018). In contrast, Kent et al. (1998) have concluded that Damodar magmatism was induced by partial melting at the margins of the Kerguelen hot spot, and it is suggested by Lehman et al. (2010) that the Kodomali and Behradih lamproites resulted from the plume that produced the Deccan traps. Note that a similar hypothesis has been advanced by Xiang et al. (2020) for the 260 Ma Baifen cratonic lamproites of the Yangtze Block (China) involving melting at the margins of the mantle plume initiating the Emeishan large igneous province. The common factor in these plume models is the rapid extension, thinning, and decompressional melting of the lithosphere induced by plume-related asthenospheric upwelling. However, as noted above with respect to the Leucite Hills other processes might be responsible for partial melting and these might be associated with a second period of incompatible enrichment of the ancient mantle metasomes.

Burke and Khan (2006) and Gurmeet Kaur et al. (2018) have interpreted the near-linear distribution of lamproites and alkaline rocks in eastern India parallel to the Eastern Ghats Mobile Belt (Fig. 20) to imply a relationship with ancient subduction processes on the basis of geophysical evidence for the presence of relict subducted oceanic slab material at depths of 160–220 km. This subducted slab is considered to be a product of the suturing of the Eastern Dharwar craton with the Eastern Ghats Mobile Belt at ~ 1600 Ma. Such subducted material might have been the source of metasomatic enrichment of the lithospheric mantle of the Dharwar and Baster cratons, but not the Singhbhum and Bundelkhand cratons. Localized partial melting of this source at ~ 1.1 Ga by asthenospheric upwelling could have resulted in the formation of the Dharwar lamproites, but not the younger Bastar lamproites or the Bundelkhand lamproites, implying different melting regimes for these magmas.

In common with the Kaapvaal craton, there has been erosion of the roots of the Dharwar and Bastar cratons. The lithospheric "keel" of the Bastar craton is estimated to have been at least 140 km in thickness at the time of emplacement of the Kodomali and Behradih lamproites, but is now only about 80–100 km in thickness, implying about one third of the craton root has been lost during the breakup of Gondwana (Lehman et al. 2010). The Eastern and Western Dharwar cratons have experienced similar modification with asthenospheric mantle now also being present at 80–100 km depth. Thus, the depleted lithospheric roots present 1.1 b.y. ago do not exist today (Griffin et al. 2009). Thermal erosion and delamination of these craton roots was considered by Lehman et al. (2010) to be due to the eastern lateral deflection of the plume which produced the 68–65 Ma Deccan Traps toward the thinner lithosphere of eastern India.

The recent geophysical studies of the Kaapvaal and Indian cratons are instructive as they indicate that the ancient metasomatic sources of lamproites are no longer present, having been removed by younger tectonic events. Hence, the depths and temperatures of lamproite magma generation in the lithospheric mantle that have been estimated by the geothermobarometry of entrained eclogite and ultrabasic xenoliths refer to the paleo-configuration of the craton and not its current state (Shaikh et al. 2019). These observations, and the work of Celli et al. (2020), have implications for the genesis and preservation of lithospheric metasomes and highlight the need for detailed studies of the current and past structure of cratons. Many of the existing models for incorporation of diamond xenocrysts in lamproites and kimberlites (e.g. Haggerty 1989; Mitchell 1995a) are now considered too simplified, as they consider cratons to have a simple boat-like shape with a relatively uniform keel-shaped lithosphere–asthenosphere boundary. The paucity of lamproite magmatism in many cratons might be related to destruction of lithospheric metasomes during the generation and ascent of more voluminous asthenosphere-derived magmas such as the basalt of large igneous provinces.

FINAL COMMENTS AND FUTURE RESEARCH

Regardless of their rarity, lamproites remain of continuing petrological interest as they are a major source of diamonds and are magma types whose origins provide unique insights into metasomatic processes in the lithospheric mantle. Lamproite magmas have similar rheological characteristics to basaltic magmas and their emplacement as hypabyssal dykes and sills or phreatomagmatic vents is well characterized, although specific fields require further investigation, as shown by the recent re-investigation of the Cancarix volcano (Spain) by Reolid et al. (2015). The mineralogy and bulk-rock geochemistry of cratonic varieties is relatively well characterized. In contrast, although the trace element and isotope bulk-rock geochemistry of orogenic lamproites is well understood, especially as a result of recent studies of Tibetan occurrences, the details of the mineralogy of the minor and trace accessory minerals are less well characterized. The origins of lamproite magmas and the tectonic events that initiated their genesis remain ambiguous as individual lamproite provinces are unique with respect both to the mineralogy and geochemistry of their mantle sources and to the thermal events which initiate partial melting. Hence, the origins of a given lamproite must be evaluated on its own basis especially with regard to orogenic lamproites whose genesis involves recent subduction and mixing processes with mantle metasomes. Some aspects of lamproite petrology that require further investigation are:

1) detailed mineralogical and petrological investigations of the Majhgawan vent and para-kimberlites of the Dharwar and Bastar cratons of India.
2) characterization of lamproites and para-lamproites in the Aldan Shield (Russia), the São Francisco craton

(Brazil) and other South American localities (e.g. eastern Paraguay, Presser 2000), the southern West African craton (Bobi, Seguela), the Kapamba lamproites of the Luangwa graben (Zambia), and the west Greenland lamproites. The potassic rocks of the Aldan Shield in particular require much re-investigation because of the presence of extremely undersaturated ultrapotassic rocks (synnyrite, yakutite, etc.) in geographic, but not necessarily genetic, relationships with lamproite- and kamafugitic-like rocks (Kostyuk et al. 1990; Chayka et al. 2020).

3) explanations are required for the apparent paucity of cratonic lamproites in some cratons (Slave, Rae, Superior, Tanzanian, Yilgarn, Amazon), and of orogenic lamproites in the South America Cordillera. High resolution studies of the structure of cratons, their delamination and erosion following the methods of Celli et al. (2020) are essential.
4) modern methods of *in situ* analytical geochemistry, such as LA–ICP–MS, should be applied to individual minerals and glasses in lamproites to determine how particular elements are distributed for general petrogenetic purposes. Examples might include Rb, Cs, Pb, NH_4, and Tl abundances in phlogopite and the role of magma mixing; Sr, C, and O isotopic studies of the origins of carbonate in Kaapvaal lamproites; determination of the abundances of Pb and the Pb isotopic compositions of K-feldspar, and how Pb is sequestered in orogenic lamproites.

ACKNOWLEDGEMENTS

This contribution is to thank the Geological Association of Canada Volcanology and Igneous Petrology Division for their recognition of my work with their 2018 Lifetime Achievement Award. My studies on the petrology of lamproites have been supported by De Beers Consolidated Mines, Inc., Seltrust Corp., Star Resources Corp., ARCO Oil And Gas, Rio Tinto Exploration (India), Natural Sciences and Engineering Council of Canada, Almaz Petrology, Lakehead University, and the Geological Society of India. All are thanked for their financial support or contributions in kind. Particular individuals to thank who have contributed in diverse ways to my work on lamproites are Barry Hawthorne, Henry Meyer, Steve Bergman, Howard Coopersmith, Barbara Scott Smith, Alan Edgar, Gurmeet Kaur, Fareeduddin, Iain Downie, John Lewis, Nikolai Vladykin, and Valerie Dennison. Georgia Pe-Piper and Lynton Jaques are thanked for reviews of the initial draft of this paper, and Rob Raeside, Cindy Murphy and Jarda Dostal for editorial handling.

REFERENCES

Becker, M., and le Roex, A.P., 2006, Geochemistry of South African on- and off-craton, Group I and Group II kimberlites: petrogenesis and source region evolution: Journal of Petrology, v. 47, p. 673–703, https://doi.org/10.1093/petrology/egi089.

Boxer, G.L., Lorenz, V., and Smith, C.B., 1989, The geology and volcanology of the Argyle (AK1) lamproite diatreme, Western Australia: Geological Society of Australia, Special Publication 14, v. 1, p. 140–152.

Burke, K., and Khan, S., 2006, Geoinformatic approach to global nepheline syenite and carbonatite distribution: testing a Wilson cycle model: Geosphere, v. 2, p. 53–60, https://doi.org/10.1130/GES00027.1.

Carmichael, I.S.E., 1967, The mineralogy and petrology of the volcanic rocks from the Leucite Hills, Wyoming: Contributions to Mineralogy and Petrology, v. 15, p. 24–66, https://doi.org/10.1007/BF01167214.

Celli, N.L., Lebedev, S., Schaeffer, A.J., and Gaina, C., 2020, African cratonic lithosphere carved by mantle plumes: Nature Communications, v. 11, 92, https://doi.org/10.1038/s41467-019-13871-2.

Chalapathi Rao, N.V., 2005, A petrological and geochemical reappraisal of the Mesoproterozoic diamondiferous Majhgawan pipe of central India: evidence for a transitional kimberlite – orangeite (group II kimberlite) – lamproite rock type: Mineralogy and Petrology, v. 84, p. 69–106, https://doi.org/10.1007/s00710-004-0072-2.

Chayka, I.F., Sobolev, A.V., Izokh, A.E., Batanova, V.G., Krasheninnikov, S.P., Chervyakovskaya, M.V., Kontonikas-Charos, A., Kutyrev, A.V., Lobastov, B.M., and Chervyakovskiy, V.S., 2020, Fingerprints of kamafugite-like magmas in Mesozoic lamproites of the Aldan Shield: Evidence from olivine and olivine-hosted inclusions: Minerals, v. 10, 337, https://doi.org/10.3390/min10040337.

Chen, J.-L., Xu., J.-F., Wang, B.-D., and Kang, Z.-Q., 2012, Cenozoic Mg-rich potassic rocks in the Tibetan Plateau: Geochemical variations, heterogeneity of subcontinental lithospheric mantle and tectonic implications: Journal of Asian Earth Sciences, v. 53, p. 115–130, https://doi.org/10.1016/j.jseaes.2012.03.003.

Clement, C.R., 1982, A comparative study of some major kimberlite pipes in the Northern Cape and Orange Free State: Unpublished Ph.D. thesis (2 volumes), University of Cape Town, South Africa, 432 p.

Coe, N., le Roex, A., Gurney, J., Pearson, D.G., and Nowell, G., 2008, Petrogenesis of the Swartruggens and Star Group II kimberlite dyke swarms, South Africa: constraints from whole rock geochemistry: Contributions to Mineralogy and Petrology, v. 156, 627, https://doi.org/10.1007/s00410-008-0305-01.

Conticelli, S., and Peccerillo, A., 1992, Petrology and geochemistry of potassic and ultrapotassic volcanism in central Italy: petrogenesis and inferences on the evolution of the mantle sources: Lithos, v. 28, p. 221–240, https://doi.org/10.1016/0024-4937(92)90008-M.

Conticelli, S., Manetti, P., and Menichetti, S., 1992, Mineralogy, geochemistry and Sr-isotopes in orendites from South Tuscany, Italy: constraints on their genesis and evolution: European Journal of Mineralogy, v. 4, p. 1359–1375.

Conticelli, S., D'Antonio, M., Pinarelli, L., and Civetta, L., 2002, Source contamination and mantle heterogeneity in the genesis of Italian potassic and ultrapotassic volcanic rocks: Sr–Nd–Pb isotope data from Roman Province and southern Tuscany: Mineralogy and Petrology, v. 74, p. 189–222, https://doi.org/10.1007/s007100200004.

Contini, S., Venturelli, G., Toscani, L., Capredi, S., and Barbieri, M., 1993, Cr–Zr-armalcolite-bearing lamproites of Cancarix, SE Spain: Mineralogical Magazine, v. 57, p. 203–216, https://doi.org/10.1180/minmag.1993.057.387.02.

Crawford, A.J., Falloon, T.J., and Green, D.H., 1989, Classification, petrogenesis and tectonic setting of boninites, *in* Crawford, A.J., *ed.*, Boninites and Related Rocks: Unwin-Hyman, London, p. 1–49.

Cross, C.W., 1897, Igneous rocks of the Leucite Hills and Pilot Butte, Wyoming: American Journal of Science, v. 4, p. 115–141, https://doi.org/10.2475/ajs.s4-4.20.115.

Das, H., Kobussen, A.F., Webb, K.J., Phillips, D., Maas, R., Soltys, A., Rayner, M.J., and Howell, D., 2018, The Bunder Diamond project, India: Geology, geochemistry and age of the Saptarshi lamproite pipes, *in* Davy, A.T., Smith, C.B., Helmstaedt, H., Jaques, A.L., and Gurney, J.J., *eds.*, Geoscience and Exploration of the Argyle, Bunder, Diavik, and Murowa Diamond Deposits: Society of Economic Geologists Special Publication, v. 20, p. 201–222, https://doi.org/10.5382/SP.20.09.

Dawson, J.B., 1987, The kimberlite clan: relationship with olivine and leucite lamproites, and inferences for upper-mantle metasomatism, *in* Fitton, J.G., and Upton, B.G.J., *eds.*, Alkaline Igneous Rocks: Geological Society, London, Special Publications, v. 30, p. 95–101, https://doi.org/10.1144/GSL.SP.1987.030.01.07.

Dawson, J.B., and Smith, J.V., 1977, The MARID (mica-amphibole-rutile-ilmenite-diopside) suite of xenoliths in kimberlite: Geochimica et Cosmochimica Acta, v. 41, p. 309–310, IN9-IN11, 311–323, https://doi.org/10.1016/0016-7037(77)90239-3.

Dunn, D.P., 2002, Xenolith mineralogy and geology of the Prairie Creek lamproite province, Arkansas: Unpublished Ph.D. thesis, University of Texas at Austin, 147 p., hdl.handle.net/2152/554.

Ekkerd, J., Stiefenhofer, J., Field, M., and Lawless, P., 2006, The geology of Finsch Mine, northern Cape Province, South Africa: 8th International Kimberlite Conference, Kimberlite Emplacement Workshop, Saskatoon, Canada, Extended Abstracts, FLA_0310, https://doi.org/10.29173/ikc3204.

Fareeduddin, and Mitchell, R.H., 2012, Diamonds and their source rocks in India: Geological Society of India, Bangalore, 434 p.

Field, M., Stiefenhofer, J., Robey, J., and Kurszlaukis, S., 2008, Kimberlite-hosted diamond deposits of southern Africa: A review: Ore Geology Reviews, v. 34, p. 33–75, https://doi.org/10.1016/j.oregeorev.2007.11.002.

Foley, S., 1992a, Petrological characterization of the source components of potassic magmas: Geochemical and experimental constraints: Lithos, v. 28, p. 187–204, https://doi.org/10.1016/0024-4937(92)90006-K.

Foley, S., 1992b, Vein-plus-wall-rock melting mechanisms in the lithosphere and the origin of potassic alkaline magmas: Lithos, v. 28, p. 435–453,

https://doi.org/10.1016/0024-4937(92)90018-T.
Foley, S.F., Venturelli, G., Green, D.H., and Toscani, L., 1987, The ultrapotassic rocks: characteristics, classification and constraints for petrogenetic models: Earth-Science Reviews, v. 24, p. 81–134, https://doi.org/10.1016/0012-8252(87)90001-8.
Franklin, J., 1822, On the diamond mines of Panna in Bundelkhand: Asia Research, v. 18, p. 100–122.
Gaeta, M., Freda, C., Marra, F., Di Rocco, T., Gozzi, F., Arienzo, I., Giaccio, B., and Scarlato, P., 2011, Petrology of the most recent ultrapotassic magmas of the Roman Province (Central Italy): Lithos, v. 127, p. 298–308, https://doi.org/10.1016/j.lithos.2011.08.006.
Gao, Y., Hou, Z., Kamber, B.S., Wei, R., Meng, X., and Zhao, R., 2007, Lamproitic rocks from a continental collision zone: Evidence for recycling of subducted Tethyan oceanic sediments in the mantle beneath southern Tibet: Journal of Petrology, v. 48, p. 729–752, https://doi.org/10.1093/petrology/egl080.
Ge, C., Sun, Y., Toksöz, M.N., Zheng, Y., Zheng, Y., Xiong, X., and Yu, D., 2012, Crustal structure of the central Tibetan plateau and geological interpretation: Earthquake Science, v. 25, p. 363–370, https://doi.org/10.1007/s11589-012-0862-2.
Giuliani, A., Phillips, D., Woodhead, J.D., Kamenetsky, V.S., Fiorentini, M.L., Mass, R., Soltys, A., and Armstrong, R.A., 2015, Did diamond-bearing orangeites originate from MARID-veined peridotites in the lithospheric mantle?: Nature Communications, v. 6, 6837, https://doi.org/10.1038/ncomms7837.
Griffin, W.L., Kobussen, A.F., Babu, E.V.S.S.K., O'Reilly, S.Y., Norris, R., and Sengupta, P., 2009, A translithospheric suture in the vanished 1-Ga lithospheric root of South India: Evidence from contrasting lithosphere sections in the Dharwar Craton: Lithos, v. 112, p. 1109–1119, https://doi.org/10.1016/j.lithos.2009.05.015.
Guo, Z., Wilson, M., Zhang, M., Cheng, Z., and Zhang, L., 2015, Post-collisional ultrapotassic mafic magmatism in south Tibet: Products of partial melting of pyroxenite in the mantle wedge induced by roll-back and delamination of the subducted Indian continental lithosphere slab: Journal of Petrology, v. 56, p. 1365–1406, https://doi.org/10.1093/petrology/egv040.
Gurmeet Kaur, and Mitchell, R.H., 2013, Mineralogy of the P2-West 'kimberlite', Wajrakarur kimberlite field, Andhra Pradesh, India: kimberlite or lamproite?: Mineralogical Magazine, v. 77, p. 3175–3196, https://doi.org/10.1180/minmag.2013.077.8.11.
Gurmeet Kaur, and Mitchell, R.H., 2016, Mineralogy of the P-12 K-Ti-richterite diopside olivine lamproite from Wajrakarur, Andhra Pradesh, India: implications for subduction-related magmatism in eastern India: Mineralogy and Petrology, v. 110, p. 223–245, https://doi.org/10.1007/s00710-015-0402-6.
Gurmeet Kaur, Mitchell, R.H., and Ahmed, S., 2018, Mineralogy of the Vattikod lamproite dykes, Ramadugu lamproite field, Nalgonda District, Telangana: A possible expression of ancient subduction-related alkaline magmatism along Eastern Ghats Mobile Belt, India: Mineralogical Magazine, v. 82, p. 35–58, https://doi.org/10.1180/minmag.2017.081.045.
Haggerty, S.E., 1989, Mantle metasomes and the kinship between carbonatite and kimberlites, *in* Bell, K., *ed.*, Carbonatites: Unwin Hyman, London, p. 546–560.
Haggerty, S.E., 1995, Upper mantle mineralogy: Journal of Geodynamics, v. 20, p. 331–364, https://doi.org/10.1016/0264-3707(95)00016-3.
Helmstaedt, H., 2018, Tectonic and structural controls on diamondiferous kimberlite and lamproite and their bearing on area selection for diamond exploration, *in* Davy, A.T., Smith, C.B., Helmstaedt, H., Jaques, A.L., and Gurney, J.J., *eds.,* Geoscience and Exploration of the Argyle, Bunder, Diavik, and Murowa Diamond Deposits: Society of Economic Geologists, Special Publication, v. 20, p. 1–48.
Hernández-Uribe, D., and Palin, R.M., 2019, Catastrophic shear-removal of subcontinental lithospheric mantle beneath the Colorado Plateau by the subducted Farallon slab: Nature Scientific Reports, v. 9, 8153, https://doi.org/10.1038/s41598-019-44628-y.
Hickey, R.L., and Frey, F.A., 1982, Geochemical characteristics of boninite series volcanics: Implications for their source: Geochimica et Cosmochimica Acta, v. 46, p. 2099–2115, https://doi.org/10.1016/0016-7037(82)90188-0.
Hyndman, R.D., 2019, Mountain building orogeny in pre-collision hot backarcs: North American Cordillera, India-Tibet, and Grenville Province: Journal of Geophysical Research, v. 124, p. 2057–2079, https://doi.org/10.1029/2018JB016697.
Jaques, A.L., Lewis, J.D., and Smith, C.B., 1986, The kimberlites and lamproites of Western Australia: Geological Survey of Western Australia, Bulletin 132, 268 p.
Jaques, A.L., Brink, F., and Chen, J., in press, Magmatic haggertyite in olivine lamproites of the West Kimberley region, Western Australia: American Mineralogist, https://doi.org/10.2138/am-2020-7456.
Kent, R.W., Kelley, S.P., and Pringle, M.S., 1998, Mineralogy and $^{40}Ar/^{39}Ar$ geochronology of orangeites (Group II kimberlites) from the Damodar Valley, eastern India: Mineralogical Magazine, v. 62, p. 313–323, https://doi.org/10.1180/002646198547701.
Kostyuk, V.P., Panina, L.L., Zhidkov, A.Y., Orlova, M.P., and Bazarova, T.Y., 1990, Potassic alkaline magmatism of the Baikal-Stanovoy Rifting System: Nauka, Novosibirsk, 200 p. (in Russian).
Krmíček, L., Cempírek, J., Havlín, A., Přichystal, A., Houzar, S., Krmíčková, M., and Gadas, P., 2011, Mineralogy and petrogenesis of a Ba–Ti–Zr-rich peralkaline dyke from Šebkovice (Czech Republic): Recognition of the most lamproitic Variscan intrusion: Lithos, v. 121, p. 74–86, https://doi.org/10.1016/j.lithos.2010.10.005.
Krmíček, L., Romer, R.L., Ulrych, J., Glodny, J., and Prelević, D., 2016, Petrogenesis of orogenic lamproites of the Bohemian Massif: Sr–Nd–Pb–Li isotope constraints for Variscan enrichment of ultra-depleted mantle domains: Gondwana Research, v. 35, p. 198–216, https://doi.org/10.1016/j.gr.2015.04.012.
Lange, R.A., Carmichael, I.S.E., and Hall, C.M., 2000, $^{40}Ar/^{39}Ar$ chronology of the Leucite Hills, Wyoming: Eruption rates, erosion rates, and an evolving temperature structure of the underlying mantle: Earth and Planetary Science Letters, v. 174, p. 329–340, https://doi.org/10.1016/S0012-821X(99)00267-8.
Lehmann, B., Burgess, R., Frei, D., Belyatsky, B., Mainkar, D., Chalapathi Rao, N.V., and Heaman, L.M., 2010, Diamondiferous kimberlites in central India synchronous with Deccan flood basalts: Earth and Planetary Sciences Letters, v. 290, p. 142–149, https://doi.org/10.1016/j.epsl.2009.12.014.
Levander, A., Schmandt, B., Miller, M.S., Liu, K., Karlstrom, K.E., Crow, R.S., Lee, C.-T.A., and Humphreys, E.D., 2011, Continuing Colorado plateau uplift by delamination-style convective lithospheric downwelling: Nature, v. 472, p. 461–465, https://doi.org/10.1038/nature10001.
Lustrino, M., Agostini, S., Chalal, Y., Fedele, L., Stagno, V., Colombi, F., and Bouguerra, A., 2016, Exotic lamproites or normal ultrapotassic rocks? The Late Miocene volcanic rocks from Kef Hahouner, NE Algeria, in the frame of the circum-Mediterranean lamproites: Journal of Volcanology and Geothermal Research, v. 327, p. 539–553, https://doi.org/10.1016/j.jvolgeores.2016.09.021.
Lustrino, M., Fedele, L., Agostini, S., Prelević, D., and Salari, G., 2019, Leucitites within and around the Mediterranean area: Lithos, v. 324–325, p. 216–233, https://doi.org/10.1016/j.lithos.2018.11.007.
Masun, K., Sthapak, A.V., Singh, A., Vaidya, A., and Krishna, C., 2009, Exploration history and geology of the diamondiferous ultramafic Saptarshi intrusions, Madhya Pradesh, India: Lithos, v. 112S, p. 142–154, https://doi.org/10.1016/j.lithos.2009.06.003.
Mathur, S.M., and Singh, H.N., 1971, Petrology of the Majhgawan pipe rocks: Geological Survey of India, Miscellaneous Publication, v. 19, p. 78–85.
McCulloch, M.T., Jaques, A.L., Nelson, D.R., and Lewis, J.D., 1983, Nd and Sr isotopes in kimberlites and lamproites from Western Australia: An enriched mantle origin: Nature, v. 302, p. 400–403, https://doi.org/10.1038/302400a0.
Meyer, H.O.A., 1976, Kimberlites of the continental United States: A Review: The Journal of Geology, v. 84, p. 377–403, https://dx.doi/10.2307/30066057.
Miller, C., Schuster, R., Klötzli, U., Frank, W., and Purtscheller, F., 1999, Post-collisional potassic and ultrapotassic magmatism in SW Tibet: Geochemical and Sr–Nd–Pb–O isotopic constraints for mantle source characteristics and petrogenesis: Journal of Petrology, v. 40, p. 1399–1424, https://doi.org/10.1093/petroj/40.9.1399.
Mirnejad, H., and Bell, K., 2006, Origin and source evolution of the Leucite Hills lamproites: evidence from Sr–Nd–Pb–O isotopic compositions: Journal of Petrology, v. 47, p. 2463–2489, https://doi.org/10.1093/petrology/egl051.
Mitchell, R.H., 1986, Kimberlites: Mineralogy, Geochemistry, and Petrology: Plenum Press, New York, 442 p.
Mitchell, R.H., 1995a, Kimberlites, Orangeites and Related Rocks: Plenum Press, New York, 410 p., https://doi.org/10.1007/978-1-4615-1993-5.
Mitchell, R.H., 1995b, Melting experiments on a sanidine phlogopite lamproite at 4–7 GPa and their bearing on the sources of lamproitic magmas: Journal of Petrology, v. 36, p. 1455–1474, https://doi.org/10.1093/petrology/36.5.1455.
Mitchell, R.H., 1996, Undersaturated potassic plutonic complexes, *in* Mitchell, R.H., *ed.*, Undersaturated Alkaline Rocks: Mineralogy, Petrogenesis and Economic Potential: Mineralogical Association of Canada Short Course, v. 24, p. 193–216.
Mitchell, R.H., 1997, Kimberlites, Orangeites, Lamproites, Melilitites, and Minettes: A Petrographic Atlas: Almaz Press, Thunder Bay, Ontario, Canada, 234 p.
Mitchell, R.H., 2006, Potassic magmas derived from metasomatized lithospheric mantle: Nomenclature and relevance to exploration for diamond-bearing rocks: Journal of the Geological Society of India, v. 67, p. 317–327.
Mitchell, R.H., 2007, Potassic rocks from the Gondwana Coalfields of India: Closing Pandora's Box of petrological confusion?: Journal of the Geological Society of India, v. 69, p. 505–512.
Mitchell, R.H., and Bergman, S.C., 1991, Petrology of Lamproites: Plenum Press,

New York, 447 p., https://doi.org/10.1007/978-1-4615-3788-5.
Mitchell, R.H., and Fareeduddin, 2009, Mineralogy of peralkaline lamproites from the Raniganj Coalfield, India: Mineralogical Magazine, v. 73, p. 457–477, https://doi.org/10.1180/minmag.2009.073.3.457.
Mitchell, R.H., Platt, RG., and Downey, M., 1987, Petrology of lamproites from Smoky Butte, Montana: Journal of Petrology, v. 28, p. 645–677.
Mitchell, R.H., Giuliani, A., and O'Brien, H., 2019, What is a kimberlite? Petrology and mineralogy of hypabyssal kimberlites: Elements, v. 15, p. 381–386, https://doi.org/10.2138/gselements.15.6.381.
Mo, X., Zhao, Z., Deng, J., Flower, M., Yu, X., Luo, Z., Li, Y., Zhou, S., Dong, G., Zhu, D., and Wang, L., 2006, Petrology and geochemistry of postcollisional volcanic rocks from the Tibetan plateau: Implications for lithosphere heterogeneity and collision-induced asthenospheric mantle flow, *in* Dilek, Y., and Pavlides, S., *eds.*, Postcollisional Tectonics and Magmatism in the Mediterranean Region and Asia: Geological Society of America Special Papers, v. 409, p. 507–530, https://doi.org/10.1130/2006.2409(24).
Mukherjee, K.K., 1961, Petrology of the lamprophyres of the Bokaro coalfield: Quarterly Journal of the Mineralogical and Metallurgical Society of India, v. 33, p. 69–87.
Nelson, D.R., McCulloch, M.T., and Sun, S.-S., 1986, The origins of ultrapotassic rocks as inferred from Sr, Nd, and Pb isotopes: Geochimica et Cosmochimica Acta, v. 50, p. 231–245, https://doi.org/10.1016/0016-7037(86)90172-9.
Niggli, P., 1923, Gesteins und Mineralprovinzen: Verlag Gebrüder Borntraegar, Berlin, 586 p.
O`Brien, H.E., Irving, A.J., McCallum, I.S., and Thirwall, M.F., 1995, Strontium, neodymium, and lead isotopic evidence for the interaction of post-subduction asthenospheric potassic mafic magmas of the Highwood Mountains, Montana, USA, with ancient Wyoming craton lithospheric mantle: Geochimica et Cosmochimica Acta, v. 59, p. 4539–4556, https://doi.org/10.1016/0016-7037(95)99266-J.
Osann, A., 1906, Über einige Alkaligestein aus Spanien: Festschrift Rosenbusch, Stuttgart, p. 283–301.
Pearson, D.G., Woodhead, J., and Janney, P.E., 2019, Kimberlites as geochemical probes of the Earth's mantle: Elements, v. 15, p. 387–392, https://doi.org/10.2138/gselements.15.6.387.
Pe-Piper, G., Zhang, Y., Piper, D.J.W., and Prelević, D., 2014, Relationship of Mediterranean-type lamproites to large shoshonite volcanoes, Miocene of Lesbos, NE Aegean Sea: Lithos, v. 184–187, p. 281–299, https://doi.org/10.1016/j.lithos.2013.11.004.
Prelević, D., and Foley, S.F., 2007, Accretion of arc-oceanic lithospheric mantle in the Mediterranean: Evidence from extremely high-Mg olivines and Cr-rich spinel inclusions in lamproites: Earth and Planetary Science Letters, v. 256, p. 120–135, https://doi.org/10.1016/j.epsl.2007.01.018.
Prelević, D., Foley, S.F., Romer, R.L., Cvetković, V., and Downes, H., 2005, Tertiary ultrapotassic volcanism in Serbia: constraints on petrogenesis and mantle source characteristics: Journal of Petrology, v. 46, p. 1443–1487, https://doi.org/10.1093/petrology/egi022.
Prelević, D., Akal, C., Foley, S.F., 2008a, Orogenic vs anorogenic lamproites in a single volcanic province: Mediterranean-type lamproites from Turkey: Don Harrington Symposium on the Geology of the Aegean, IOP Conference Series: Earth and Environmental Science 2; IOP Publishing, 012024, https://doi.org/10.1088/1755-1307/2/1/012024.
Prelević, D., Foley, S.F., Romer, R., and Conticelli, S., 2008b, Mediterranean Tertiary lamproites derived from multiple source components in postcollisional geodynamics: Geochimica et Cosmochimica Acta, v. 72, p. 2125–2156, https://doi.org/10.1016/j.gca.2008.01.029.
Prelević, D., Stracke, A., Foley, S.F., Romer, R.L., and Conticelli, S., 2010, Hf isotope compositions of Mediterranean lamproites: Mixing of melts from asthenosphere and crustally contaminated mantle lithosphere: Lithos, v. 119, p. 297–312, https://doi.org/10.1016/j.lithos.2010.07.007.
Presser, J.L.B., 2000, Lamproites of the Ybytyruzú field, Guairá Department, Eastern Paraguay (Abstract): International Brazil 2000, First International Geological Congress.
Rao, T.K., 2007, Panna Diamond Belt, Madhya Pradesh – A critical review: Journal of the Geological Society of India, v. 69, p. 513–522.
Rayner, M.J., Jaques, A.L., Boxer, G.L., Smith, C.B., Lorenz, V., Moss, S.W., Webb, K., and Ford, D., 2018, The geology of the Argyle (AK1) diamond deposit, Western Australia, *in* Davy, A.T., Smith, C.B., Helmstaedt, H., Jaques, A.L., and Gurney, J.J., *eds.,* Geoscience and Exploration of the Argyle, Bunder, Diavik, and Murowa Diamond Deposits: Society of Economic Geologists, Special Publication, v. 20, p. 89–117, https://doi.org/10.5382/SP.20.04.
Reolid, M., Abad, I., and Sanchez-Gomez, M., 2015, Phreatomagmatic activity and associated hydrothermal processes in the lamproitic volcano of Cancarix (Southeast Spain): Journal of Iberian Geology, v. 41, p. 183–204, https://doi.org/10.5209/rev_JIGE.2015.v41.n2.46696.
Roffey, S., Rayner, M.J., Davy, A.T., and Platell, R.W., 2018, Evaluation of the AK1 Deposit at Argyle Diamond Mine, *in* Davy, A.T., Smith, C.B., Helmstaedt, H., Jaques, A.L., and Gurney, J.J., *eds.,* Geoscience and Exploration of the Argyle, Bunder, Diavik, and Murowa Diamond Deposits: Society of Economic Geologists, Special Publication, v. 20, p. 65–87, https://doi.org/10.5382/SP.20.03.
Scott Smith, B.H., 1989, Lamproites and kimberlites in India: Neues Jahrbuch für Mineralogie Abhandlungen, v. 161, p. 193–225.
Scott Smith, B.H., 2008, The Fort à la Corne kimberlites, Saskatchewan, Canada: Geology, emplacement and economics: Journal of the Geological Society of India, v. 71, p. 11–55.
Scott Smith, B.H., and Skinner, E.M.W., 1984, Diamondiferous lamproites: Journal of Geology, v. 92, p. 433–438, https://doi.org/10.1086/628877.
Scott Smith, B.H., Nowicki, T.E., Russell, J.K., Webb, K.J., Mitchell, R.H., Hetman, C.M., and Robey, J.vA., 2018, A Glossary of Kimberlite and Related Terms Part 1: Scott-Smith Petrology Inc., North Vancouver, British Columbia, Canada, 144 p.
Shaikh, A.M., Patel, S.C., Bussweiler, Y., Kumar, S.P., Tappe, S., Ravi, S., and Mainkar, D., 2019, Olivine trace element compositions in diamondiferous lamproites from India: Proxies for magma origins and the nature of the lithospheric mantle beneath the Bastar and Dharwar cratons: Lithos, v. 324–325, p. 501–518, https://doi.org/10.1016/j.lithos.2018.11.026.
Shand, S.J., 1922, The problem of the alkaline rocks: Proceedings of the Geological Society of South Africa, v. 25, p. xix–xxxii.
Smith, C.B., 1983, Pb, Sr and Nd isotopic evidence for sources of southern African Cretaceous kimberlites: Nature, v. 304, p. 51–54, https://doi.org/10.1038/304051a0.
Smith, C.B., Skinner, E.M.W., Clement, C.R., Gurney, J.J., and Ebrahim, N., 1985, Geochemical character of southern African kimberlites: A new approach based on isotopic constraints: Transactions of the Geological Society of South Africa, v. 88, p. 267–280.
Venturelli, G., Capedri, S., Di Battistini, G., Crawford, A., Kogarko, L.N., and Celestini, S., 1984, The ultrapotassic rocks from southeastern Spain: Lithos, v. 17, p. 37–54, https://doi.org/10.1016/0024-4937(84)90005-7.
Vollmer, R., Ogden, P., Schilling, J.-G., Kingsley, R.H., and Waggoner, D.G., 1984, Nd and Sr isotopes in ultrapotassic volcanic rocks from the Leucite Hills, Wyoming: Contributions to Mineralogy and Petrology, v. 87, p. 359–368, https://doi.org/10.1007/BF00381292.
Wade, A., and Prider, R.T., 1940, The leucite-bearing rocks of the West Kimberley area, Western Australia: Quarterly Journal of the Geological Society, v. 96, p. 39–98, https://doi.org/10.1144/GSL.JGS.1940.096.01-04.04.
Wagner, P.A., 1914, The Diamond Fields of Southern Africa: Transvaal Leader, Johannesburg, 355 p.
Wagner, P.A., 1928, The evidence of the kimberlite pipes on the constitution of the outer part of the Earth: South African Journal of Science, v. 25, p. 127–148.
Woolley, A.R., Bergman, S.C., Edgar, A.D., Le Bas, M.J., Mitchell, R.H., Rock, N.M.S., and Scott Smith, B.H., 1996, Classification of lamprophyres, lamproites, kimberlites, and the kalsilitic, melilitic, and leucitic rocks: Canadian Mineralogist, v. 34, p. 175–186.
Xia, L., Li, X., Ma, Z., Xu, X., and Xia, Z., 2011, Cenozoic volcanism and tectonic evolution of the Tibetan plateau: Gondwana Research, v. 19, p. 850–866, https://doi.org/10.1016/j.gr.2010.09.005.
Xiang, L., Zheng, J., Zhai, M., and Siebel, W., 2020, Geochemical and Sr–Nd–Pb isotopic constraints on the origin and petrogenesis of Paleozoic lamproites in the southern Yangtze Block, South China: Contributions to Mineralogy and Petrology, v. 175, 29, https://doi.org/10.1007/s00410-020-1668-1.
Xiao, Z., Fuji, N., Iidaka, T., Gao, Y., Sun, X., and Liu, Q., 2020, Seismic structure beneath the Tibetan Plateau from iterative finite-frequency tomography based on ChinArray: New insights into the Indo-Asian collision: Journal of Geophysical Research, v. 125, e2019JB018344, https://doi.org/10.1029/2019JB018344.
Zhang, L., Guo, Z., Zhang, M., Cheng, Z., and Sun, Y., 2017, Post-collisional potassic magmatism in the eastern Lhasa terrane, South Tibet: Products of partial melting of mélanges in a continental subduction channel: Gondwana Research, v. 41, p. 9–28, https://doi.org/10.1016/j.gr.2015.11.007.

Received June 2020
Accepted as revised August 2020

SERIES

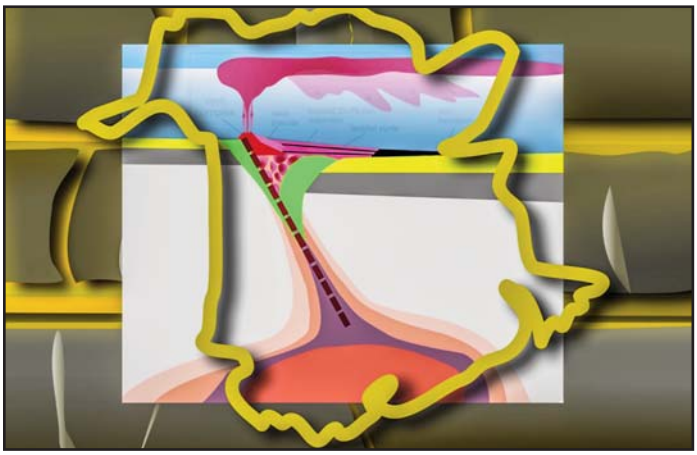

Great Mining Camps of Canada 8. The Bathurst Mining Camp, New Brunswick, Part 2: Mining History and Contributions to Society

Steven R. McCutcheon[1] and James A. Walker[2]

[1]McCutcheon Geo-Consulting
1935 Palmer Drive, Bathurst, New Brunswick, E2A 4X7, Canada
Email: steve.mccutch@gmail.com

[2]New Brunswick Department of Natural Resources and Energy Development
Minerals and Petroleum Division
2574 Route 180, South Tetagouche, New Brunswick, E2A 7B8 Canada

SUMMARY

In the Bathurst Mining Camp (BMC), 12 of the 45 known massive sulphide deposits were mined between 1957 and 2013; one was mined for iron prior to 1950, whereas three others had development work but no production. Eleven of the deposits were mined for base metals for a total production of approximately 179 Mt, with an average grade of 3.12% Pb, 7.91% Zn, 0.47% Cu, and 93.9 g/t Ag. The other deposit was solely mined for gold, present in gossan above massive sulphide, producing approximately one million tonnes grading 1.79 g/t Au. Three of the 11 mined base-metal deposits also had a gossan cap, from which gold was extracted. In 2012, the value of production from the Bathurst Mining Camp exceeded $670 million and accounted for 58 percent of total mineral production in New Brunswick.

Base-metal production started in the BMC in 1957 from deposits at Heath Steele Mines, followed by Wedge in 1962, Brunswick No. 12 in 1964, Brunswick No. 6 in 1965, Caribou in 1970, Murray Brook, Stratmat Boundary and Stratmat N-5 in 1989, Captain North Extension in 1990, and lastly, Half Mile Lake in 2012. The only mine in continuous production for most of this time was Brunswick No. 12. During its 49-year lifetime (1964–2013), it produced 136,643,367 tonnes of ore grading 3.44% Pb, 8.74% Zn, 0.37% Cu, and 102.2 g/t Ag, making it one of the largest underground base-metal mines in the world.

The BMC remains important to New Brunswick and Canada because of its contributions to economic development, environmental measures, infrastructure, mining innovations, and society in general. The economic value of metals recovered from Brunswick No. 12 alone, in today's prices exceeds $46 billion. Adding to this figure is production from the other mines in the BMC, along with money injected into the local economy from annual exploration expenditures (100s of $1000s per year) over 60 years. Several environmental measures were initiated in the BMC, including the requirement to be clean shaven and carry a portable respirator (now applied to all mines in Canada); ways to treat acid mine drainage and the thiosalt problem that comes from the milling process; and pioneering studies to develop and install streamside-incubation boxes for Atlantic Salmon eggs in the Nepisiguit River, which boosted survival rates to over 90%. Regarding infrastructure, provincial highways 180 and 430 would not exist if not for the discovery of the BMC; nor would the lead smelter and deep-water port at Belledune. Mining innovations are too numerous to list in this summary, so the reader is referred to the main text. Regarding social effects, the new opportunities, new wealth, and training provided by the mineral industry dramatically changed the living standards and social fabric of northern New Brunswick. What had been a largely poor, rural society, mostly dependent upon the fishing and forestry industries, became a thriving modern community. Also, untold numbers of engineers, geologists, miners, and prospectors `cut their teeth' in the BMC, and many of them have gone on to make their mark in other parts of Canada and the world.

Geoscience Canada, v. 47, https://doi.org/10.12789/geocanj.2020.47.163 pages 143–166

RÉSUMÉ

Dans le camp minier de Bathurst (CMB), 12 des 45 gisements de sulfures massifs connus ont été exploités entre 1957 et 2013; un de ces gisements a été exploité pour le fer avant 1950, tandis que trois autres étaient en développement mais pas en production. Onze gisements ont été exploités pour des métaux communs pour une production totale d'environ 179 Mt, avec une teneur moyenne de 3,12% Pb, 7,91% Zn, 0,47% Cu et 93,9 g/t Ag. L'autre gisement était uniquement exploité pour l'or, présent dans le gossan au-dessus du sulfure massif, produisant environ un million de tonnes titrant 1,79 g/t Au. Trois des 11 gisements de métaux communs exploités avaient également un gossan, d'où l'or était extrait. En 2012, la valeur de la production du camp minier de Bathurst dépassait 670 millions de dollars et représentait 58% de la production minérale totale au Nouveau-Brunswick.

La production de métaux communs a commencé dans le CMB en 1957 à partir des gisements de Heath Steele Mines, suivie de Wedge en 1962, Brunswick no 12 en 1964, Brunswick no 6 en 1965, Caribou en 1970, Murray Brook, Stratmat Boundary et Stratmat N- 5 en 1989, Captain North Extension en 1990, et enfin Half Mile Lake en 2012. La seule mine en production continue pendant la majeure partie de cette période était Brunswick no 12. Au cours de sa durée de vie de 49 ans (1964–2013), elle a produit 136 643 367 tonnes de minerai titrant 3,44% Pb, 8,74% Zn, 0,37% Cu et 102,2 g/t Ag, ce qui en fait l'une des plus grandes mines souterraines de métaux communs au monde.

Le CMB demeure important pour le Nouveau-Brunswick et le Canada en raison de sa contribution au développement économique, aux mesures environnementales, à l'infrastructure, aux innovations minières et à la société en général. La valeur économique des métaux récupérés du seul gisement Brunswick n° 12, aux prix d'aujourd'hui, dépasse 46 milliards de dollars. S'ajoute à ce chiffre la production des autres mines du CMB, ainsi que l'argent injecté dans l'économie locale par les dépenses d'exploration annuelles (des centaines à des milliers de $ par an) sur 60 ans. Plusieurs mesures environnementales ont été lancées dans le CMB, y compris l'exigence d'être rasé de près et de porter un respirateur portatif (maintenant appliqué à toutes les mines au Canada); les moyens de traitement des effluents miniers acides et le problème des thiosels qui proviennent du processus de broyage; et les études pionnières pour développer et installer des boîtes d'incubation en bord de rivière pour les œufs de saumon de l'Atlantique dans la rivière Nepisiguit, ce qui a fait passer les taux de survie à plus de 90%. En ce qui concerne les infrastructures, les routes provinciales 180 et 430 n'existeraient pas sans la découverte du CMB; la fonderie de plomb et le port en eau profonde de Belledune non plus. Les innovations minières sont trop nombreuses pour être énumérées dans ce résumé, le lecteur est donc renvoyé au texte principal. En ce qui concerne les effets sociaux, les nouvelles possibilités, la nouvelle richesse et la formation offertes par l'industrie minière ont radicalement changé le niveau de vie et le tissu social du nord du Nouveau-Brunswick. Ce qui avait été une société rurale en grande partie pauvre, principalement tributaire des industries de la pêche et de la sylviculture, est devenu une communauté moderne florissante. De plus, un nombre incalculable d'ingénieurs, de géologues, de mineurs et de prospecteurs «se sont fait les dents» au CMB, et bon nombre d'entre eux ont continué à faire leurs marques dans d'autres régions du Canada et du monde.

Traduit par la Traductrice

INTRODUCTION

The Bathurst Mining Camp (BMC) is known worldwide for its volcanogenic massive sulphide (VMS) deposits, especially the Brunswick No. 12 Mine, which closed on April 30, 2013 after 49 years in operation. During its lifetime, this mine produced 136,643,367 tonnes of ore grading 3.44% Pb, 8.74% Zn, 0.37% Cu, and 102.2 g/t Ag (Table 1), making it one of the world's largest underground VMS mines. This paper describes the history of mine developments in the BMC up to closure of Brunswick No. 12. A companion paper (McCutcheon and Walker 2019) entitled: *The Bathurst Mining Camp, Part 1: Geology and Exploration History* describes the geological setting of the BMC and the history of exploration.

Camp Overview

The location and definition of the BMC are described in McCutcheon and Walker (2019). Suffice it to say that the BMC occupies an area of approximately 3800 km^2 in the central part of northern New Brunswick (Fig. 1). Twelve of the 45 known massive sulphide deposits were mined between 1957 and 2013; whereas Austin Brook was mined prior to 1950 (Table 1). Although there has been development work on three others (Chester, Key Anacon and Hachey-Shaft), there was no production. Most of these deposits were discovered in the 1950s and 1960s by a combination of airborne geophysical, geological and stream geochemical methods (McCutcheon et al. 2003).

The BMC is one of Canada's most important base metal mining districts, accounting for approximately 2.8% of total metal production in 2012 (https://sead.nrcan-rncan.gc.ca/MIS/MISTable.aspx?FileT=01&Year=2012), the last full year of production at Brunswick No. 12. This includes approximately 30% of Canada's production of Zn, 81% of its Pb, 21% of its Ag, and 2% of its Cu. Eleven massive sulphide deposits have been mined for a total production to 2013 of approximately179 Mt, with an average grade of 3.12% Pb, 7.91% Zn, 0.47% Cu, and 93.9 g/t Ag (Table 1). In addition, 0.337 Mt of copper ore was mined from the Caribou supergene zone and 1.254 Mt of gold-bearing gossans, collectively from Caribou, Murray Brook, and Heath Steele (Boyle 2003), of which one million tonnes came from Murray Brook (Table 1). In 2012, the value of production from the Bathurst Mining Camp exceeded $650 million and accounted for approximately 57% of total mineral production in New Brunswick (https://sead.nrcan-rncan.gc.ca/MIS/MISTable.aspx?FileT=01&Year=2012).

Information Sources

Much has been written about the geology and mineral deposits of the BMC since its discovery in 1952 but the best place to

Table 1. List of Bathurst Mining Camp deposits with Unique Record Numbers (URN) in the New Brunswick 'Mineral Occurrence Database', which have been mined since 1957, showing tonnages and average grades.

URN	Deposit	Tonnage	%Pb	%Zn	%Cu	g/t Ag	g/t Au	Date	Source
054	Brunswick No. 12	136,643,367	3.44	8.74	0.37	102.2		1964–2013	Production to mine closure in 2013 (P. Bernard written communication)
144	Brunswick No. 6	12,762,962	2.15	5.45	0.4	66.5		1966–1983	Milled at Brunswick No. 12 (P. Bernard written communication)
444	Caribou	4,426,874	2.8	6.1				to 2017	Includes production from several operators: Anaconda, East-West Caribou, Breakwater, Blue Note and Trrevali to end of 2017 (Jensen et al. 2018)
170	Captain North Extension (CNE)	39,000	4.42	9.97		134.7		1990–1992	Ore milled at Heath Stele (Luff 1995)
170	Captain North Extension (CNE)	62,720	3.22	8.13	0.44	111		2013	Ore milled at Brunswick No. 12; P. Bernard written communication)
409	Halfmile	125,569	1.61	4.83	0.45	44.0		2012	Ore milled at Brunswick No 12; P. Bernard written communication)
395	Heath Steele ACD Zone	553,100	4.18	11.26	0.29	111		to 1998	Heath Steele Mines (A. Hamilton written communication)
396	Heath Steele B Zone	20,723,000	1.75	4.79	0.98	65.5		to 1999	Heath Steele Mines (A. Hamilton written communication)
255 & 257	Heath Steele N-5 and Stratmat Boundary	1,137,000	2.98	8.11	0.35	44		1991	Luff (1995)
414	Murray Brook	1,014,000				61.4	1.79	1989–1993	Gossan production (Luff 1995)
138	Restigouche	795,801	5.00	6.5				to 2017	Jensen et al. (2018)
052	Wedge	1,503,500	0.65	1.61	2.88	20.6		1962–1968	Ore milled at Heath Steele (Luff 1995)
Total tonnage and average grade:		**178,772,893**	**3.12**	**7.91**	**0.47**	**93.91**			

URN = Unique Record Number; Total tonnage excludes Murray Brook; Caribou and Restigouche are excluded for average Cu and Ag grades

start is with *Economic Geology Monograph 11* (Goodfellow et al. 2003), because this volume provides extensive lists of references to previous work on various topics. There are also two special issues of *Exploration and Mining Geology* that are devoted to mineral deposits of the BMC (Davies et al. 1992; Lentz 2006). The website of the Geological Surveys Branch of New Brunswick Department of Natural Resources and Energy Development (NBNRED) (http://www2.gnb.ca/content/gnb/en/departments/erd/energy/content/minerals.html) has online databases that contain a wealth of information, including a 'Mineral Occurrence Database' that has information about mine development and production in the Province. Finally, Technical Reports filed on the 'System for Electronic Document Analysis and Retrieval' (SEDAR) website (https://www.sedar.com/homepage_en.htm) contain post-2008 mine development data for some deposits.

Historical information about mining in the BMC comes from published books and articles, most notably: *The Birth of the Bathurst Mining Camp* (Belland 1992), which describes the development history of the Austin Brook Iron Mine and Brunswick No. 6 base-metal deposit; Heath Steele (Gallagher 1999), which describes the history of that mine and the people who worked there; and *Brunswick Mine* (Jarratt 2012), which describes the history of the Brunswick No. 6 and No. 12 mines. A journal article by Kenny (1997) describes the development of New Brunswick's base metal industry. In addition, articles from *The Northern Miner*, and New Brunswick newspapers, such as *The Northern Light*, *The Daily Gleaner*, and *Telegraph Journal* are too numerous to list. Finally, unpublished correspondence and photographs in the files of the New Brunswick NRED provide useful historical information.

HISTORY OF MINE DEVELOPMENT AND PRODUCTION

The history of mine development in the BMC begins with the Austin Brook Mine, originally called Drummond Mines, which produced approximately 145,000 tonnes (164,282 tons) of iron ore between 1911 and 1913, when Canada Iron Corporation closed the mine (Belland 1992). The mine was reopened in 1943 by the Dominion Steel and Coal Company (DOSCO) of Nova Scotia to obtain a secure supply of ore for its steel mill in Sydney. Prior to this, DOSCO's ore had been coming from the Wabana Iron Mines in Newfoundland (Pollock 2019), but

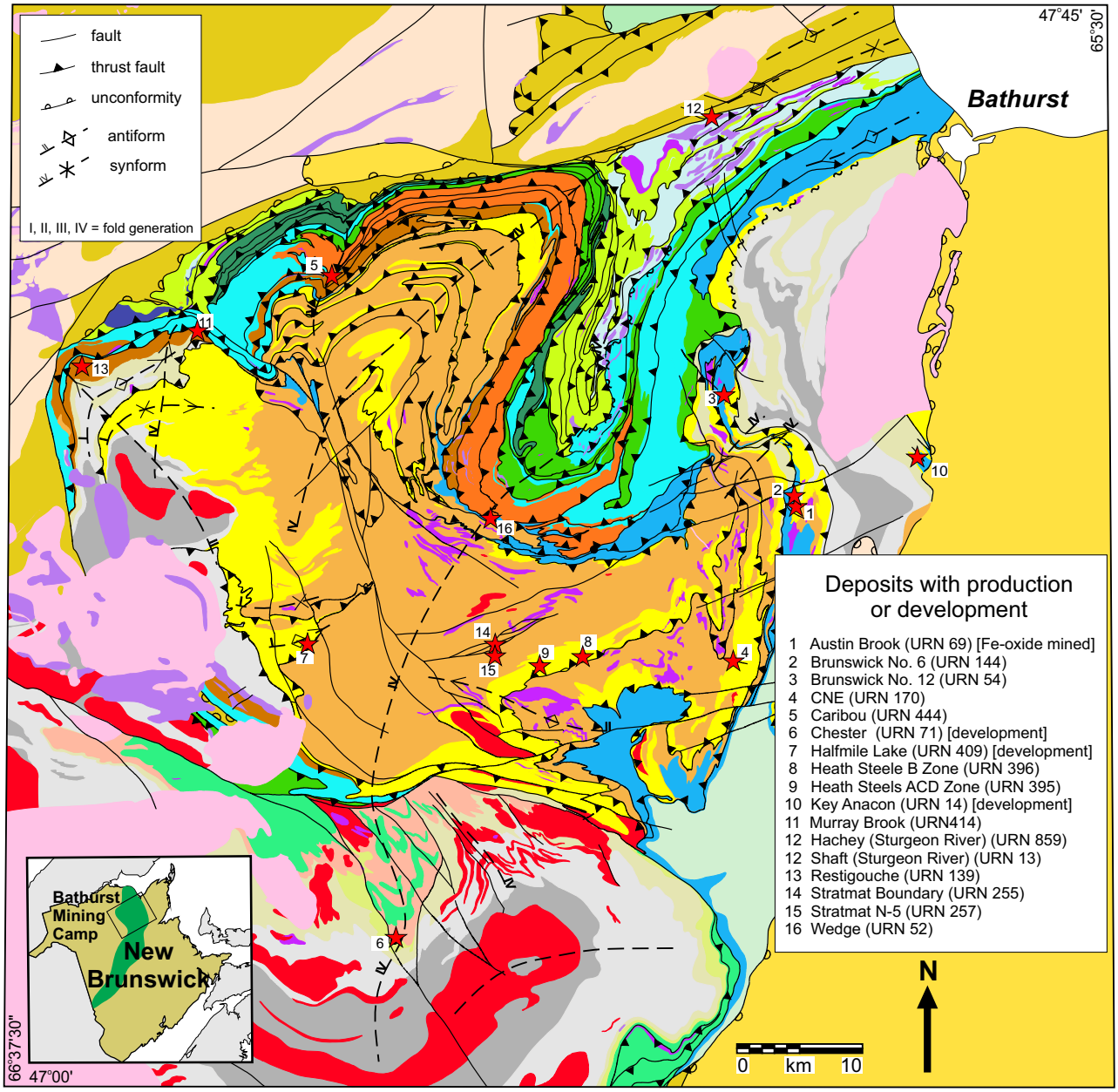

Carboniferous
- Sedimentary rocks

Upper Silurian - Devonian
- Granite
- Gabbro
- Sedimentary and volcanic rocks

Silurian
- Sedimentary and volcanic rocks

- Gabbro
- Granite

Fournier Supergroup
- Elmtree Formation (E)
- Millstream Formation (M)
- Sormany Formation

Bathurst Supergroup

California Lake Group
- Boucher Brook Formation (BB)
- Mount Brittain Formation (B)
- Spruce Lake Formation (S)
- Canoe Landing Lake Formation (CL)

Middle Ordovician - Lower Silurian
- Blueschist nappe

Tetagouche Group
- Tomogonops Formation (T)
- Little River Formation (LR)
- Flat Landing Brook Formation (FB)
- Nepisiguit Falls Formation

Sheephouse Brook Group
- Slacks Lake Formation (SK)
- Sevogle River Formation
- Clearwater Stream Formation (C)

Cambrian - Lower Ordovician

Miramichi Group
- Patrick Brook Formation
- Knights Brook Formation
- Chain of Rocks Formation

Late Neoproterozoic - Lower Cambrian
- Upsalquitch gabbro

Figure 1. Simplified geological map of the Bathurst Mining Camp (BMC) showing the distribution of deposits and their Unique Record Numbers (URN) in the New Brunswick Mineral Occurrence Database, which have had development and/or been mined.

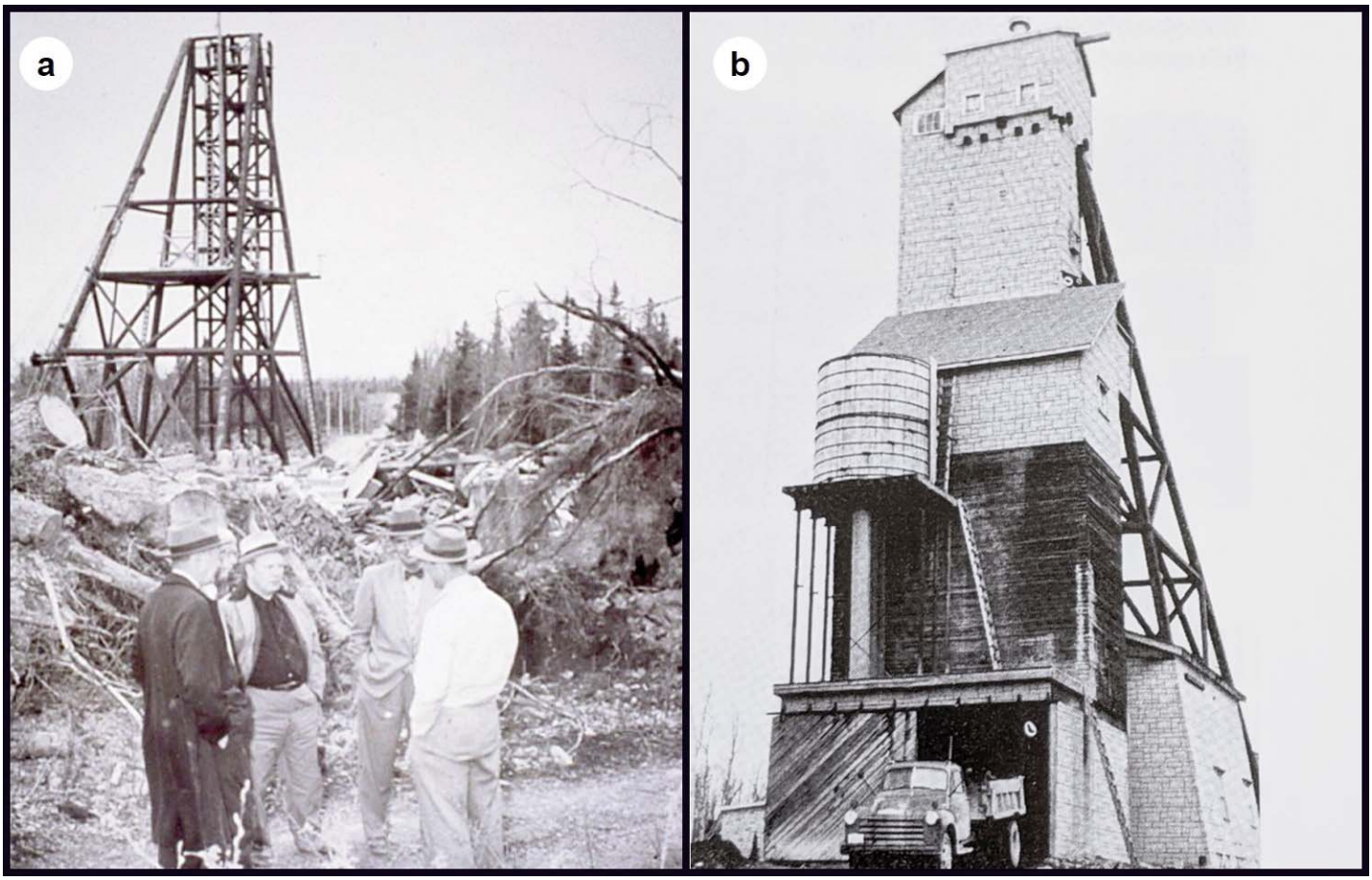

Figure 2. 1950s developments: a) Key Anacon (New Larder U) 1954, looking east with M.J. Boylen being the shortest guy, others unknown (New Brunswick Natural Resources and Energy Development archives); b) Brunswick No. 12 (#1 shaft), circa 1957, looking northwest (Brunswick Mining and Smelting archives).

in late 1942, German U-boats had attacked, and sunk ore carriers destined for Sydney, so the company acquired the mining rights to Austin Brook. During 1943, DOSCO mined approximately 118,000 tonnes (129,778 tons) of ore from Austin Brook before closing it at the end of the year.

The connection between iron ore at Austin Brook and the base-metal deposits of the BMC was not discovered until 1952 when Bennett (Ben) Baldwin, a graduate student at the University of New Brunswick, was examining samples of Austin Brook ore that had been collected by his supervisor, Dr. Graham MacKenzie, in 1943. Baldwin found lead and zinc in samples near the footwall of the iron ore deposit, which ultimately led to the discovery of the Brunswick No. 6 deposit in October of 1952, and the birth of the BMC (Belland 1992).

Subsequent mine development activity is described chronologically below by decade from the 1950s and ending with developments that postdate 2000. Deposits that have been mined or had some production work are shown in Figure 1 and production and resource numbers are shown in Table 1. Photographs of mine sites at various stages of development are also included.

1950s Development

The chronology of mine development in the 1950s is recorded in the pages of *The Northern Miner*, starting with the front page of the September 10, 1953 edition, entitled: "*Multi-Million Dollar Deal for New Brunswick Mines*". In this article, it was announced that the jointly owned property of Anacon Lead Mines and Leadridge Mining (Canadian subsidiary of St. Joseph Lead Co.) would be merged with the property of Brunswick Mining and Smelting Corporation. St. Joe would loan Brunswick $7.5 million (with provision for another $17.5 million) to develop both properties (now known as No. 12 and No. 6, respectively) and to do metallurgical research on the ores. St. Joe was to manage the project, but control of Brunswick was to remain with the Anacon–Boylen group.

In 1954, more developments were reported in *The Northern Miner* newspaper. The April 8th edition had the following text: "*Preparations for shaft sinking are going right ahead at New Larder U Island Mines* [now Key Anacon]*, near Bathurst N.B.*" The bridge over Nepisiguit River "*was completed this week and heavy equipment, which had been piled up on the west side of the river, can now be brought across and assembled at the shaft site*" (Fig. 2a). The May 13th edition reported: "*Plans of Brunswick Mining and Smelting Corp. for 1954 call for continuation of the present research program on ore treatment and it is planned to build a pilot mill for testing ore from both deposits* [No. 6 and No. 12]*, on a larger scale*". The June 10th edition reported: "*Erection of the headframe* [at No. 12] *is nearing the final stages of*

https://doi.org/10.12789/geocanj.2020.47.163

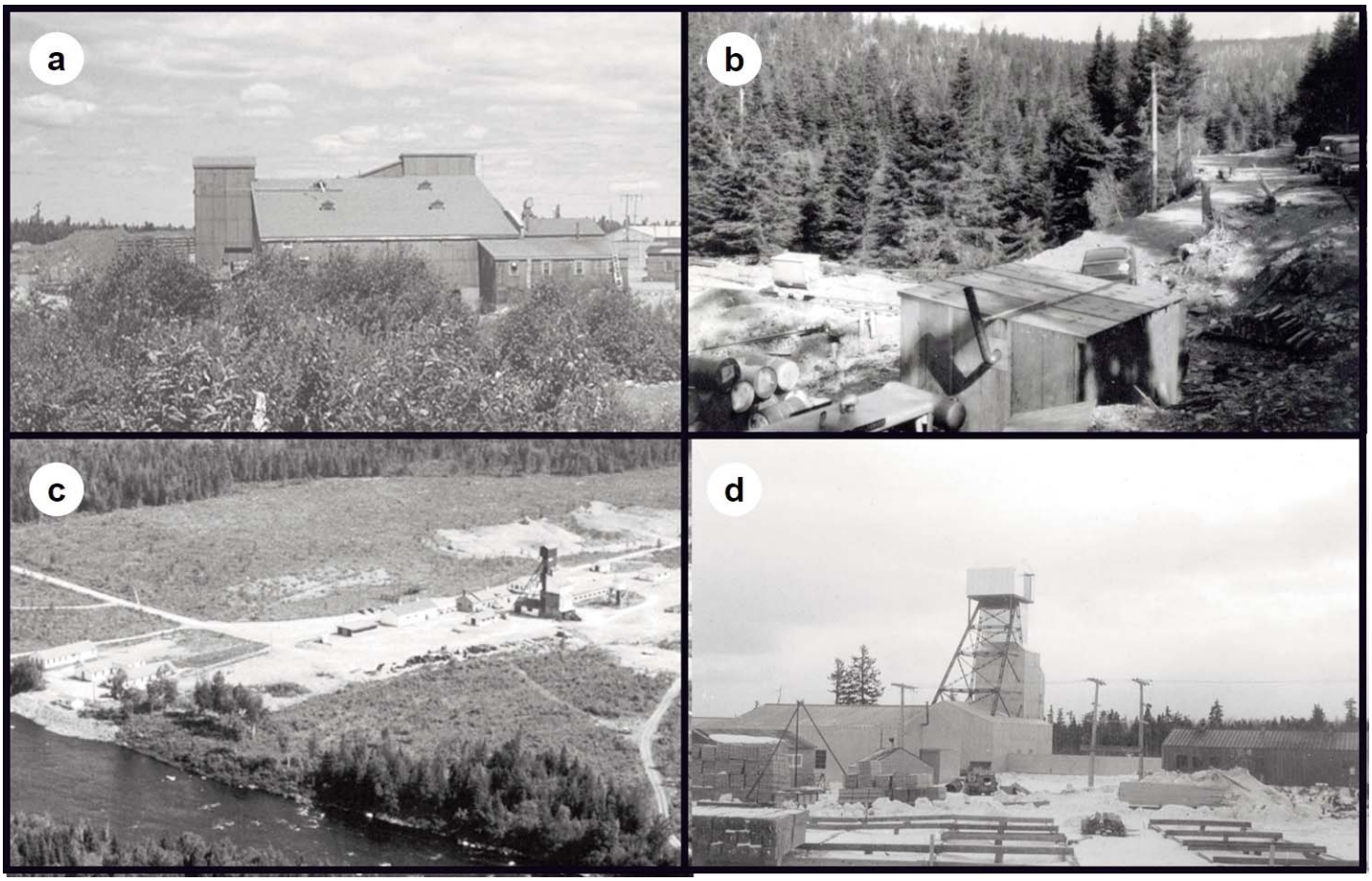

Figure 3. 1950s developments: a) Brunswick No. 6 pilot plant circa 1957, looking east (New Brunswick Natural Resources and Energy Development archives); b) view looking northeast over the Caribou adit entrance or portal (behind shed at bottom right; note ore car to the left of shed) circa 1959 (courtesy of Richard Cavellero); c) aerial view of Key Anacon (New Larder U) circa 1956, looking northeast with Nepisiguit River in the foreground (NBNRED archives); d) Brunswick No. 12 (#2 shaft) circa 1957, looking northeast (Brunswick Mining and Smelting archives).

completion…". Then on November 18th: "*The present development shaft* [Fig. 2b]…*will open up the orebody on two levels (200 and 350 ft.) and provide muck for feeding the 150-ton test mill* …[that] *is expected to be ready for operation by the end of January……The test mill is situated close to the Brunswick* [No. 6] *orebody, about six miles from the Anacon* [No. 12] *shaft*." Not much mine development work was reported in 1955. One article entitled: "*Magnificent Orebody Unfolds in Brunswick Crosscutting*" appeared on the front page of the May 26th edition of *The Northern Miner*. It states: "*The 150-ton pilot plant, situated six miles away on the No. 6 project* [the original Brunswick or Austin Brook orebody], *is in regular operation* [Fig. 3a]. *Currently it is working on ore from development headings at No. 12 but later in the season will start testing ore from the open pit at No. 6 mine."* Further along it is reported that: "*Lateral work is well along at the 350-ft. level but the crosscut from the (#1) shaft is only just now getting started at the 200-ft.*" The September 22nd edition reported that "*Construction of a permanent collar for the sinking of a second shaft (#2) to a depth of 2000 feet is rapidly nearing completion*".

Anaconda Minerals Company carried out preliminary surface mapping and exploration work on their Caribou property in 1955 and began drilling the deposit in 1956. In 1959, Anaconda excavated a 380 m long 2.4 m by 2.7 m adit (Fig. 3b) to obtain a bulk sample of the mineralization (Zhang et al. 2014).

The Northern Miner focused on other mine developments in 1956. A front-page article in the April 26th edition reports: "*In New Brunswick, lateral development is getting under way at Anacon's New Larder 'U' property* [Fig. 3c]. *The long job of sinking the shaft to 1,500 ft. depth has finally been completed and crosscuts to the ore zone ore* [*sic*] *now advancing on the 550, 850 and 1,300-ft. levels.*" Then on June 7th, the following headline appeared: "*Amco's Heath Steele Operation Hive of Construction Activity*". It states:

> "*A large area has been cleared at the site of the main plant, foundations for the mill and other buildings are pretty well completed and erection of the structures should be starting shortly...* [Fig. 4a, b]. *Additionally, four orebodies are being prepared for production. Two are being developed underground from shafts and two are being exposed in surface open pits.*" Furthermore: "*Underground development is farthest advanced on the D orebody, the most westerly of the known deposits. Here, the No. 1 shaft has been sunk to 480 ft. and some 1,500 ft. of lateral work completed on the 200 and 350-ft. levels…. To the east of the mill is the No. 2 shaft* [Fig. 4c] *and to the east of it is B open pit* [Fig. 4d]. *So far, only temporary plant and headframe have been erected at No. 2 shaft. Sinking has advanced to 250 ft. on the way to an objective of 480 ft.*"

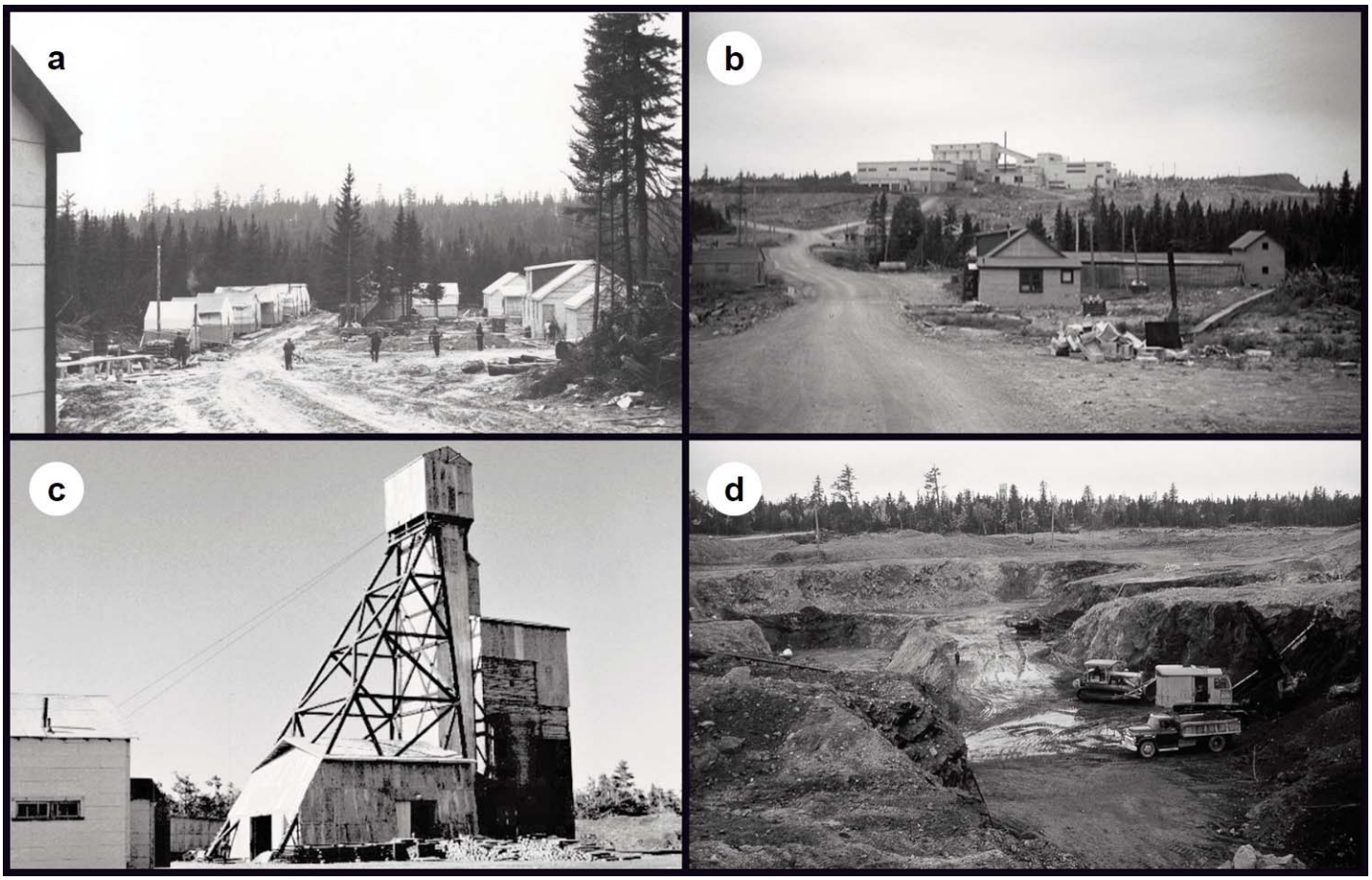

Figure 4. 1950s developments: a) site of Heath Steele gatehouse with construction camps in the background in1955, looking north (Our Miramichi Heritage Family archives); b) entrance to Heath Steele (foreground) with the mill complex on the hill in the background in late 1956, looking north (OMHF archives); c) headframe of No. 2 shaft at the B-Zone circa 1957, looking northwest (OMHF archives); d) Heath Steele B-Zone open-pit circa 1957, looking west with the headframe of No. 2 shaft (arrow) barely visible in the tree line (New Brunswick Natural Resources and Energy Development archives).

Then on June 14th, the following text appeared: "*At its No. 12 project, formerly termed the Anacon–Leadridge orebody, Brunswick Mining and Smelting Corp. is going ahead with preparations for the new 5-compartment No. 2 shaft which will be sunk to a depth of 2000 ft.*" (Fig. 3d). Finally, on June 21st, this headline appeared: "*Production Planned by Sturgeon River*". It states: "*This summer should see construction started on a concentrator of at least 400 tons capacity and the development underground of the indicated orebodies* [Shaft and Hachey deposits] *on the New Brunswick property of Sturgeon River Mines….A mining plant has been installed, electric power provided, and sinking is now underway to initial depth of 600 ft.*"

In 1957, *The Northern Miner* did not report on any new mine developments but provided updates on operations that existed in 1956. In the February 28th edition, there was a headline: "*Rush Construction on Railway Line for Heath Steele*". This article describes a 37 km spur line under construction betwehen the CNR main line and Heath Steele (Fig. 5a). The June 6th edition reports that:

> "*East drift headings on both the 200 and 500-ft. levels at Sturgeon River Mines* [Fig. 5b] *have just come into ore…. These east faces are into the west end of what is known as the Original shaft showing* [now Shaft deposit]. *The west drifts, headed for the Hachey showing* [now Hachey deposit], *have still some distance to go before they can expect to tap the start of the ore*". The May 30th edition had the following news: "…*Brunswick Mining and Smelting Corp. is proceeding with plans to bring the property into production…. The initial production unit will consist of a 2,000-ton flotation mill, plus a lead smelter and associated sulphuric acid plant…. The target date for production has been set for the spring of 1960.*" Further along, the article states: "*The production plan contemplates mining the high grade north end of the No. 12 orebody* [Fig. 5c] *for the first three and one half years and then swinging over to the No. 6 orebody for the next three and one half years ….A total of eight stopes has been laid out which will provide the 2,500,000 tons needed for the first 3$^{1/2}$ years production.*"

The front page of the June 20th edition has the following headline: "*Amco's Heath Steele Embarked on Profitable Metal Output*". The article states: "*The mill* [Fig. 5d], *with a rated capacity of 1,500 tons daily, was put into operation last February and tuning up has been in process since…. Two separate circuits are being operated in the mill. One is for treating the chalcocite* [copper] *ore and the other is for han-*

https://doi.org/10.12789/geocanj.2020.47.163

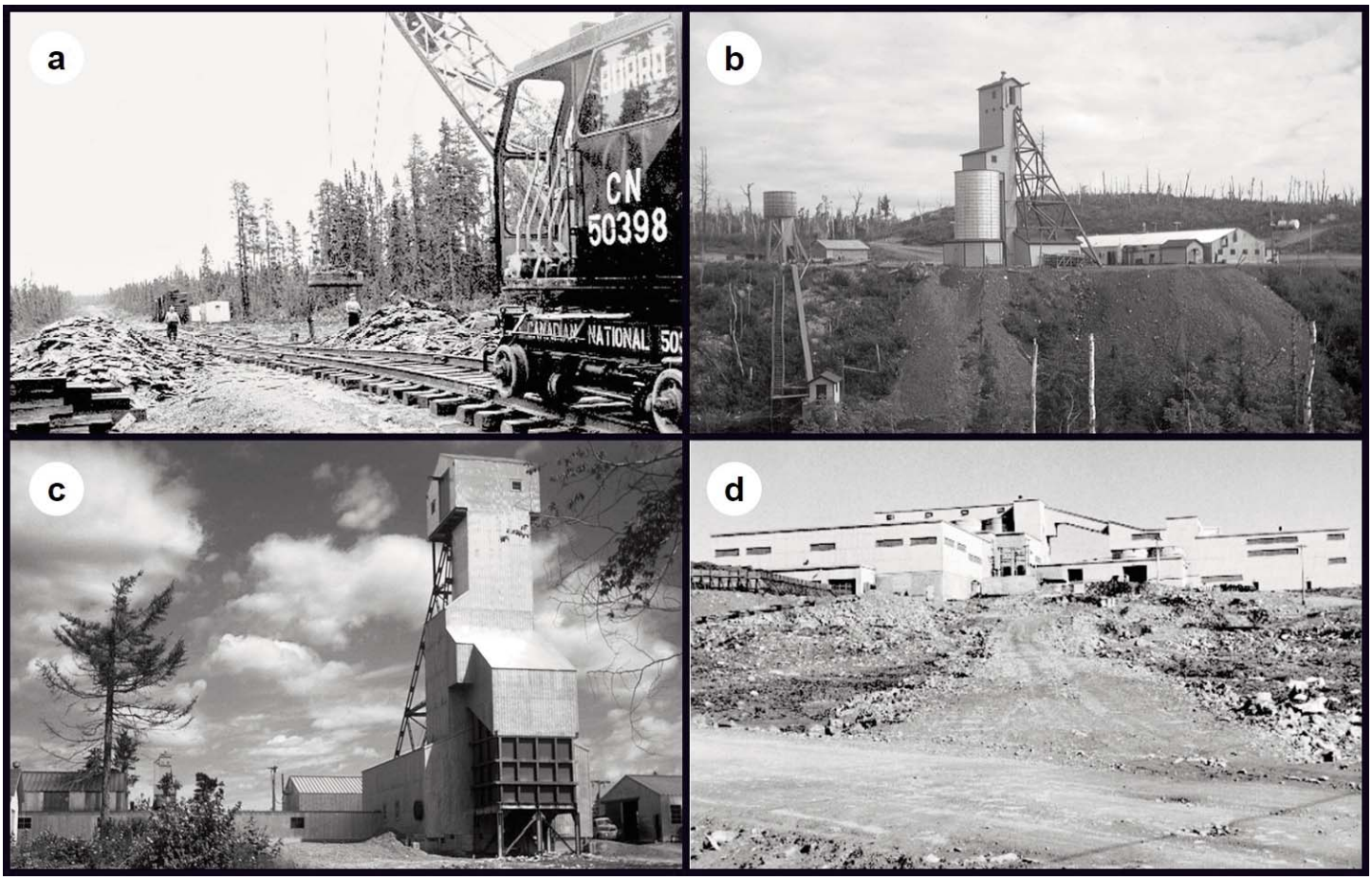

Figure 5. 1950s developments: a) construction of the CN spur line to Heath Steele in 1957, looking west (CN Images of Canada Collection); b) Sturgeon River Mines headframe at the Hachey-Shaft deposit circa 1957, looking north (New Brunswick Natural Resources and Energy Development archives); c) Brunswick No. 12 (#2 shaft in foreground with #1 shaft in background above bushes to the left) circa 1957, looking north (NBNRED archives); d) view of the Heath Steele mill in 1957, looking north (Our Miramichi Heritage Family archives).

dling the lead–zinc…. The three concentrates presently being made are: chalcocite, lead–copper and zinc. They are trucked out to Newcastle and shipped by rail to the smelter, but concentrates are now being accumulated for shipment by boat."

Gallagher (1999) noted: "*In June, the first shipload with 3,000 tons of Heath Steele copper concentrates left for a smelter in New Jersey.*"

Finally, the December 12, 1957 edition of *The Northern Miner* had the following headline: "*Continued Selling in Base Metals Leads Toronto Market Downward*", heralded a downturn in the metals markets and changed development plans. In April 1958, Heath Steele Mines, the first producer in the BMC, was shut down because of low metal prices (Gallagher 1999) and because the United States imposed a quota on lead–zinc imports in 1958 (Kenny 1997). Conversely, in early 1959, the Consolidated Mining and Smelting Company of Canada Limited (Cominco) decided to proceed with development of its Wedge deposit, by extending the power line from Heath Steele to the site, improving the road access, constructing a permanent camp, and sinking an exploration shaft (Douglas 1965). Other operations were put on care and maintenance mode in the late 1950s, including the project of Sturgeon River Mines, which was ultimately abandoned.

1960s Development

Mine development in the 1960s is largely described in books by Gallagher (1999) and Jarratt (2012) as well as a paper by Kenny (1997), but a paper by Douglas (1965) provides details about development of the Wedge Mine, and a Technical Report (Barrett 2014) describes developments at the Caribou Mine. The mining methods used at Brunswick No. 12 up to 1970 are described by Grebenc and Welwood (1971).

Shaft sinking began at Wedge in July, 1959, and "*was completed to a depth of 1,136 feet in 1960…….Arrangements were completed with the Heath Steele Company to use one half of their mill for treating the Wedge ore…..It was agreed that the portion of the road between Heath Steele and Nepisiquit* [*sic*] *river, as well as the bridge across the river, could be built under the Federal "Road to Resources" program, in which the Federal and Provincial Governments share the costs equally*" (Douglas 1965). The 4.8 km access road from the north side of the bridge to the Wedge property would be cost shared between Cominco and Government. Finally, the decision to proceed with production at 680 tonnes (750 tons) per day was made in early 1961 (Douglas 1965). Production began at Wedge, the second producer in the BMC, in January of 1962 (Fig. 6a, b) and ended in May of 1968.The following text is extracted from Gallagher (1999):

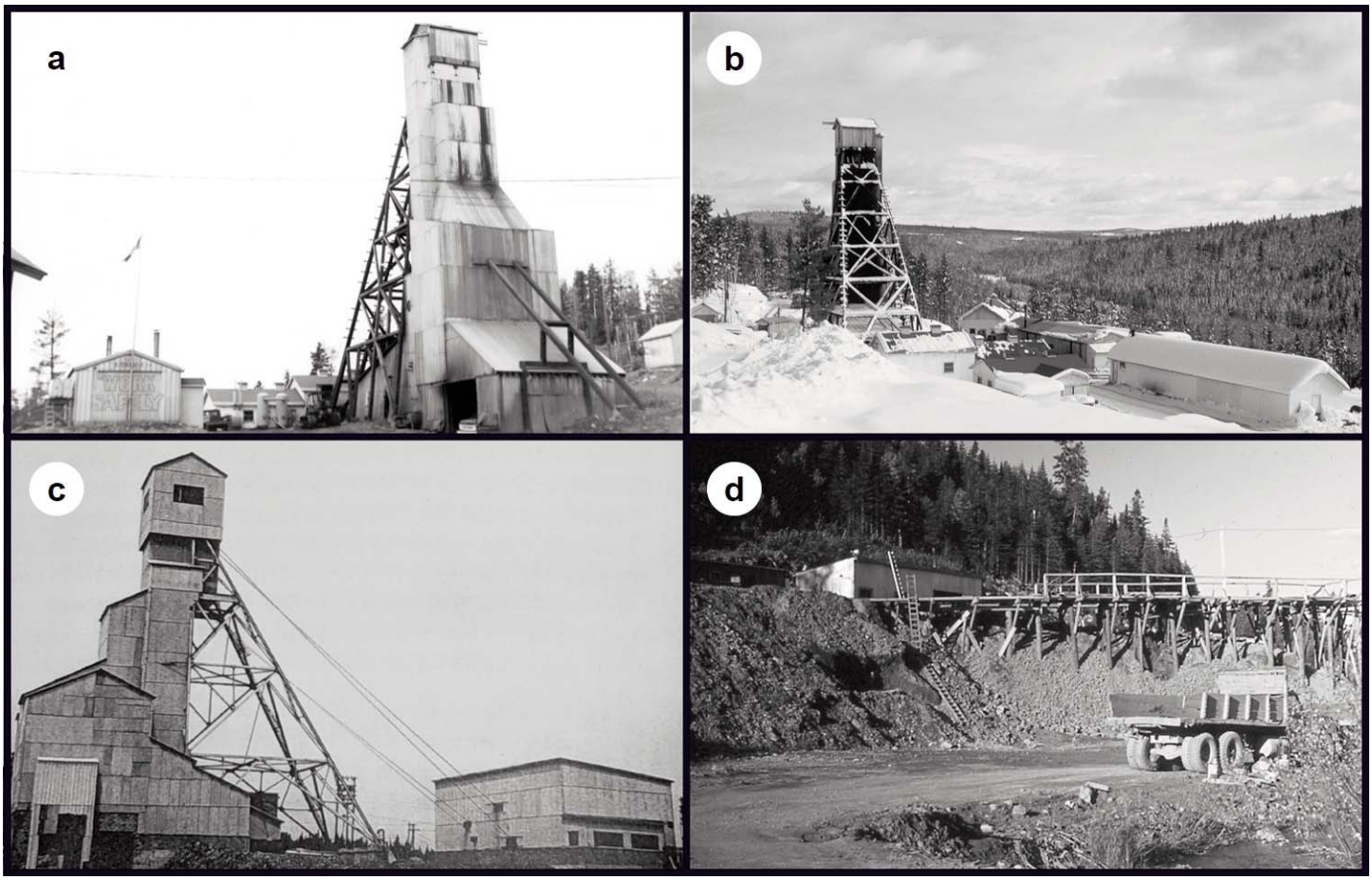

Figure 6. 1960s developments: a) Wedge circa 1962, looking northwest (New Brunswick Natural Resources and Energy Development archives); b) Wedge mine site looking east with the Nepisiguit River valley to the right, winter 1966 (NBNRED archives); c) Heath Steele #3 headframe looking north?, circa 1966 (Our Miramichi Heritage Family archives); d) entrance (portal) to the Caribou adit looking southwest, fall 1966 (courtesy of Richard Cavellero).

"*On June 5, 1962 the first Heath Steele ore, since February 1958, went through the mill – 16,445 tons of it that first month, including 9,659 tons directly from B-zone, and another 6,786 tons from the development stockpile…. For the next few years, the mill ran at 1,500 tons a day, with about half the ore coming from Wedge, and the other half from B-Zone.*"

In 1965, a comprehensive exploration program in the 'ACD' zone area resulted in the discovery of two new ore zones, as well as extensions to the known zones. In 1966, the No. 3 shaft was sunk to a depth of 518 m to further develop the 'B' Zone (Fig. 6c). In May 1968, ore shipments from the Wedge Mine ceased, and production from Heath Steele increased to 1600 tons per day to utilize the concentrator circuit previously used to process Wedge Mine ore. In July 1969, the concentrator was temporarily closed to permit expansion to 3000 tons per day.

At Caribou, in 1965, Anaconda extended the adit (Fig. 6d) that it had begun in 1959 to cover the entire deposit, as it was known at the time, and in the process of excavating a ventilation raise discovered a near-surface, supergene-copper gossan that was mined in 1971 and stockpiled.

Meanwhile, Brunswick Mining and Smelting Corporation's plan to bring its No. 12 and No. 6 properties into production in 1960 fell through when St. Joseph Lead withdrew its financing in 1958 (Jarratt 2012). In 1960, Jim Boylen turned to the provincial government of Louis J. Robichaud (Fig. 7a) to guarantee $20 million in bonds for East Coast Smelting, a company that he promised to establish to smelt lead–zinc concentrates on the north shore of New Brunswick. In March of 1961, Robichaud's government agreed to the guarantee, with the caveat that Boylen had to find investors (within 45 days) to buy out St. Joseph's 40% interest in Brunswick (Kenny 1997). Subsequently, Boylen recruited Patiño Mines, a Bolivian mining multinational, and K.C. Irving, an industrialist, (Fig. 7b) to join his own Maritimes Mining Corporation in buying St. Joseph's share of Brunswick. Under the agreement, they contributed $3.16, $2.52, and $4.82 million, respectively (Kenny 1997).

With St. Joseph out of the picture, Brunswick lawyers set about negotiating a list of legislative concessions for Brunswick and East Coast from Robichaud's government (Kenny 1997). The concessions included: 1) the right to enter tax agreements with municipalities for up to 30 years; 2) the right to divert rivers and streams for its operations; 3) protection from 'nuisance' suits arising from pollution caused by their operations, although the attorney general could authorize a suit against the company; and 4) the exclusive right to smelt

https://doi.org/10.12789/geocanj.2020.47.163

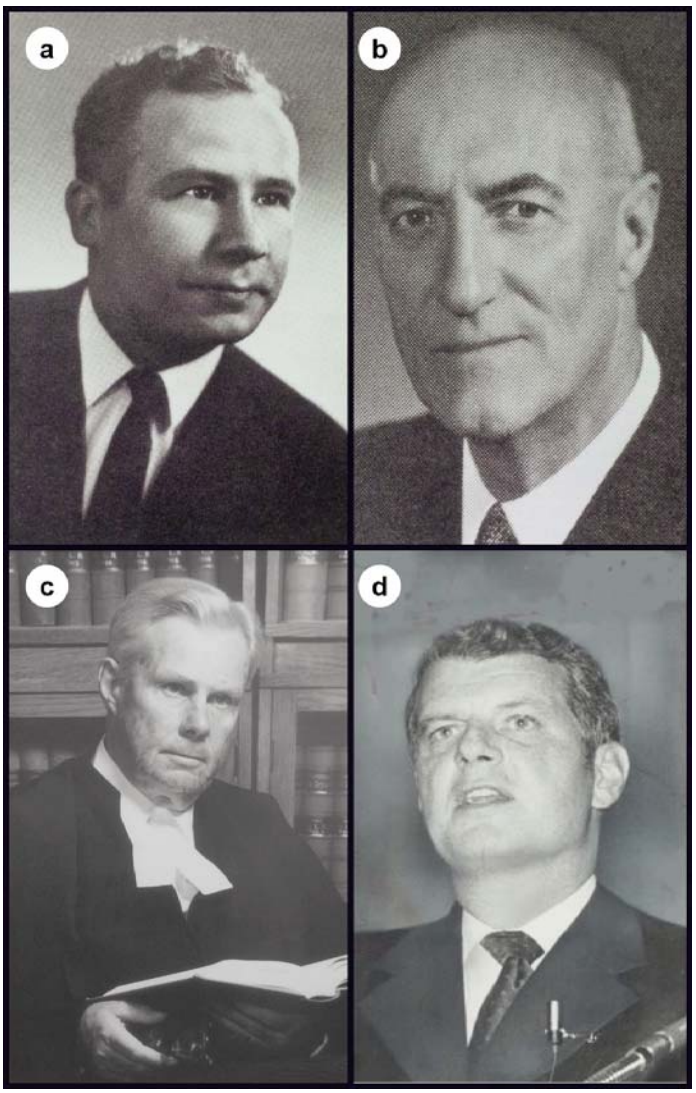

Figure 7. Important participants in the development of Brunswick Mining and Smelting (BMS) during the 1960s: a) Premier Louis J. Robichaud, circa 1963 (BMS archives); b) Kenneth C. Irving, circa 1965 (BMS archives); c) Edward G. Byrne, circa 1970 (courtesy of Terrance Lenihan); d) Alfred Powis, circa 1974 (Toronto Public Library).

New Brunswick base metals for 10 years, but East Coast had to offer its smelting services at a competitive rate. In 1962, these concessions were supplemented by orders in council that gave three additional concessions: 5) ownership of the 'mines and minerals held under lease' by Brunswick was transferred from the Crown to the company; 6) the province pledged that it would not increase mining taxes; and 7) the export tax on unprocessed minerals leaving the province would not be imposed. The latter concession allowed Brunswick to enter an agreement with Sogemines, a Belgian company in Brussels, whereby an exclusive five-year right to buy Brunswick's concentrates was given to Sogemines, in return for an investment in Brunswick of $11.52 million; at the end of the five-year period, Sogemines was permitted to purchase surplus concentrates (those not needed by East Coast) for an additional seven years (Kenny 1997).

The 1961 buyout of St. Joseph had left Boylen with a 40% controlling interest in Brunswick, with K.C. Irving and Patiño Mines having 27% and 14%, respectively (Kenny 1997). However, Irving's influence in the company was much greater than his minority shareholder status suggested, and he was able to exercise a great deal of control over its development. In fact, in 1962 one of his newly formed companies, Engineering Consultants Ltd., was given the contract to manage construction of the mill at Brunswick No. 12 and the smelter at Belledune. Construction began at Brunswick No. 12 on May 15, 1962 (Fig. 8a, b, c) and continued through to June 30, 1964. Mine production began in April of that year (Luff 1995), although the official opening occurred on June 12, 1965 (Jarratt 2012).

In 1964, Anacon Lead Mines Limited was reorganized as Key Anacon Mines Limited. Underground work resumed at New Larder 'U' (Fig. 9a) and continued until 1966 (New Brunswick Mineral Occurrence Database). In 1955, all assets of New Larder 'U' Mines had been acquired by Anacon Lead Mines Ltd.; a pilot plant (mill) had been installed, and a 457 m (1499 ft) deep shaft was sunk, and nine levels excavated. Work was suspended on the property in 1957. By 1964, Irving had acquired 38% of Brunswick and controlling interest in the company, by quietly purchasing (through his shipping company, Kent Line) shares of Boylen's Key Anacon Mines, which held 11% of Brunswick's stock (Kenny 1997).

As Irving's share in Brunswick got larger, so did the size of the smelter development that began at Belledune in 1964 (Kenny 1997). In October of that year, Robichaud announced that an additional $117 million was to be invested to expand the project. Two new mines, Brunswick No. 6 and Key Anacon's New Larder 'U', were to be opened, with a new concentrator to be constructed at each one. In addition, fertilizer and acid plants were to be built at the smelter as well as an electric refinery to process iron pyrite into steel. Lastly, a $12 million ore carrier was to be constructed by Irving's Saint John Shipbuilding and Dry Dock Co. and chartered by Brunswick to ship base metals. Originally, the smelter was to be built at Daly Point on the east side of Bathurst Harbour (*The Northern Miner*, May 30, 1957), but ultimately, Belledune Point was selected as the site for construction (Kenny 1997). Furthermore, the Robichaud government, at Brunswick's insistence, helped convince Ottawa to contribute $9 million to the construction of a new year-round, deep-water harbour at Belledune, to be used almost exclusively by Brunswick.

By the summer of 1965, pre-production stripping was under way at the No. 6 site (Jarratt 2012). Production began in the fall of 1966 at 2,041 tonnes per day (t/d) but periodically increased to as much as 4,100 t/d to supplement under-production at the Brunswick No. 12 mine.

By 1966, Brunswick was having serious financial problems, created in large part by the cost of smelter construction by East Coast (Fig. 9b), so in September of that year Boylen asked the Robichaud government to guarantee another $20 million in long-term East Coast bonds and another $10 million in short-term notes. At the time, East Coast owed $2.7 million to suppliers and more than $7 million to mostly Irving-owned com-

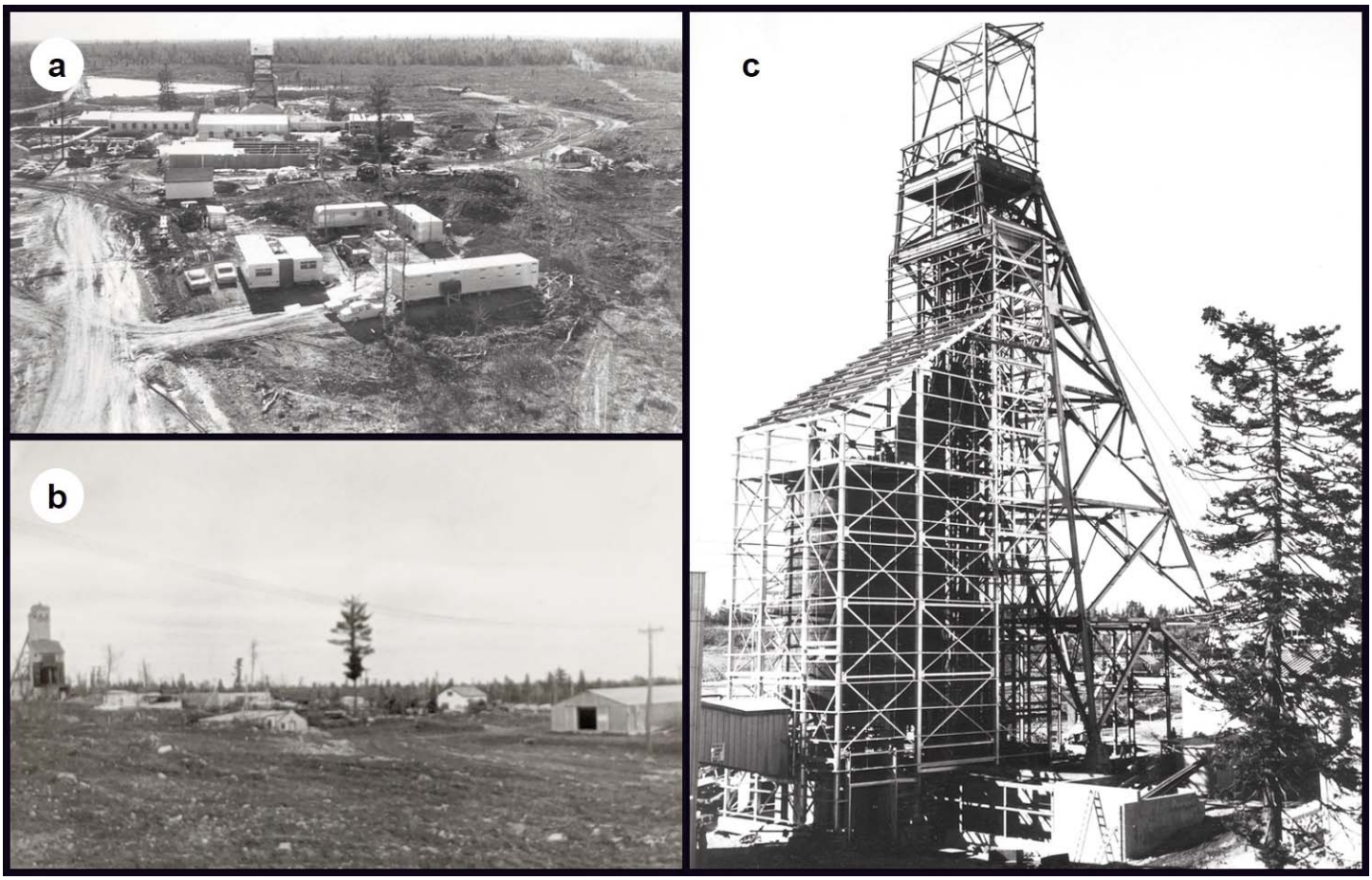

Figure 8. 1960s developments: a) Brunswick No. 12 (#2 shaft in background) in December 1962, looking south from #1 shaft (Brunswick Mining and Smelting archives); b) Brunswick No. 12 (#1 shaft at left) in December 1962, looking east (BMS archives); c) Brunswick No. 12 (#2 shaft expansion) in May 1963, looking northwest (BMS archives).

panies (Kenny 1997). The government reluctantly approved Boylen's request but considered it a temporary solution, realizing that the real problem lay in Irving's management of Brunswick. The local population was also dissatisfied with K.C. Irving's monopoly on construction contracts and his plan to build a large town site at Belledune (Kenny 1997). Furthermore, the personal relationship between L.J. Robichaud and K.C. Irving was also souring. The combination of three factors: 1) distrust of Irving's management, 2) local discontent, and 3) the growing animosity between Irving and Robichaud, made a compelling case for government to find a way to remove Irving from the picture (Kenny 1997).

In early 1967, Robichaud initiated a secret search for a new investor to wrest control of Brunswick from Irving (Kenny 1997). His confidante Edward Byrne (Fig. 7c), with the help of Boylen and Carte of Patiño, both of whom wanted Irving out of the project, convinced Noranda's Alfred Powis (Fig. 7d) to take over Brunswick. Noranda agreed to pay off $50 million in Brunswick debts and to loan $20 million to complete the smelter, in return for 51% control of the company. Noranda also insisted on a $20 million loan guarantee. The shareholders approved the takeover in June of that year, the same year that the No. 2 shaft at Brunswick No. 12 was deepened to 925 m (Luff 1995). At the time, Brunswick's accounts payable amounted to more than $19 million, of which nearly $15 million was owed to Irving companies. Eventually, Noranda paid off all the Irving group's outstanding accounts (Kenny 1997).

Under Noranda's management, the Belledune industrial complex was brought into production, but on a less grand scale than originally planned and with mixed results (Kenny 1997). The steel project and the construction of Belledune Harbour were shelved, with Noranda choosing instead to use Dalhousie Harbour, approximately 57 km to the northwest. The Brunswick smelter came into production in 1967 but was plagued with problems and did not reach maximum operating capacity until 1970; then it was converted from a zinc–lead to a lead only smelter in 1972. The fertilizer plant, Belledune Fertilizer, came into production in 1968 but had trouble finding buyers for its product.

In late 1968, a fire (oxidizing sulphides) started in the No. 6 open pit (Fig. 9c) when a blast was touched off in a pyrrhotite-rich part of the deposit; the spontaneously oxidizing sulphides were spread out on the waste-pyrite dump. It was expected that the fire would burn itself out, but instead the fire spread to the pyrite creating acid mine drainage that killed juvenile salmon in the Nepisiguit River in 1969. To extinguish the fire, the burning material was mixed with waste rock and over 1.3 million tonnes were trucked to the No. 12 mine (Fig.

https://doi.org/10.12789/geocanj.2020.47.163

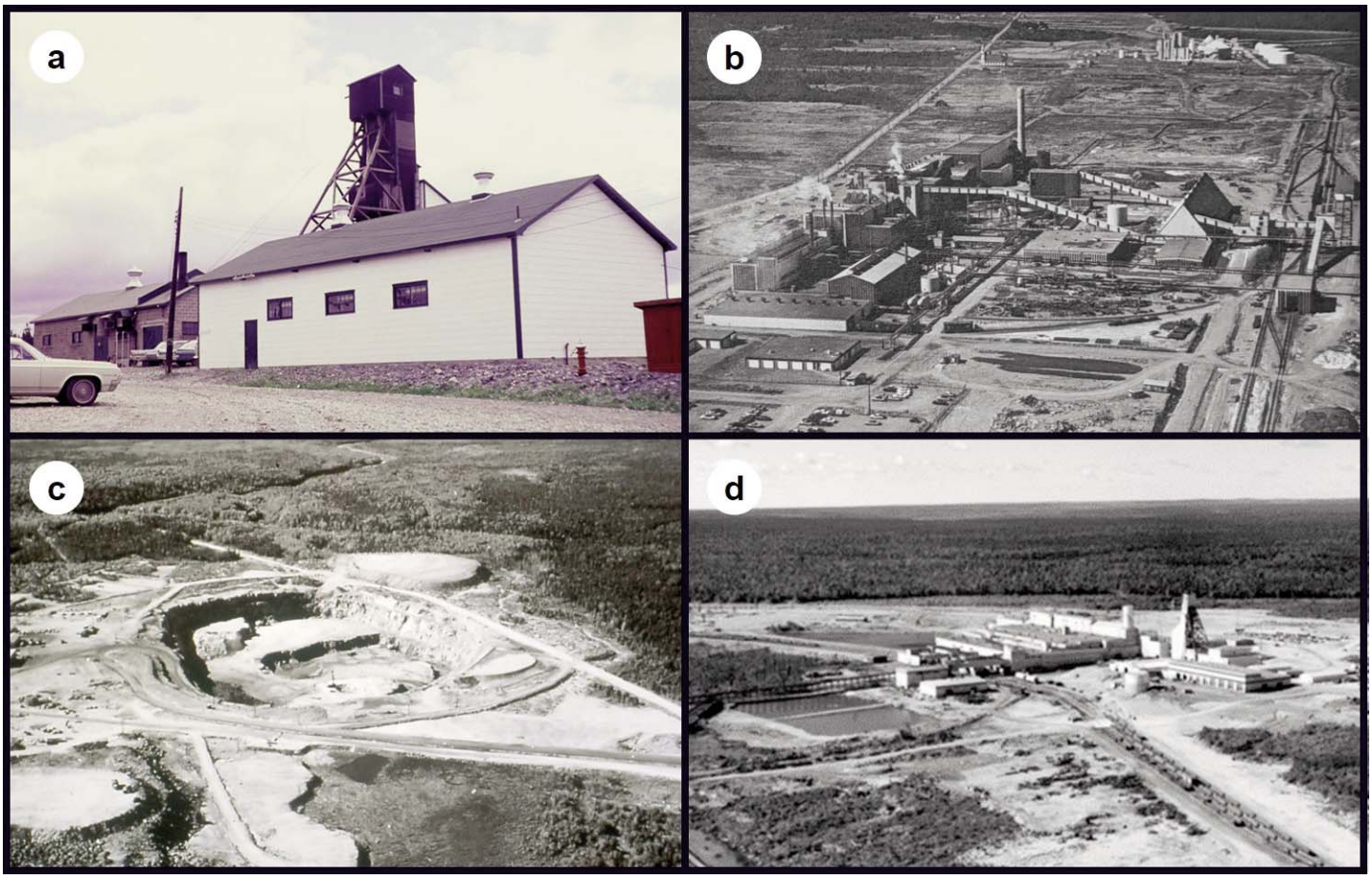

Figure 9. 1960s developments: a) Key Anacon (New Larder U) in 1966 looking east (New Brunswick Natural Resources and Energy Development archives); b) aerial view of Belledune smelter in 1966, looking northwest (Brunswick Mining and Smelting archives); c) aerial view of Brunswick No. 6 in 1969, looking southwest (NBNRED archives); d) aerial view of Brunswick No. 12 in 1969, looking southeast with #2 shaft to the right (BMS archives).

9d) and used as backfill underground in the upper part of the orebody. However, this caused oxidation of sulphides (spread the fire) in the mined-out stopes and subsequently necessitated the installation of bulkheads, a separate ventilation course and a 23 m stack to exhaust the resulting sulphur dioxide (SO_2) gas that was generated by the fire (Belland 1992).

1970s Development

Mine development in the 1970s is briefly described by Luff (1995), and Brunswick No. 12 is specifically described by Jarratt (2012). The mining methods used at Brunswick during the 1970s are described by Dufresne (1981). Additional information is found in the NBNRED online Mineral Occurrence Database (http://dnr-mrn.gnb.ca/mineraloccurrence/). Subsequently, some deposits were more fully described in Technical Reports, one for Trevali Mining Corporation (Zhang et al. 2014) and the other for First Narrows Resources Corporation (Sim and Davis 2008), which are filed on SEDAR. Two deposits, in addition to those first developed in the 1960s, saw development during this decade, namely Caribou and Chester. Surface exploration was carried out on the Key Anacon property in the early 1970s, but it saw no further mine development (Fig. 10a).

In 1970, the oxidized (gossan) zone at the Caribou deposit was mined to extract the supergene copper (Fig. 10b); in 1971, mining continued in the sulphide body, which was accessed from a ramp. Production ended in December of 1971, but Anaconda initiated a second phase of production in 1973–74 (Fig. 10c), which ceased in November of 1974 (Zhang et al. 2014).

In 1970, Sullico Mines Limited (Sullivan Mining Group) acquired 100% interest in the Chester deposit (Fig. 1). When initial plans for open pit mining were abandoned, Sullico drove a 470-metre decline in 1974–75 in order to explore the Copper Stringer Zone (i.e. Chester West Zone) and confirm diamond drill-indicated grade and tonnage, as well as to check rock competency and water flows for a potential underground mine operation (Sim and Davis 2008). Reportedly, 31,750 tonnes (35,000 tons), grading 2.06% Cu, were taken from underground in 1977 and processed at the Nigadoo mill, a Sullivan operation north of the BMC (Luff 1995). Further development was postponed, reportedly due to low copper prices, and the project was later abandoned (Fig. 10d).

In 1971–72, the No. 4 shaft at Heath Steele was sunk to 417 m on the C-Zone (Luff 1995). From 1974 to 1976, mining of the A and C zones was conducted from a ramp driven from

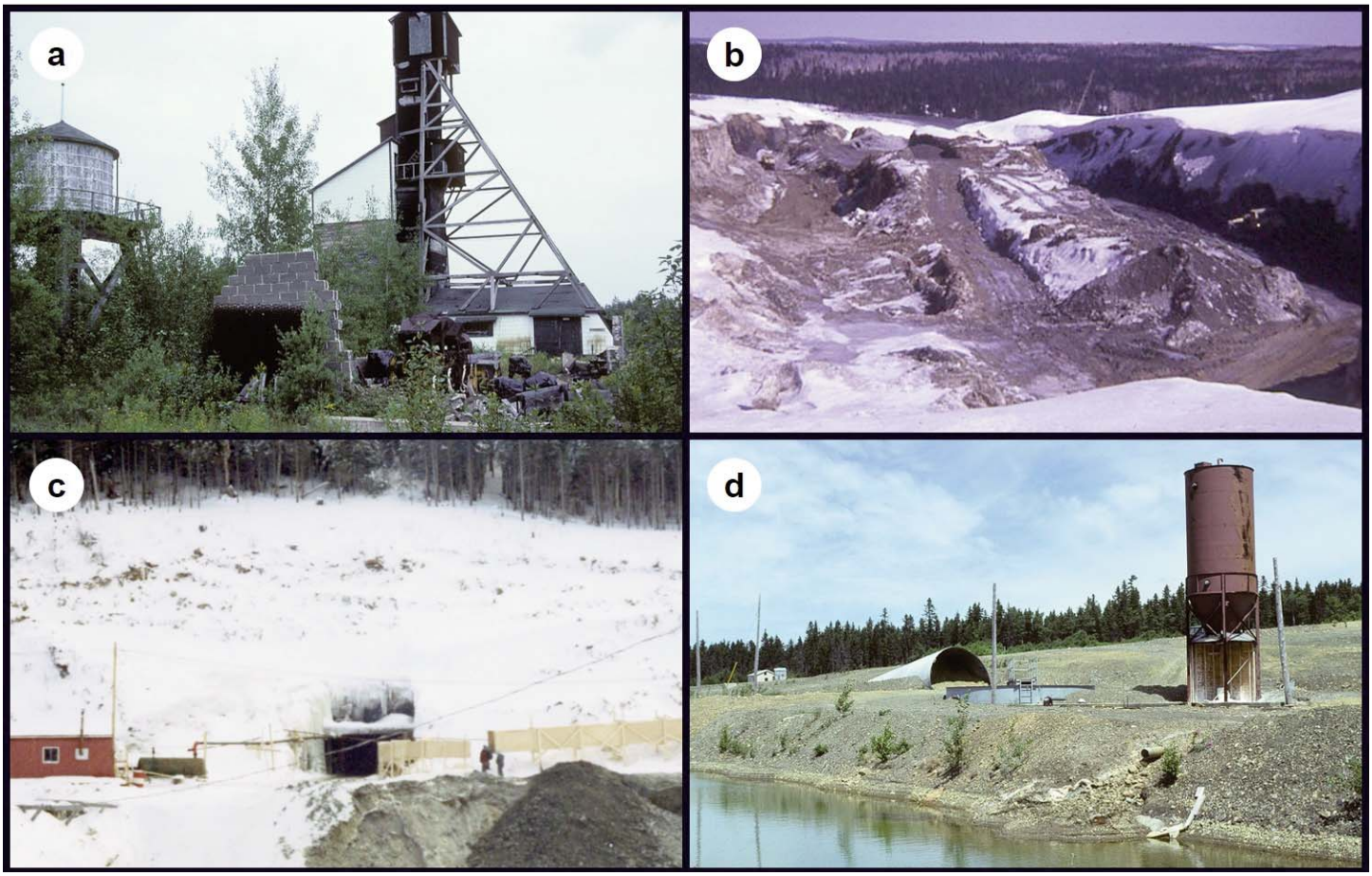

Figure 10. 1970s developments: a) Key Anacon 1979, looking southwest (New Brunswick Natural Resources and Energy Development archives); b) Caribou open pit looking north, circa 1971 (courtesy of Richard Cavellero); c) the mine portal at Caribou looking south, circa 1973 (courtesy of Richard Cavellero); d) the portal at the Chester deposit in 1978, looking northeast (NBNRED archives).

the A Zone open pit (Fig. 11a). In 1975–76, the No. 5 shaft on the B Zone was sunk to a depth of 890 m (Fig. 11b, c). In 1979, Noranda acquired a 75% interest in Heath Steele from American Metal Climax (Amax) and Asarco Inc. acquired 25% from Inco; in 1986, Asarco sold its 25% share to Noranda's Brunswick Mining Division (Gallagher 1999).

At Brunswick, open pit mining in the northern part of the No. 12 deposit occurred in 1971 (Luff 1995). In 1974, the No. 3 shaft, with an 88 m (288.5 feet) headframe, was collared and by 1977, it had been sunk to approximately 1125 m (3700 feet) (Fig. 12a, b, c). By 1977, the No. 6 open pit bottomed out at approximately 170 m (547 feet). Underground production began at 205 m via a ramp driven from the bottom of the pit, and production continued until 1983 when the ore was exhausted (Fig. 13a, b, c).

1980s Development

Mine developments in the 1980s are briefly described by Luff (1995), Gallagher (1999), and Jarratt (2012). Additional information is found in the NBNRED online Mineral Occurrence Database. A Technical Report for Trevali Mining Corporation (Zhang et al. 2014) has details about development at Caribou during this period. The Murray Brook (Fig. 14a) and Stratmat deposits saw developments during this decade, as did deposits that were worked in the 1970s.

In 1980, Anaconda conducted additional drilling on its Caribou property to test the continuity of the deposit at depth. The company also carried out limited test mining, extracting a 25,400-tonne bulk sample that was milled at Brunswick No. 12 (Zhang et al. 2014). In 1982–83, Anaconda operated a gold–silver heap leach plant at Caribou, the first heap-leach gold operation in Canada (Luff 1995). Approximately 61,500 tonnes of gossan, which were stockpiled in 1970, were processed, yielding 106,000 ounces of silver and 8100 ounces of gold (Zhang et al. 2014).

Heath Steele shut down in April 1983, but the company decided to mill its stockpile (approximately 1000 tonnes) of gossan ore from the B-1 Zone to recover gold and silver, which was completed in June 1984 (Gallagher 1999). Heath reopened in 1989, milling ore from the Stratmat Boundary and Stratmat N-5 deposits (Table 1) until 1993 (Fig. 15a), and continued mining from the B-Zone until 1999, when Heath Steele closed permanently (Fig. 11d).

In 1985, Northumberland Mines Ltd. optioned the Murray Brook property (Table 1, Fig. 1), primarily to look at the precious metal content of the gossan (oxidized sulphides) cap on

https://doi.org/10.12789/geocanj.2020.47.163

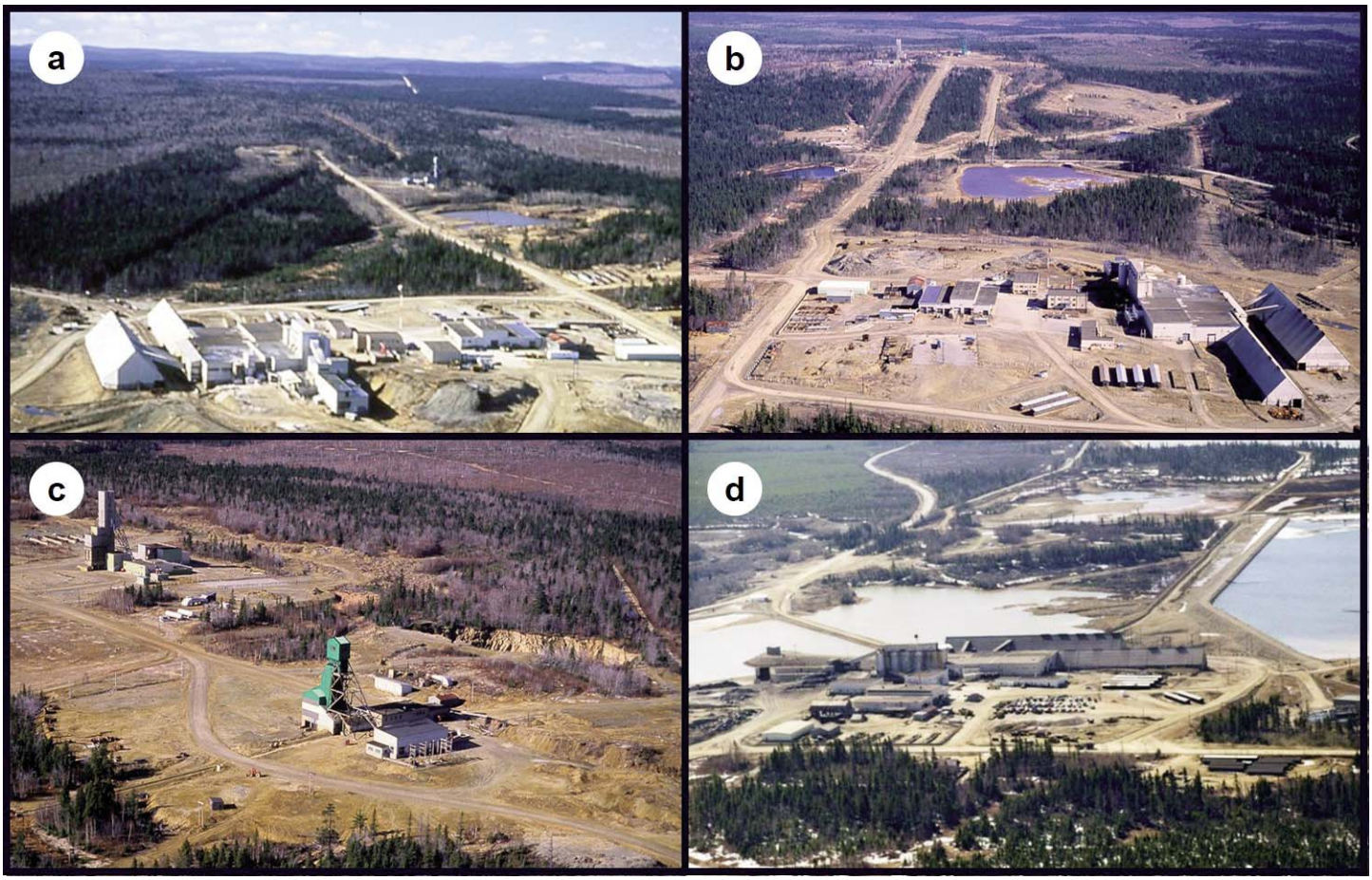

Figure 11. 1980s Heath Steele: a) aerial view of the Heath Steele mill in the foreground with the headframe to the No. 4 shaft (C-Zone) in the middle distance and the A-Zone open pit (flooded) in between, circa 1988, looking west (New Brunswick Natural Resources and Energy Development archives); b) aerial view of the Heath Steele mill in the foreground with the headframes to the No. 3 and No. 5 shafts (C-Zone) in the distance, circa 1988, looking east (NBNRED archives); c) close-up of the No. 3 (foreground) and No. 5 (left rear) headframes at the C-Zone, circa 1988, looking northwest (NBNRED archives); d) aerial view of the Heath Steele mill and water treatment ponds looking southeast, circa 1999 (Our Miramichi Heritage Family archives).

this massive sulphide deposit. In 1986, an open pit mine development and vat-leach processing facility were approved by government regulatory authorities. In 1988, Northumberland Mines and the Murray Brook deposit were acquired by Nova Gold Resources Ltd. The latter company commenced production in September 1989 and continued until 1992, at which time the gossan ore was exhausted (Fig. 14a, b).

In 1986, Caribou was acquired by East-West Minerals NL of Australia and in 1988 became East West Caribou Mining Ltd. Between 1987 and 1988, East West initiated pre-production construction, which included underground development and the construction of a concentrator on the property (Fig. 14c, d). East West began production in 1989 but the mine was shut down shortly afterward because of operating problems. In 1989, Caribou was acquired by Breakwater Resources Ltd.; the mine briefly re-opened, producing 728,400 tonnes, before closing in 1990 due to poor metal recoveries (Zhang et al. 2014), which resulted from the fine-grained nature of the ore.

Meanwhile at Brunswick, the $56 million expansion program at No. 12, which began in 1974, was completed in 1981; this included increasing the mill capacity to 10,000 tonnes per day (Jarratt 2012). The No. 6 mine closed in 1983 after 18 years of production (Fig.13a). In 1987, the No. 12 mine produced its 50 millionth tonne of ore, and the No. 3 shaft (Fig. 12b, c) was deepened to 1325 m the following year. In 1989, the 25th anniversary of the mine opening, a new sulphide zone was discovered 1.5 km north of the No. 12 deposit at a depth of 1100 m.

1990s Development

Mine developments of this decade are described in the New Brunswick Mineral Occurrence Database, in Jarratt (2012), Luff (1995), Whaley (1992), and in Technical Reports for Trevali Mining Corporation, which are filed on SEDAR. New mining operations were established at the Restigouche (in conjunction with Caribou) and Captain North Extension (CNE) deposits (Table 1, Fig. 1). During the 1990s, reclamation projects began at Heath Steele and Brunswick. The Port of Belledune, which was originally built in 1968 to address the shipping needs of what was then the Noranda Smelter (Glencore), expanded in 1995 and again in 1998 (https://www.portofbelledune.ca/history.php).

Stratabound Minerals Corporation optioned the CNE deposit in 1988. Trenching in 1989 and 1990 exposed a 20 by

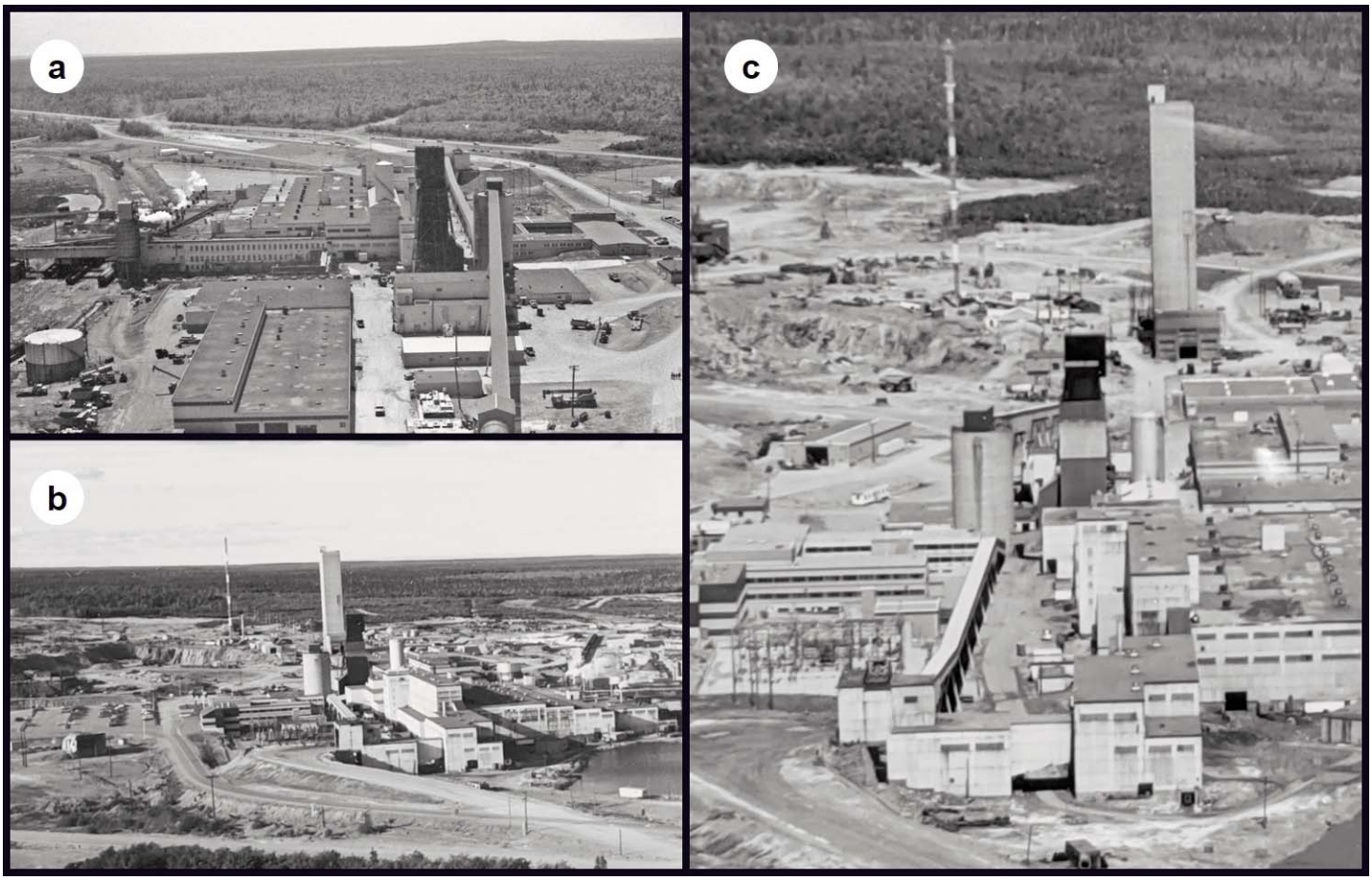

Figure 12. 1980s Brunswick No. 12: a) view from #3 headframe looking south over the mill and #2 headframe in the late1970s (Brunswick Mining and Smelting archives); b) aerial view looking north at the mill (foreground), #2 headframe (dark grey) and #3 headframe (light grey) with the ventilation stack (striped) and the nearby open pit in 1983 (BMS archives); c) close-up aerial view looking north at the mill (foreground), #2 headframe (dark grey) and #3 headframe (light grey), with the ventilation stack (striped) and the nearby open pit in 1987 (BMS archives).

45 m area of bedrock beneath 5 to 6 m of till, from which Stratabound mined an 11,000-tonne bulk sample in 1990. The ore was trucked to the Heath Steele mill and processed successfully in September of that year (Whaley 1992). Between then and 1992, Stratabound mined another 28,000 tonnes (Fig. 15b) that was milled at Heath Steele (Luff 1995).

In 1995, Breakwater Resources Ltd. announced a metallurgical breakthrough, namely introduction of new mills (designed at the Mt. Isa Mine in Australia) capable of processing fine-grained ores, which would enable the company to reopen the Caribou mine. Reopening plans included the mining and processing of ore from the nearby Restigouche deposit, which was purchased from Marshall Minerals Corporation, following a positive feasibility study and testing of Restigouche ore. In 1996, Breakwater Resources, through its subsidiary East West Caribou Mining Ltd., received regulatory approval to mine the Restigouche deposit. Both the Caribou and Restigouche mines began production in 1997 (Figs.15c, 16a, b), with the first ore going through the Caribou mill in July, at a combined rate of 3000 t/d. Production ceased in August 1998, when both mines went into care and maintenance mode.

At Brunswick, a new high-density, sludge-water treatment plant was completed at the No. 12 mine by 1994 (Jarratt 2012). In 1995, reclamation work at the No. 6 mine was completed, including installation of three drainage trenches (Fig. 16c) to capture run off from the waste-rock piles, which were contoured and seeded, and construction of an 8.5 km pipeline and pump station to transfer pit water to No. 12 for treatment (R. Schwenger written comm. 2017). In 1999, the underground ore handling and ventilation systems at the No. 12 mine were upgraded to support new mining areas in the south end of the orebody, and process changes were made to the grinding and flotation circuits to enhance metallurgical recovery.

At Heath Steele, a new water-treatment plant and buffer-storage pond were completed in 1997 (R. Schwenger written comm. 2017). Acid generating waste rock was removed from the vicinity of the B-Zone mine and from the haulage road to the B-Zone in 1998–99, and in November 1999 the Heath Steele mine and mill were closed (Figs. 11d, 16d).

Post-2000 Development

Since 2000, mine closure and reclamation have been as prevalent as mine development in the BMC. A new mining opera-

https://doi.org/10.12789/geocanj.2020.47.163

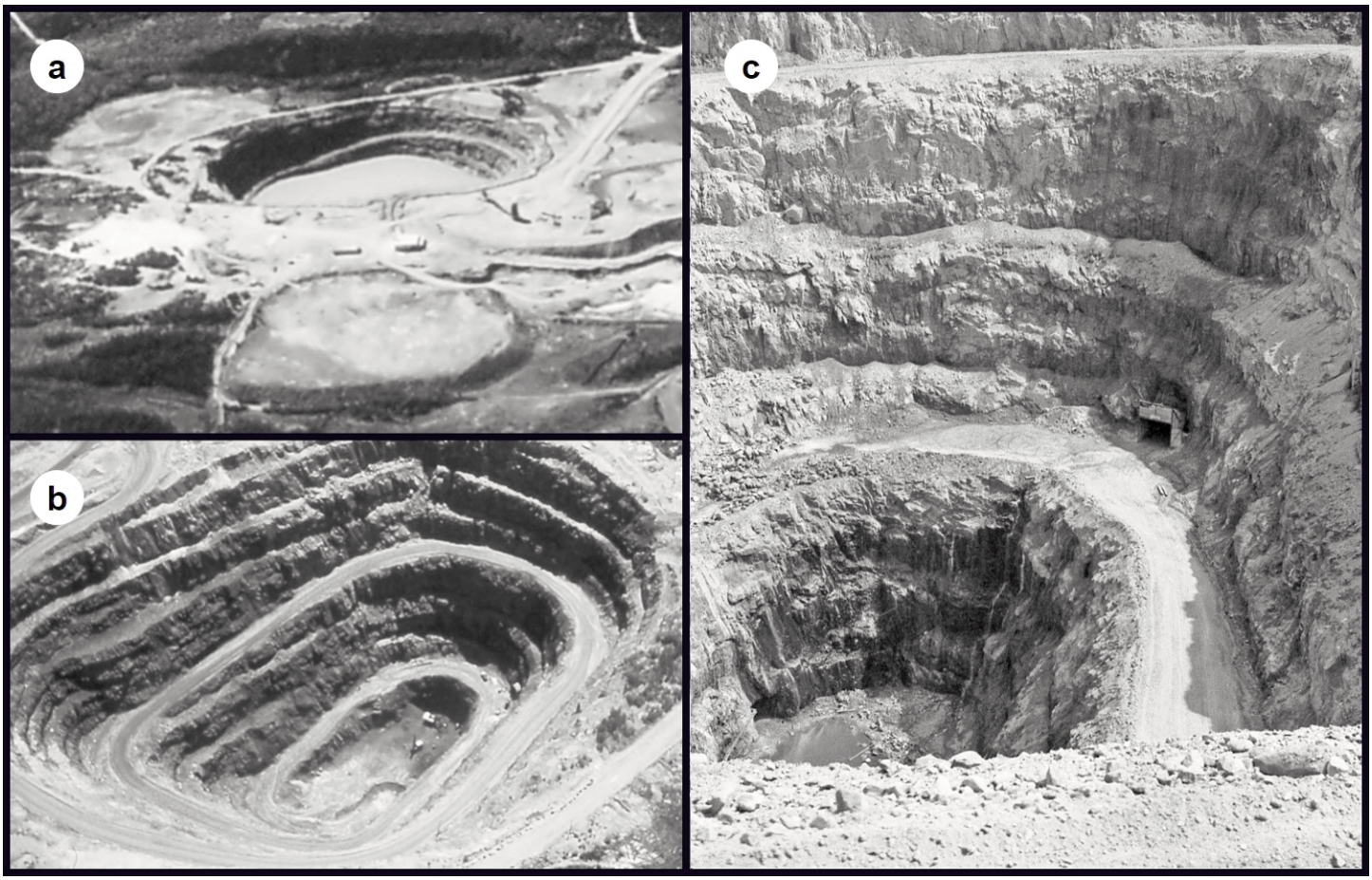

Figure 13. 1980s Brunswick No. 6: a) aerial view looking west of No. 6 pit (flooded) in 1989 , with waste-rock piles at bottom center and top left (New Brunswick Natural Resources and Energy Development archives); b) aerial view looking southerly into No. 6 pit circa 1980 (Brunswick Mining and Smelting archives); c) ground view looking southerly into No. 6 pit, circa 1980 (courtesy of Ronald Jessulat).

tion was established at the Halfmile Lake deposit (Table 1, Fig. 1) and further developments occurred at Brunswick No. 12, Caribou, and CNE. Reclamation work occurred at Heath Steele and Brunswick.

In 2008, Kria Resources entered an agreement with Xstrata Canada Corporation – Xstrata Zinc Canada Division (now Glencore Canada), whereby Kria had the right to gain 100% interest in the Halfmile Lake and Stratmat deposits for $18 million (US) and by issuing units worth $7 million (CAD) (www.trevali.com). On April 7, 2011, Trevali Resources Corporation merged with Kria Resources Ltd. and changed its name to 'Trevali Mining Corporation'. In August of that year, construction of a portal and underground ramp (Fig. 17a) to the upper part of the Halfmile Lake orebody began. The mine permitting did not allow ore processing on site, or permanent storage of waste rock on surface; it also limited surface storage of ore, directing all run off away from the Northwest Miramichi River. All site discharge was controlled and there was a commitment to meet strict Canadian Council of Ministers of the Environment (CCME) guidelines using state of the art Veolia water treatment. (J. Griggs written comm. 2017). In the first seven months of 2012, approximately 100,000 tonnes were mined (on a trial basis) from the Upper Zone of the deposit; the ore was trucked to the Brunswick No. 12 mill for toll processing, which was considered a technical success (www.trevali.com). However, since then, the mine has been on care and maintenance mode while Trevali focuses on its Caribou operation.

In 2003, new technology was implemented at Brunswick No. 12 that significantly lengthened the life of the mine. The introduction of paste backfill (80% tailings with water and cement) in 1998 allowed re-entry to the long-abandoned upper part of the orebody ('425 Main Ore Zone'); permitted mining without having to leave pillars of ore; reduced rock stress, and quenched oxidation of waste sulphides (Jarratt 2012). The fire (oxidizing sulphides) that had burned in that part of the orebody since 1970 was finally extinguished by 2005, and the 23 m exhaust stack that was used to vent SO_2 gas was dismantled (compare Figs. 12c and 17b). In July 2005, Brunswick's owner, Noranda, acquired the remaining shares of Falconbridge Ltd., a Toronto-based mining company, and changed its name to 'Falconbridge Limited', but in 2006 Xtrata Zinc, an Anglo–Swiss multinational mining company, purchased Falconbridge (Jarratt 2012) and the name changed to 'Xstrata Canada Corporation – Xstrata Zinc Canada Division'. Xstrata closed the Brunswick No. 12 mine on April 30, 2013, but not before pro-

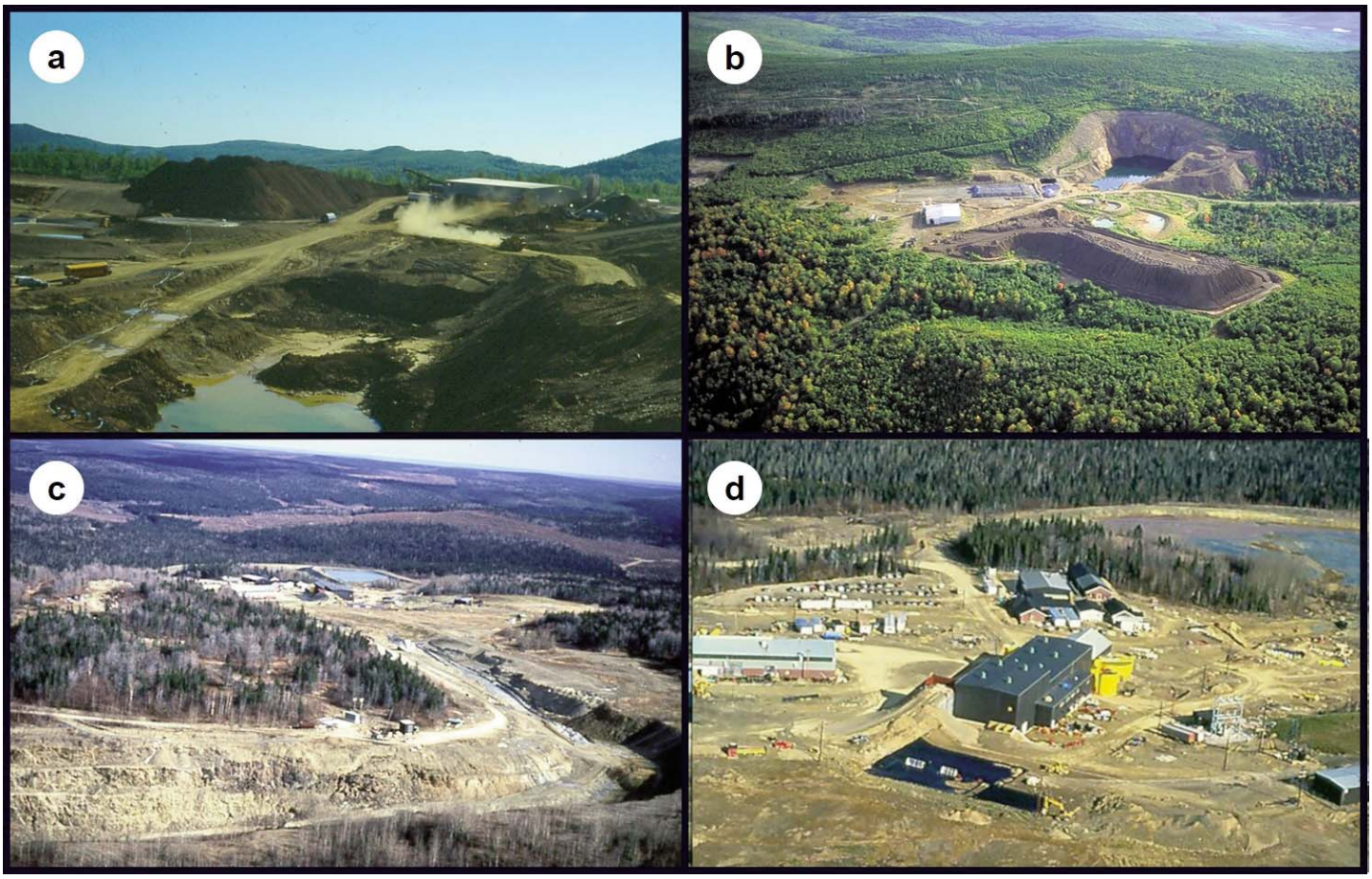

Figure 14. 1980s developments: a) Murray Brook open pit in1989 with pit in the foreground and leach-plant in the background (to right) and gossan tailings (to left) , looking northeast (New Brunswick Natural Resources and Energy Development archives); b) aerial view looking south of Murray Brook open pit (flooded) and gossan tailings pile in the foreground in1997 (NBNRED archives); c) aerial view of Caribou mine site looking northeast, with open pit in the foreground and mine buildings in the background in 1988 (NBNRED archives); d) close-up of Caribou mine buildings looking north, with mill in the foreground and office in the background in 1988 (NBNRED archives).

cessing 62,720 tonnes of ore (between March 6 and April 12) from Stratabound Minerals Corporation's CNE open pit mine (Fig. 17c).

Between 2008 and 2017, reclamation work was done at the Brunswick No. 12 mine site (R. Schwenger written comm. 2017). Covering the slopes of the tailings began in 2008 and was completed in 2015. The covering of tailings benches started in 2011 and was completed in 2017. A south perimeter ditch was constructed in 2012; a north perimeter ditch was started in 2013 and completed in 2017. Demolition of the mine buildings began in 2014 and was complete by 2016. All openings to surface were capped and fenced in 2016. Reclamation of the mine site itself began in 2015 and was completed in 2018.

In August 2006, Blue Note Mining Inc. acquired an 80% interest in the Caribou and Restigouche mines from Breakwater Resources. Blue Note Caribou Mines Inc. invested approximately $116 million to revive the two mines; operations started in July 2007 with commercial production declared at the start of 2008 (*The Northern Miner*, October 27, 2008). Operations achieved full capacity at 3000 tonnes daily, and recoveries exceeded 83% for zinc and 70% for lead. Restigouche ore (Fig. 17d) was hauled to Caribou and blended with Caribou ore in the mill. Production ceased in late 2008 because of the global economic slowdown and the accompanying drop in metal prices. Following a legal battle, control of the Caribou deposit passed to Maple Minerals Corportion in April of 2011 (visit the New Brunswick Mineral Occurrence Database).

Between 2000 and 2007, demolition and reclamation work were completed at Heath Steele (R. Schwenger written comm. 2017). Demolition began in 2000 and was finished in 2001. During the same period, a dike was constructed around the Stratmat open-pit to increase its storage capacity; shafts at Heath Steele were capped; a pump station was constructed at the B-Zone mine; the main tailings dam and buffer pond dam were raised 0.6 m to increase their storage capacity, including constructing permanent and emergency spillways in the main dam. In 2005, dams on North Little River Lake and McCormack Reservoir were decommissioned, and a fish way was installed in South Little River Dam. In 2007, two pump stations were decommissioned, and one was upgraded; a collection ditch to the B-Zone open pit was constructed; the cave-in of a crown pillar at the B-Zone mine was filled and capped with clay, and finally, fences were constructed around all crown pillars.

Figure 15. 1990s developments: a) aerial view looking northeast of the flooded Stratmat Boundary (foreground) and N5 (background) open pits in 1997 (New Brunswick Natural Resources and Energy Development archives); b) view looking east of the partly flooded CNE open pit in 1991 (NBNRED archives); c) aerial view looking north of the Caribou mine site in 1997 (NBNRED archives).

Mine Production

The production history of the BMC is described in Luff (1995); an update is shown in Table 1. Twelve of the known 45 deposits in the BMC have been mined.

The Heath Steele deposit was the first producer, beginning in 1957, and was mined under a joint agreement between INCO and AMAX. The B zone (Fig. 11b) to the east and ACD zones (Fig. 11a) to the west provided most of the mill feed, with over 20 million tonnes being mined from the B zone and over 0.5 million tonnes from the ACD zones (Table 1). In addition, approximately 178,000 tonnes of gold–silver-bearing gossan from the ACD and B zones was processed at the Heath Steele mill between 1983 and 1984 (Luff 1995).

Other deposits were processed at the Heath Steele mill (Table 1). For example, the Wedge deposit, which was mined for copper by Cominco from 1962 to 1968, produced about 1.5 million tonnes, all of which was milled at Heath Steele. From 1989 to 1993, over one million tonnes were mined from the Stratmat Boundary and N-5 zones and processed there (Table 1). Finally, between 1990 and 1992, Stratabound Minerals extracted approximately 39,000 tonnes from the CNE deposit and trucked it to the Heath Steele mill. Total throughput at the Heath Steele mill from all sources was over 26 million tonnes.

The Brunswick No. 12 deposit started production in 1964, followed in 1966 by the Brunswick No. 6 deposit. The No. 12 deposit is the 'elephant' of the BMC, with total production of nearly 137 million tonnes to the end of mine life in 2013 (Table 1). The combined production from the No. 6 and No. 12 deposits exceeded 149 million tonnes (Table 1). In addition, approximately 126,000 tonnes of ore, mined at Halfmile Lake by Trevali Mining Corporation in 2012 and approximately 63,000 tonnes of ore mined at CNE by Stratabound Minerals Corporation in 2013, were processed at the Brunswick mill (Table 1).

The first production from the Caribou deposit, roughly 340,000 tonnes, was from the supergene copper zone between 1970 and 1974 (Luff 1995). Between 1982 and 1983, approximately 60,000 tonnes of gold–silver-bearing gossan were processed at Caribou, making it the first heap leach gold recovery operation in Canada (Luff 1995). A test stope of the primary massive sulphide was mined at Caribou in 1983 and processed at Brunswick. Further underground production took place from 1988 to 1990 and was processed at the Cari-

Figure 16. 1990s developments: a) aerial view looking north of Restigouche open pit in 1997 (New Brunswick Natural Resources and Energy Development archives); b) ground view looking north of Restigouche pit face in 1997 (NBNRED archives); c) aerial view looking west of drainage trench at Brunswick No. 6 open pit in 1997 (NBNRED archives); d) view looking north of the gate to the Heath Steele mine site in 2003, with water-treatment ponds (foreground) and water-treatment plant in the background at left (NBNRED archives).

bou mill. In 1997, production resumed at Caribou and began at Restigouche by open pit. Production continued until July of 1998. The ore from the two deposits was blended and processed at the Caribou mill. Total combined lead–zinc production from these deposits to the end of 2018 was over five million tonnes (Table 1).

The Murray Brook deposit has also been mined (Table 1). Over one million tonnes of gossan was successfully vat-leached (indoors) for gold and silver between 1989 and 1993 and represented the first application of indoor leaching in Canada. Also, over 50 thousand tonnes of primary and secondary massive sulphides, rich in copper (2.5%), were mined at Murray Brook in 1992 and placed on an outdoor leach pad. A bio-assisted leach operation was attempted in the fall but was unsuccessful (Luff 1995).

IMPORTANCE OF THE BATHURST MINING CAMP

The Bathurst Mining Camp (BMC) was, and still is, important to New Brunswick and Canada for many reasons, encompassing such things as infrastructure, mining innovations, economic impact, social effects, and environmental initiatives. Details about each of these topics are provided below.

Infrastructure

Prior to the discovery of the BMC, access to remote parts of Gloucester and Northumberland counties was mainly by seasonal lumber roads or by canoe. When Heath Steele was being brought into production in the mid-1950s, the road from Newcastle (now Miramichi City) to Wayerton had to be extended northwestward to the mine site, including construction of a bridge, known as the 'Miners Bridge' over the Northwest Miramichi River (described in some detail by Gallagher 1999). A spur railway line from the main CNE track was also constructed from Bartibog Station to the Heath Steele mine site (Fig. 5a); the tracks were taken up after the mine closed in 1999, and the roadbed is now used as a snowmobile trail. Then in the early 1960s, when the Wedge mine was being readied for operation, the road was extended north from Heath Steele, across the Nepisiguit River, and northwest along the river to the mine site. This road included construction of a major bridge over the Nepisiguit River, referred to locally as the 'Heath Steele Bridge' (Fig. 18a). A bit later, when Brunswick No. 12 was being made ready for production a road (the 'Mines Road') was constructed from Big River, just south of Bathurst, to the mine site. A spur railroad line was also built

https://doi.org/10.12789/geocanj.2020.47.163

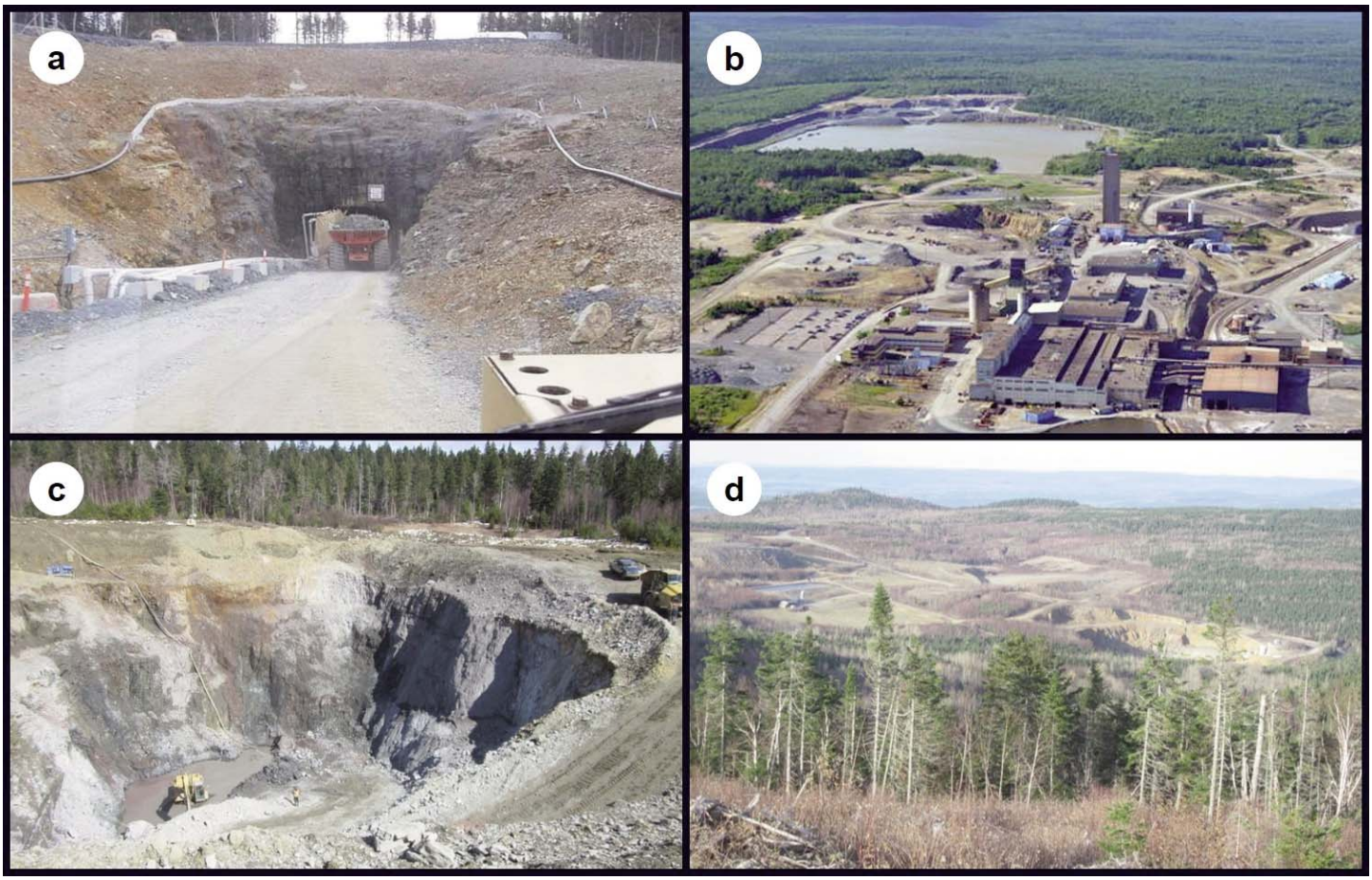

Figure 17. 2000s developments: a) portal to the Halfmile Lake decline in 2012 (New Brunswick Natural Resources and Energy Development archives); b) aerial view looking north of Brunswick No. 12 in 2010, showing the absence of the ventilation stack between the #3 headframe and the open pit, with the flooded rock-backfill quarry in the background (Bathurst Heritage Museum); c) open-pit at CNE in 2013 (NBNRED archives); d) Restigouche mine site looking northeast across the open pit (to the right) and waste rock piles (to the left) in 2012 (NBNRED archives).

from Nepisiguit Junction to the mine site. Furthermore, a smelter and deep-water port facilities were constructed at Belledune (Fig.18b) and are still there today, although the smelter closed at the end of 2019. Ultimately, the roads to Brunswick and Heath Steele were linked and are now known as provincial Highway 430.

Similarly, the southeastern part of Restigouche County was difficult to reach, even up to the 1980s, when the 'Road to Resources' was completed. However, it was development work at the Caribou mine site in the late 1950s and 1960s that led to construction of the road from South Tetagouche (just west of Bathurst) to Caribou Depot in 1965. In the early 1980s, the road was extended westward, past the Murray Brook and Restigouche deposits, to connect with a main lumber haulage road coming east from St. Quentin. Subsequently, it has been upgraded and it is now a paved provincial highway (Route 180) from Bathurst to St. Quentin. Finally, the lead smelter and the deep-water port at Belledune would not exist if not for the discovery of the BMC.

Mining Innovations

The BMC has been the site of multiple mining innovations. Many of them pertain to Brunswick No. 12 and are described in papers that were published in the CIM Bulletin over the years. In fact, a 1971 issue of the CIM Bulletin (V. 64, no.713) was devoted to "The Brunswick Story". Many innovations that occurred at Brunswick No. 12 are mentioned in Jarratt's (2012) book. More specifically, the BMC was where:

- the first heap-leach gold operations in Canada, both indoor at Murray Brook and outdoor at Caribou, were conducted (Luff 1995);
- a state-of-the-art underground-seismic-monitoring network was installed in 1986 at Brunswick No. 12; it was upgraded in 1997; and was used until 2013 to guide mining activity and maintain safety (Simser and Falmagne 2004);
- a large-scale panel-distress blast was fired in 1999 to reduce ground stresses in a critically important part of the Brunswick No. 12 mine, which allowed more ore to be mined and thereby extended mine life (Andrieux et al. 2003);
- modified cone bolts and 00-gauge metal straps were employed at Brunswick No. 12 to control rock bursts (White and Rose 2012);

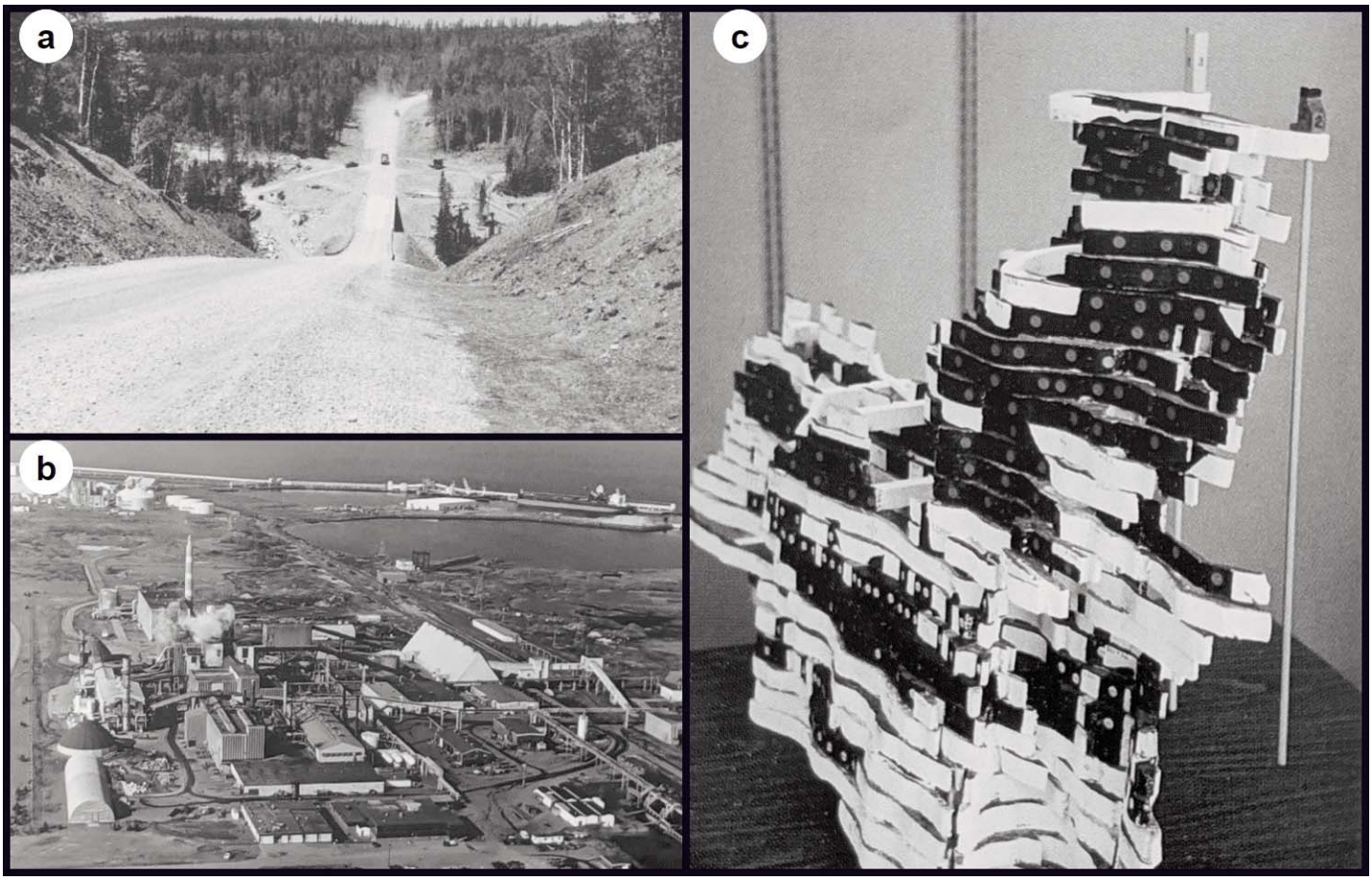

Figure 18. Other photos: a) road and bridge ('Heath Steele Bridge') over Nepisiguit River circa 1962, looking north (Our Miramichi Heritage Family archives); b) aerial view looking northwest at the Belledune smelter with the docks for the Port of Belledune in the background in 2000 (Bathurst Heritage Museum); c) a 3D model, created by Rhéal Godin, of the Brunswick No. 12 orebody in the mid-1990s, showing the #2 and #3 headframes (top), the #2 shaft and the various levels in the mine; black areas are mined-out stopes and white areas are unmined (from Gallagher 1997).

- the 'Mechanic's Stethoscope', a diagnostic software tool for underground vehicle maintenance, was developed and successfully employed at Brunswick No. 12 (Fauteux et al. 1995);
- the remotely controlled 'Weasel drill' was developed in 1992 for use in open stopes (Jarratt 2012) and beginning in 1997 was manufactured commercially by Marcotte Mining Machinery Services of Sudbury, Ontario, for other mining operations (Gallagher 1997);
- a 3D scale model (Fig. 18c) of the orebody that dwarfed Toronto's CN Tower was constructed in the mid-1990s by an employee, Rhéal Godin, to help develop a computerized model of the No. 12 mine, and so visitors could better visualize the underground extent of the mine workings (Gallagher 1997);
- an underground incentives program, the 'Brunswick Incentive System', was developed in 1972 and used for many years to keep Brunswick Mining near the top of the list of producers in terms of productivity and near the bottom, with respect to labour and bonus costs (Baker 1995);
- paste backfill was commissioned at Brunswick No. 12 in 1998 (Bernier et al. 1999), and implemented in 2000 (Cormier 2010), leading to increased ore recovery, improved safety and reduced mining costs;
- studies were done on composite soil covers (Bell et al. 1995) and the geochemistry of mine tailings (Blowes et al. 1992) at Heath Steele;
- studies were done on grinding media (Petruk and Hughson 1977; Cooper et al. 1994), mineral liberation (Petruk and Schnarr 1981), and flotation practices (McTavish 1980; Cooper et al. 2004) to enhance metal recoveries at Brunswick and Heath Steele (Chen and Petruk 1980);
- a method was developed to neutralize thiosalts, which form during the milling process and contribute to acid mine drainage (AMD), in wastewater from the Brunswick mill (Cormier 2010);
- and innovative mills designed at the Mt. Isa mine, Australia, were first used in Canada at the Caribou Mine by Breakwater Resources in the late 1990s.

Economic Impact

The economic impact of the mining industry for northern New Brunswick (and Canada) has been immense. During its lifetime, the Brunswick No. 12 mine alone produced over 136

million tonnes of ore grading 3.44% Pb, 8.74% Zn, 0.37% Cu, and 102.2 g/t Ag. The total value of metals recovered, in today's prices, is over $46 billion of new wealth that was injected into the economy. This figure does not account for production from Heath Steele or the other metal mines in the BMC. Additionally, 100s of $1000s per year have been injected into the regional economy from exploration expenditures for over 60 years. Furthermore, additional monies were injected into the economy by suppliers and service providers to the mining operations, such as the Brunswick Smelter at Belledune.

Social Effects

The discovery of the BMC started a transformational change in the social fabric of Bathurst and its surrounding communities. What had been a largely poor, rural society, mostly dependent upon the fishing and forestry industries, was faced with an influx of people and a new economic reality in the 1950s. Initially most of the miners and explorationists were from away, but over time local people were trained to do the well-paid jobs and were employed in the mines and exploration crews, as well as the smelter. The living standard in Bathurst and the surrounding communities improved, local businesses flourished, and Bathurst became a city in 1966, two years after Brunswick No. 12 went into production. The new opportunities, new wealth, and training provided by the mineral industry changed the social fabric of northern New Brunswick. Untold numbers of engineers, geologists, miners, and prospectors 'cut their teeth' in the BMC, and many of them have gone on to make their mark in other parts of Canada and the world.

Over the years, Brunswick Mining and Smelting Corporation contributed to virtually every non-profit organization and charity in the Bathurst area and beyond, encompassing such things as health, safety, education, sports, arts, culture, and the environment. For example, the list of recipient organizations for a two-year period (2010–2012) numbers 192 (Jarratt 2012).

Environmental Initiatives

Several environmental measures were initiated in the BMC. One of the results of the underground fire that began at Brunswick No. 12 in 1970, was a change in safety regulations; specifically, anyone working underground was required to be clean shaven and carry a portable respirator, in case SO_2 gas escaped from the fire zone into other parts of the mine. Ultimately, this regulation has been applied to all underground mines in Canada.

Originally, the lead smelter at Belledune was supposed to be built on the east side of Bathurst Harbour at Daly Point, where land (mostly marshland) had been purchased for this purpose in the early 1960s. The land remained undeveloped until 1988, when Brunswick decided to turn Daly Point into a nature preserve, with the cooperation of the City of Bathurst and the NBNRED. In September of 1989, the Daly Point Nature Reserve officially opened as a joint venture between Brunswick and NBNRED (Jarratt 2012). A wildlife interpretation centre, parking lot, footpaths, boardwalks, and an observation tower were constructed, complete with bilingual signage, to enhance the area. In October of 2002, Brunswick officially signed over Daly Point to the City of Bathurst. Today, Daly Point is a popular tourist attraction, with 20,000 visitors annually, and it also serves to educate the public about the coastal wetland environment.

Acid mine drainage (AMD) is a common problem at most base-metal mines because sulphide minerals are unstable in the surface environment, where they react with oxygen. In the presence of water, oxidizing sulphides produce sulphuric acid, iron oxides (rust) and they release water soluble metals into the environment, which are harmful to aquatic life, unless the acid is neutralized naturally by limestone host rocks, or deliberately by adding lime. Since limestone host rocks are extremely rare in the BMC, AMD is a problem, which Brunswick discovered in 1969 at its No. 6 mine site, when spring run-off from the waste piles ran into Knights Brook and ultimately killed fish in the Nepisiguit River. To resolve this issue, Brunswick began to collect and treat AMD from both the No. 6 and No. 12 sites after that incident.

At Brunswick No. 12, the treatment consisted of mixing lime with the AMD, which was then sent to settling ponds where approximately 98% of the solids settled to the bottom as a sludge phase, and the remaining water was released to the environment. However, the water quality was not always acceptable, so a new wastewater treatment plant was commissioned in 1993 and went into operation in 1994 (Jarratt 2012). Initially, this plant did not treat water from Brunswick No. 6, which had its own liming station that treated AMD from the waste piles, and then pumped the treated water into the mined-out pit. By the late 1990s, however, the pit was nearly full, so a pipeline and pump station were constructed to send water from No. 6 to the No. 12 site for treatment. Drainage trenches from the waste piles at No. 6 to the pit were constructed and the liming station was removed.

However, the wastewater treatment plant did not resolve the thiosalt problem that is created by the milling process. Thiosalts are partially oxidized sulphur compounds that are not neutralized by lime, but become oxidized after release into the surface environment, where they lead to acidification of down-stream waters. To minimize the amount of wastewater (and thiosalts) released to the environment, Brunswick established recycling loops in the mill. However, the water reclamation system had limited storage capacity until after 2000, when paste backfill was implemented at Brunswick No. 12. This made the rock quarry, which had provided conventional backfill for the mine (Fig. 17b), redundant, so it became a big (500 x 500 x 20 m) storage reservoir for the reclamation system. This enabled the mill to increase the recycling rate from 48% to 64%, while reducing the freshwater withdrawal rate from the Nepisiguit River by 20% (Cormier 2010). One unforeseen effect was a dramatic increase in the concentrations of sulphates and thiosalts in the reclamation quarry over time. Sulphate-reducing bacteria proliferated and generated copious quantities of H_2S (rotten egg gas). In order to reduce the odour of H_2S (and other reduced sulphur compounds) generated in the reclaim quarry, AMD water from the No. 6 pipeline was re-directed to the reclamation quarry in 2009. As a result, the rotten-egg odour was immediately reduced and eventually

eliminated, the pH hovered around 7 (neutral), and the concentrations of sulphates and thiosalts both declined (Cormier 2010).

Also, in the late 1990s, a new wastewater treatment plant was constructed at the Heath Steele Mine to control AMD from that site. Since active mining had ceased by then, there was no thiosalt problem to deal with there.

Brunswick (and Noranda Research) had a long history with the Nepisiguit Salmon Association (NSA), which was formed in 1976 by a small group of local anglers who wanted to rebuild the Atlantic Salmon population in the Nepisiguit River. In 1981, only 312 grilse and salmon returned to the counting fence near the mouth of the River, so the NSA decided to start its own salmon enhancement program, with the blessing of the Federal Department of Fisheries and Oceans. Since 1981, nearly $2.5 million has been spent on this program, with money mainly coming from Brunswick, the Environmental Trust Fund, and the Wildlife Trust Fund. In 1985, the NSA began pioneering studies with Noranda Research to develop and install streamside-incubation boxes for salmon eggs; survival rates of over 90% were achieved. By 1988, the salmon population in the Nepisiguit River had increased significantly; a total of 4,268 grilse and salmon passed through the counting fence that year. After 2009, NB Power and the Atlantic Salmon Conservation Foundation also became contributing sponsors to the NSA. Today, the Nepisiguit River is one of the premier salmon rivers of New Brunswick (Jarratt 2012).

ACKNOWLEDGEMENTS

We would like to thank the two Geoscience Canada reviewers (Neil Rogers and Reginald Wilson) for their helpful comments on the manuscript; most of their suggested changes have been incorporated in this final version. We would also like to thank the following people for providing data and/or information about specific mine sites, namely: Pierre Bernard, John Griggs, Arthur Hamilton, Kenneth Moore, Richard Schwenger and Melbourne Scott. Others provided photographs, or pointed out where they could be found, namely: Charles Asoyuf, Richard Cavellero, Roger Clinch, Florence Gray, Ronald Jessulat, Terrence Lenihan, Terrance MacDonald, and Mark Mullin. Thanks to all.

REFERENCES

Andrieux, P.P., Brummer, R.K., Liu, Q., Simser, B.P., and Mortazavi, A., 2003, Large-scale panel destress blast at Brunswick mine: Canadian Mining and Metallurgical Bulletin, v. 96, no. 1075, p. 78–87.

Baker, R.W., 1995, Underground incentives - their development, application and effect at Brunswick No. 12 mine, Bathurst, New Brunswick: Canadian Mining and Metallurgical Bulletin, v. 87, no. 985, p. 73–76.

Belland, M., 1992, The birth of the Bathurst Mining Camp: a development history of the Austin Brook iron mine and the No. 6 base metal deposit: New Brunswick Department of Natural Resources and Energy, Mineral Resources Popular Geology Paper 92–1, 56 p.

Bell, A.V., Riley, M.D., and Yanful, E.K., 1995, Evaluation of a composite soil cover to control acid waste rockpile drainage: Canadian Mining and Metallurgical Bulletin, v. 88, no. 995, p. 41–46.

Bernier, L.R., Li, M.G., and Moerman, A., 1999, Effects of tailings and binder geochemistry on the physical strength of paste backfill, *in* Goldsack, D., Belzile, N., Yearwood, P., and Hall, G., *eds.,* Proceedings of Mining and the Environment II: Laurentian University, Sudbury, ON, p. 1113–1122.

Blowes, D.W., Jambor, J.L., Appleyard, E.C., Reardon, E.J., and Cherry, J.A., 1992, Temporal observations of the geochemistry and mineralogy of a sulfide-rich mine tailings impoundment, Heath Steele Mines, New Brunswick: Exploration and Mining Geology, v.1, p. 251–264.

Boyle, D.R., 2003, Preglacial weathering of massive sulfide deposits in the Bathurst Mining Camp: economic geology, geochemistry, and exploration applications: Economic Geology Monograph 11, p. 689–721.

Chen, T.T., and Petruk, W., 1980, Mineralogy and characteristics that affect recoveries of metals and trace elements from the ore at Heath Steele Mines, New Brunswick: Canadian Mining and Metallurgical Bulletin, v. 73, no. 823, p. 167–179.

Cooper, M., Bazin, C., and Grant, R., 1994, Grinding media evaluation at Brunswick Mining: Canadian Mining and Metallurgical Bulletin, v. 88, no. 987, p. 29–31.

Cooper, M., Scott, D., Dahlke, R., Finch, J.A., and Gomez, C.O., 2004, Impact of air distribution profile on banks in a Zn cleaning circuit: Canadian Mining and Metallurgical Bulletin, v. 97, no. 1083, p. 1–6.

Cormier, J., 2010, Acid mine drainage as a sustainable solution to eliminate risk and reduce costs, *in* The Organizing Committee of the 14th International Conference on Tailings and Mine Waste, *editor,* Tailings and Mine Waste 2010: Taylor and Francis, London, UK.

Davies, J.F., Gibson, H.L., and Whitehead, R.E.S., *editors*, 1992, Exploration and Mining Geology, Special Issue, v. 1, p. 93–207.

Douglas, R.P., l965, The Wedge mine – Newcastle–Bathurst area: Canadian Mining and Metallurgical Bulletin, v. 58, no. 635, p. 290–296.

Dufresne, N., 1981, The evolution of mining methods used at Brunswick Mining and Smelting: Canadian Mining and Metallurgical Bulletin, v. 74, no. 825, p. 101–109.

Fauteux, L., Dasys, A., Gaultier, P., and Johnson, R., 1995, Mechanic's stethoscope: a technology transfer model: Canadian Mining and Metallurgical Bulletin, v. 88, no. 994, p. 47–50.

Gallagher, D., *editor*, 1997, Noranda Mining and Exploration: New Brunswick Divisions Magazine, May, 11 p.

Gallagher, D., 1999, Heath Steele: Noranda Inc., Bathurst, NB, 87 p.

Goodfellow, W.D., McCutcheon, S.R., and Peter, J.M., *editors*, 2003, Massive sulfide deposits of the Bathurst Mining Camp, New Brunswick, and northern Maine: Economic Geology Monograph 11, 930 p.

Grebenc, F.J., and Welwood, R.J.R., 1971, The Brunswick Story: Brunswick Mining Operations: Canadian Mining and Metallurgical Bulletin, v. 64, no. 713, p. 37–43.

Jarratt, M., *editor*, 2012, Brunswick Mine, The End of an Era: Xstrata Zinc Canada, Bathurst, NB, 195 p.

Jensen, T., Blakley, I.T., Jacquemin, T., and Woods, S.C., 2018, Technical report on the Caribou Mine, Bathurst, New Brunswick, Canada: Roscoe Postle Associates Inc., prepared for Trevali Mining Corporation, 238 p. Available from: https://www.sedar.com/search/search_en.htm.

Kenny, J.L., 1997, A new dependency: state, local capita l, and the development of New Brunswick's base metal industry, 1960–70: The Canadian Historical Review, v. 78, p. 1–39, https://doi.org/10.3138/CHR.78.1.1.

Lentz, D.R., *editor*, 2006, Volcanic-hosted massive sulfide deposits and their geological settings in the Bathurst Mining Camp, New Brunswick: Exploration and Mining Geology, Special Issue, v. 15, p. 1–261.

Luff, W.M., 1995, A history of mining in the Bathurst area, northern New Brunswick, Canada: Canadian Mining and Metallurgical Bulletin, v. 88, no. 994, p. 63–68.

McTavish, S., 1980, Flotation practices at Brunswick Mining: Canadian Mining and Metallurgical Bulletin, v. 73, no. 821, p.115–120.

McCutcheon, S.R., and Walker, J.A., 2019, Great mining camps of Canada 7. The Bathurst Mining Camp Part 1: Geology and exploration history: Geoscience Canada, v. 46, p. 137–154, https://doi.org/10.12789/geocanj.2019.46.150.

McCutcheon, S.R., Luff, W.M., and Boyle, R.W., 2003, The Bathurst Mining Camp, New Brunswick, Canada: History of discovery and evolution of geologic models: Economic Geology Monograph 11, p. 17–35.

Petruk, W., and Hughson, M.R., 1977, Image analysis evaluation of the effect of grinding media on selective flotation of two zinc–lead–copper ores: Canadian Mining and Metallurgical Bulletin, v. 70, no. 782, p. 128–135.

Petruk, W., and Schnarr, J.R., 1981, An evaluation of the recovery of free and unliberated mineral grains, metals and trace elements in the concentrator of Brunswick Mining and Smelting Corporation Ltd.: Canadian Mining and Metallurgical Bulletin, v. 74, no. 833, p. 132–159.

Pollock, J.C., 2019, Great mining camps of Canada 6. Geology and history of the Wabana Iron Mines, Bell Island, Newfoundland: Geoscience Canada, v. 46, p. 69–83, https://doi.org/10.12789/geocanj.2019.46.148.

Sim, R.C., and Davis, B.M., 2008, Technical report Chester copper property New Brunswick, Canada: First Narrows Resources Corporation, Technical Report NI 43–101 June 3, 2008, 88 p. Available from: https://www.sedar.com/search/search_en.htm.

Simser, B., and Falmagne, V., 2004, Seismic source parameters used to monitor rock-mass response at Brunswick mine: Canadian Mining and Metallurgical Bulletin, v. 97, no. 1080, p.58–63.

Whaley, K.D.A., 1992, The Captain North Extension (CNE) Zn–Pb–Ag deposit,

Bathurst District, New Brunswick: Exploration and Mining Geology, v. 1, p. 143–150.

White, R., and Rose, B., 2012, Rockburst support in high stress areas at Brunswick Mines (Presentation): Xstrata Zinc Canada, Sudbury, ON. Available from https://www.workplacesafetynorth.ca/sites/default/files/resources/Rockburst%20Support%20in%20High%20Stress%20Areas%20at%20Brunswick%20Mines.pdf.

Zhang, Y.H., Arsereau, G., Holland, L., and Barrett, J., 2014, Technical Report on preliminary economic assessment for the Caribou massive sulphide zinc–lead–silver project, Bathurst, New Brunswick, Canada: SRK Consulting (Canada) Inc., prepared for Trevali Mining Corporation, 169 p. Available from: https://secure.kaiserresearch.com/i/jk/tr16/TRTV20140513.pdf.

Received March 2020
Accepted as revised July 2020

GEOLOGICAL ASSOCIATION OF CANADA (2020-2021)

Corporate Members

PLATINUM

MEMORIAL UNIVERSITY

GOLD

NORTHWEST TERRITORIES GEOLOGICAL SURVEY

SILVER

ROYAL TYRRELL MUSEUM

YUKON GEOLOGICAL SURVEY

BRITISH COLUMBIA GEOLOGICAL SURVEY

NICKEL

UNIVERSITY OF WATERLOO

GEOSCIENCE CANADA AND THE GEOLOGICAL ASSOCIATION OF CANADA ARE GRATEFUL TO THE CANADIAN GEOLOGICAL FOUNDATION FOR THEIR FINANCIAL SUPPORT OF THIS JOURNAL

Canadian Geological Foundation — Fondation Géologique du Canada

Officers

President
Deanne van Rooyen
Past President
Kathryn Bethune
Vice-President
Alwynne Beaudoin
Treasurer
Michael Michaud
Secretary
Holly Steenkamp

Councillors

Paul Alexandre
Andrea Amortegui
Alwynne Beaudoin
Kathryn Bethune
Stefanie Bruekner
Hendrik Falck
Alana Hinchey
Rebecca Hunter
Andy Kerr
Phil McCausland
Michael Michaud
Camille Partin
Roger Paulen
Holly Steenkamp
Deanne van Rooyen
Reg Wilson

Standing Committees

Communications: Rebecca Hunter
Finance: Michael Michaud
GAC Lecture Tours: Stefanie Bruekner
Publications: Roger Paulen
Science Program: Phil McCausland

GEOSCIENCE CANADA

JOURNAL OF THE GEOLOGICAL ASSOCIATION OF CANADA
JOURNAL DE L'ASSOCIATION GÉOLOGIQUE DU CANADA

2020 VOLUME 47 GSCNA7 47 103-166
PRINT EDITION ISSN 0315-0941
ONLINE EDITION ISSN 1911-4850